

American University in Cairo

AUC Knowledge Fountain

Theses and Dissertations

2-1-2015

Development of inhalable microparticles for drug delivery to deep lung tissues

Yasmine Houssam ElDin Abbas

Follow this and additional works at: <https://fount.aucegypt.edu/etds>

Recommended Citation

APA Citation

Abbas, Y. (2015). *Development of inhalable microparticles for drug delivery to deep lung tissues* [Master's thesis, the American University in Cairo]. AUC Knowledge Fountain.

<https://fount.aucegypt.edu/etds/1282>

MLA Citation

Abbas, Yasmine Houssam ElDin. *Development of inhalable microparticles for drug delivery to deep lung tissues*. 2015. American University in Cairo, Master's thesis. *AUC Knowledge Fountain*.

<https://fount.aucegypt.edu/etds/1282>

This Thesis is brought to you for free and open access by AUC Knowledge Fountain. It has been accepted for inclusion in Theses and Dissertations by an authorized administrator of AUC Knowledge Fountain. For more information, please contact mark.muehlhaeusler@aucegypt.edu.



School of Sciences and Engineering

**Development of Inhalable Microparticles for Drug
Delivery to Deep Lung Tissues**

A Thesis Submitted to

The Nanotechnology Master's Program

In partial fulfilment of the requirements for

The degree of Master of Science

By:

Yasmine Houssam EIDin Hassan Abbas

Under the supervision of:

Prof. Dr. Hassan M.E. Azzazy (Advisor)

Department of Chemistry, The American University in Cairo, Egypt

Fall 2014

The American University in Cairo

Development of Inhalable Microparticles for Drug Delivery to Deep Lung Tissues

A Thesis Submitted by

Yasmine Houssam ELDin Hassan Abbas

To the Nanotechnology Graduate Program

Fall 2014

In partial fulfillment of the requirements for

The degree of Master of Science

Has been approved by

Thesis Committee Chair and Thesis Supervisor: Prof. Dr. Hassan M.E. Azzazy

Affiliation: Professor of Chemistry, School of Sciences and Engineering, The American University in Cairo.

Thesis Committee Internal Examiner: Prof. Dr. Tarek M. Madkour

Affiliation: Professor of Polymer Chemistry, School of Sciences and Engineering, The American University in Cairo.

Thesis Committee External Examiner: Prof. Dr. Nagia N. Afifi

Affiliation: Department of Pharmaceutical Technology, Faculty of Pharmacy and Biotechnology, German University in Cairo.

Thesis Committee Moderator: Dr. Ahmed Moustafa

Affiliation: Associate Professor and Director of Biotechnology Graduate Program, School of Sciences and Engineering, The American University in Cairo.

Dept. Chair/Director

Date

Dean

Date

ACKNOWLEDGEMENTS

First I would like to express my sincere gratitude to my advisor; Prof. Hassan Azzazy for believing in me and my work. This thesis would have not been accomplished without his research guidance, encouragement and support that motivated me to put my best effort in completing this project.

I would also like to extend my deepest thanks to Prof. Sanjay Mathur and the whole research group for providing me with the best hospitality and immense kindness.

Special thanks to my teammates (Mrs. Mai Mansour, Miss Heba Adel, Miss Marwa Hussein, Mr Mahmoud Abdel Ati, Mr Karim Abdel Hady, Miss Heba Othman, Miss Ayaat Mohamed, Mrs. Mai SaadZaghloul and Mrs. Amira Mansour) at Dr. Hassan Azzazy's research group at the American University in Cairo for their help, support, and encouragement; especially to Mrs. Salma Tamam for her great help and technical advice.

I am also thankful to all my professors at the American University in Cairo who taught me through the multidisciplinary courses I have attended in the Nanotechnology program. Their guidance and experience were very valuable.

Special thanks to the researchers and colleagues here at the American University in Cairo and Cologne University who participated in teaching me some research skills and provided me with continuous guidance during my work; Rami Wasfi, Alaa EIDin Gad and Shifaa Siribbal for helping me in the SEM imaging, Mr. Mahmoud AbdelMoez and Ahmed Omaia for the FTIR experiments, Johannes Schläfer for the STEM measurements and Dr. Nahed Yacoub for FAAS measurements. Thanks for the research group at the Nanotechnology Characterization Center (NCC), Agriculture Research Center (ARC) for VSM, DLS, XRD and CLSM measurements as well as research group at the Egyptian Petroleum Research Institute for HR-TEM measurement. Thanks to Prof. Annette Schmidt and Silvio Sollazzo at the Institute of Physical Chemistry of Cologne University and to Prof. Alf Lamprecht and Mohamed Ehab Ali at the Laboratory of Pharmaceutical Technology and Biopharmaceutics, University of Bonn for helping me to complete two of the main milestones of my thesis (The drug release experiment in the presence of MNPs with the application of alternating magnetic field and the spray freeze drying with evaluation of lung deposition by next generation impactor; respectively).

I would like also to sincerely thank my beloved family; my mother, father and brother for always believing in me, supporting me and providing me with the right environment for work and study. I dedicate this work to them.

Finally, I would like to express my endless thanks to my dearest friends Miss Heba Samaha, Mrs. Salma ElMenawi, Miss Mai Kessba, Miss Shaimaa Kassem, Miss Merihane Nosseir and Miss Rania Ayman for their continuous support and being with me through thick and thin and always pushing me forward. And to my University colleagues Miss Ruaa Nur, Miss Yomna Emad, Miss Isra Ali, Mrs. Samar Fadl, Mr. Mohamed ElLeithy and Mr. Ahmed ElGhazaly for their continuous advice, support, prayers and encouragement since I decided to start this track. I will never forget their help and contribution in pushing me to achieve my goals.

Abstract

Lung cancer is the deadliest solid tumor, leading to the deaths of more individuals than the combination of the three next most lethal cancers which are colon, prostate and breast cancer. According to the IARC, in 2012 lung cancer accounted for 13% (1.83 million) of cancer cases and caused 19% (1.56 million) of cancer deaths worldwide. Despite advances in surgery and drug discovery, lung cancer remains difficult to treat. This is a result of unavoidable exposure to carcinogens, poor diagnosis and the lack of targeted drug delivery platforms. The aim of this study was to develop a non-invasive, patient convenient platform for the targeted delivery of chemotherapeutic drugs to cancer in deeper lung tissue. The formulation consisted of inhalable maltodextrin (MD)-based microparticles (MPs) encapsulating chitosan (CS) nanoparticles (NPs) loaded with magnetic nanoparticles (MNPs) and a chemotherapeutic drug. Ionotropic gelation was used for CS NPs synthesis. MNPs were synthesized via hydrothermal method and they were superparamagnetic with magnetic saturation (M_s), coercivity (H_c) and remanence (M_r) of 48.4 Am^2/Kg , 9.9×10^{-4} T and 0.5 Am^2/Kg emu/g; respectively. CS NPs provided a sustained release of drug, whereas MNPs encapsulated in CS NPs were able to increase the NP drug release in response to an external magnetic field by 1.7 fold. Cell uptake studies conducted using lung cancer cells (A549) indicated that the CS NPs are rapidly uptaken, and show preferential toxicity to tumor cells in comparison to cultured fibroblasts. NPs were modified with anti-epidermal growth factor receptor antibodies and this modification showed to hinder cellular uptake of NPs. Afterwards, the prepared CS NPs and CS-MNPs were co-spray freeze dried (SFD) with MD. The prepared SFD powders had fine particle fraction ($\text{FPF} \leq 5.2 \mu\text{m}$) of 40-42 % w/w and mass median aerodynamic diameter (MMAD) of 5-6 μm as determined by the next generation impactor (NGI). A mixture of CS NPs and CS-MNPs could be able to provide a continuous sustained release of drug, with intermittent blouses of drug in response to external stimuli; a drug profile desirable in cancer therapy. In conclusion, the targeted delivery to the lung cancer using the developed formulation seems to be a promising approach.

Table of Contents

ACKNOWLEDGEMENTS	iii
Abstract	iv
Chapter 1: Introduction and Literature Review	1
1. Lung Cancer:	1
1.1. Burden:	1
1.2. Pathophysiology:	1
1.3. Lung cancer classification:	2
2. Chemotherapy in Non-Small Cell Lung Cancer (NSCLC):	2
3. Drawbacks of intravenously (I.V.) administered chemotherapy:	3
4. NSCLC targeting; Endobronchial intratumoral chemotherapy (EITC):	4
5. NSCLC targeting; Oral chemotherapeutic drugs?	5
6. NSCLC targeting; Inhaled nanoparticle (NP)/microparticle (MP) based chemotherapy:	5
6.1. In-vivo fate of inhaled particulate carriers:	6
6.2. The Proposed Formulation: Nanoparticle embedded in microparticles (NEMs) for airway tumor delivery:	7
6.2.1. Why CS NPs?	7
6.2.2. Why MNPs?	7
6.3. Route and method of administration:	8
6.4. Deposition in the lung:	8
6.5. Specific targeting and entry into tumor cell:	8
6.6. Drug release and theranostic potential:	9
7. State of the art:	10
Thesis Scope and Objectives	12
Chapter 2: Materials and Methods	14
1. Materials:	14
2. Methodology:	15
2.1. Nanoparticles (NPs) formulation and characterization:	15
2.1.1. Chitosan Nanoparticles (CS NPs):	15
2.1.2. Magnetic Nanoparticles (MNPs):	16
2.1.3. Void MNPs-loaded CS NPs (CS-MNPs):	17
2.2. Drug loading and its effect on NPs physicochemical properties:	17
2.2.1. Encapsulation Efficiency % (EE %) of CS NPs:	17

2.2.2.	Determining the effect of drug encapsulation on the physicochemical properties of CS NPs:	19
2.2.3.	Determination of MNPs encapsulation's effect on drug-loaded CS NPs size, surface charge and EE %:	19
2.3.	Drug Release:	20
2.3.1.	Determination of drug release profile from drug-loaded NPs:	20
2.3.2.	Determination of MNPs effect on drug release upon the application of high frequency magnetic field (HFMF):	20
2.4.	NPs modification:	22
2.4.1.	Tagging of EGFR-antibody to CS NPs surface:	22
2.4.2.	Quantification of tagged EGFR-antibody:	23
2.5.	NPs-cell interaction:	23
2.5.1.	Cellular cultivation:	23
2.5.2.	Extent of NP uptake determination; effect of NP:	23
2.5.3.	Efficiency of Cisplatin-loaded NPs via MTT assay:	24
2.6.	Spray freeze drying (SFD) and evaluation of Lung deposition by next generation impactor (NGI):	25
2.6.1.	Incorporation of NPs in Polyvinylpyrrolidone (PVP): Maltodextrin (MD) microparticles (MPs):	25
2.6.2.	Evaluation of aerodynamic properties of MPs using NGI:	26
2.7.	Statistical analysis:	26
Chapter 3: Results		27
1.	NPs formulation and characterization:	27
1.1.	CS NPs:	27
1.1.1.	Morphology and size:	27
1.1.2.	Surface charge measurement with LDE:	27
2.	MNPs:	27
2.1.	Morphology, size and surface charge:	28
2.1.1.	DLS and LDE Measurement:	28
2.1.2.	STEM Measurement:	28
2.2.	Functional groups determination with FT-IR:	28
2.3.	Magnetic properties measurement using VSM:	29
2.4.	Determination of MNPs crystallography using XRD:	29
3.	Void CS-MNPs:	29
3.1.	Morphology, size and surface charge:	29
3.1.1.	DLS and LDE Measurement:	29

3.1.2. HR-TEM:.....	29
4. Drug loading and its effect on NPs physicochemical properties:.....	30
4.1. Determining the effect of drug encapsulation on the physicochemical properties of CS NPs: 30	
4.1.1. EE % of CS NPs:	30
4.1.2. Morphology, size and surface charge:	30
4.2. Determination of MNPs encapsulation's effect on drug-loaded CS NPs size, surface charge and EE %:	30
5. Drug Release:	31
5.1. Determination of drug release profile from drug-loaded CS NPs:.....	31
5.2. Determination of drug release profile from drug-loaded CS NPs and CS-MNPs:	31
5.3. Determination of MNPs effect on drug release upon the application of HFMF:.....	31
6. Quantification of EGFR-antibody used to modify the surface of drug and MNP-loaded CS NPs:.....	32
7. NPs-cell interaction:	32
7.1. Extent of NP uptake determination; effect of NP:	32
7.1.1. MTT assay:	32
7.1.2. Effect of NPs concentration and modification on the cell's uptake magnitude:.....	32
7.1.3. NPs Uptake confirmation by CLSM:.....	32
7.1.4. Efficiency of Cisplatin-loaded NPs via MTT assay:	33
8. SFD and evaluation of Lung deposition by NGI:	33
8.1. Incorporation of NPs in PVP: MD MPs:.....	33
8.2. Evaluation of aerodynamic properties of MPs using NGI:	33
Chapter 4: Discussion	34
1. NP formulation and characterization:.....	34
1.1. CS NPs:	34
1.2. MNPs:.....	34
1.3. Void CS-MNPs:	36
2. Drug loading and its effect on NPs physicochemical properties:.....	36
2.1. Determining the effect of drug encapsulation on the physicochemical properties of CS NPs: 36	
2.2. Determination of MNPs encapsulation's effect on CS NPs size, surface charge, morphology and drug loading:	37
3. Drug Release:	37
3.1. Determination of drug release profile from drug-loaded NPs:	37

3.2.	Determination of drug release profile from FL-loaded NPs in the absence of magnetic field:	38
3.3.	Determination of MNPs effect on drug release upon the application of magnetic field:	39
4.	NP modification:	39
5.	NP-cell interaction:	40
5.1.	MTT assay:	41
5.2.	Extent of NP uptake determination; effect of NP:	41
5.3.	Efficiency of Cisplatin-loaded NPs via MTT assay:	43
6.	SFD and evaluation of Lung deposition by NGI:	43
6.1.	Incorporation of NPs in PVP: MD MPs:	43
6.2.	Evaluation of aerodynamic properties of MPs using NGI:	44
	Conclusions and Future Perspectives:	45
	Tables:	47
	Figures:	60
	References:	90

List of Abbreviations

AC: Adenocarcinoma

AD: Aerodynamic Diameter

AFM: Atomic Force Microscope

Cisplatin: Cis-Diammineplatinum (II) Dichloride

CLSM: Confocal Laser Scanning Microscopes

CS: Chitosan

DLS: Dynamic Light Scattering

DMSO: Dimethyl sulfoxide

EDC: N-(3-Dimethylaminopropyl)-N'-ethylcarbodiimide hydrochloride

EDTA: Disodium Ethylenediaminetetraacetate

EGFR-Antibody or Ab: Monoclonal Anti-Epidermal Growth Factor Receptor Antibody

EGFR: Epidermal Growth Factor Receptor

EITC: Endobronchial Intratumoral Chemotherapy

Ellman's reagent (DTNB): 5, 5'-Dithiobis(2-nitrobenzoic acid)

FAAS: Flame Atomic Absorption Spectrometer

FBS: Fetal Bovine Serum

FE-SEM: Field Emission-Scanning electron microscope

FT-IR: Fourier Transform-Infrared Spectrometer

FL: Fluorescein

HFMF: High Frequency Magnetic Field

HR-TEM: High Resolution Transmission Electron Microscope

IgG-FITC: Anti-Mouse IgG (whole molecule)- Fluorescein isothiocyanate

I.V.: Intravenous

LDE: Laser Doppler Electrophoresis

MD: Maltodextrin

MNPs: Magnetic Nanoparticles

MP: Microparticle

MTT: 3-(4, 5-dimethylthiazolyl-2)-2, 5-diphenyltetrazolium bromide

NAC: N-Acetyl-L-Cysteine

NGI: Next Generation Impactor

NP: Nanoparticle

NSCLC: Non-Small Cell Lung Cancer

PBS: Phosphate Buffered Saline

PVP: Polyvinylpyrrolidone

SCLC: Small Cell Lung Cancer

SCC: Squamous Cell Carcinoma

SFD: Spray Freeze Dryer

STEM: Scanning Transmission Electron Microscope

TPP: Sodium Tripolyphosphate

USPIONS: Ultra-Small Superparamagnetic Nanoparticles

Vit. C: L-Ascorbic Acid/Vitamin C

VSM: Vibrating Sample Magnetometer

WGA-AF: Wheat Germ Agglutinin, Alexa Fluor 488 Conjugate

XRD: X-ray Diffractometer

List of Figures

Figure 1: Cancer Worldwide.....	60
Figure 2:TNM staging for NSCLC	61
Figure 3: Nanoparticles embedded in microparticles (NEMs) for airway tumor delivery.	62
Figure 4: Role of EGFR in cell growth and division.	63
Figure 5: Desirable release profile of chemotherapeutic drug from proposed formulation.	64
Figure 6: Model Drugs: (a) N-acetyl cysteine (NAC) and (b) Fluorescein (FL)	65
Figure 7: Indirect determination of N-acetyl cysteine (NAC).	66
Figure 8: Cisplatin.....	67
Figure 9: Drug release profile determination from Drug-loaded NPs	68
Figure 10: EDC (carbodiimide) cross-linking reaction scheme.....	69
Figure 11: Spray Freeze Drying (SFD) apparatus.....	70
Figure 12: NGI Assembly (Induction port, Preseparator, Stages 1-7 and MOC).	71
Figure 13: Initial assessment of formulated NPs using SEM.	72
Figure 14: AFM analysis.	73
Figure 15: STEM image for MNPs.....	74
Figure 16: FT-IR of (a) MNPs and (b) Precursors (vitamin C and FeCl ₃ .6H ₂ O) with product (MNPs).	75
Figure 17: Hysteresis loop of prepared MNPs.....	76
Figure 18: XRD chart showing the crystal structure of prepared MNPs	77
Figure 19: HR-TEM images for MNPs-loaded CS NPs.	78
Figure 20: SEM images of drug-loaded CS NPs.	79
Figure 21: Figure 4- N-acetyl cysteine (NAC) drug release profile	80
Figure 22: Fluorescein (FL) drug release profile.....	81
Figure 23: Logarithmic presentation for the release profile of a) FL-loaded CS NPs and b) FL-loaded CS-MNPs.	82
Figure 24: τ for CS NPs and CS-MNPs.	82
Figure 25: IgG-FITC calibration curve.....	83
Figure 26: MTT assay for (a) CS NPs, CS-MNPs and (b) MNPs on A549 and L929 cell lines	84
Figure 27: Cellular Uptake of tagged and non-tagged NPs for A549 cell lines.....	85
Figure 28: CLSM images for intact A549 cells.	86
Figure 29: MTT assay for free cisplatin versus NPs-loaded cisplatin and cisplatin released.....	87
Figure 30: SEM images for SFD NPs.....	88
Figure 31:The NGI dispersion results for CS NPs and CS-MNPs.....	88
Figure 32: CS NPs preparation by Iontropic Gelation	89

Figure 33: Active targeting moieties attached to the surface of nanoparticle..... 89

Figure 34: Schematic diagram of monoclonal antibody. 89

List of Tables

Table 1: Recently developed biodegradable NP/MP drug delivery platforms used in lung cancer targeting.	47
Table 2: Opalescent NP formulations with varied parameters and their assessment using SEM.	54
Table 3: Further analysis of NPs (formulas 9-11) using DLS.	55
Table 4: Various formulations for MNPs synthesized with varied parameters that were attracted by externally applied magnet.	56
Table 5: Mean size and potential for different MNPs formulations.	57
Table 6: Different Concentrations of AC with their corresponding CS NPs EE %.....	58
Table 7: EE% and size comparison between the developed formula and same formulas in different studies.	59

List of Equations

Entrapment Efficiency (1).....	18
Determination of FL concentration released at each timepoint (2).....	21
Determination of time constant (τ) (3)	22
Logarithmic Conversion of Equation (3) (4)	22
Debye-Scherrer Formual (5)	35

Chapter 1: Introduction and Literature Review

1. Lung Cancer:

1.1. Burden:

The dread and terror that come with a cancer diagnosis have their roots in its killer nature. Though tragic in general some types of cancer seem to have a lighter impact on patients' ears than others; lung cancer surely not included. Lung cancer is the deadliest solid tumor, leading to the deaths of more individuals than the combination of the three next most lethal cancers which are colon, prostate and breast cancer [1]. As stated by the International Agency for Research on Cancer (**Figure 1**) in 2012, lung cancer accounted for 13% (1.83 million) of cancer cases and caused 19% (1.56 million) of cancer deaths worldwide [2]. The numbers seem to leap; the World Health Organization estimates that lung cancer will account for 19.35% of all cancer deaths by 2020 [3]. Elevated lung cancer cases and associated deaths could be attributed to a number of reasons. Poor diagnosis; because the lungs are large, tumors can grow undetected for a while. In addition to that symptoms are unspecific (coughing and fatigue), failing to illicit serious worry [4]. For such reasons, early-stage lung cancer is difficult to detect. Smoking and increased exposure to carcinogens are other main causes [5]. The lungs' epithelial surface represents the largest surface area of the human body, being concurrently in direct contact with the environment [6] makes inhalation the most important exposure route for airborne carcinogens such as such as arsenic, asbestos, polycyclic aromatic hydrocarbons, and radon [2, 7].

1.2. Pathophysiology:

Lung cancer's pathophysiology can be described as a "multi-hit" condition; where several carcinogens (from different sources) induce genetic mutation affecting essential biological mechanisms such as growth control, vascular supply, proliferation and death of normal cells. Along with genetic susceptibility, the cumulative effect of several "hits" results in irreversible effects; dysregulation of these mechanisms and cancer development [8].

1.3. Lung cancer classification:

There are two types of lung cancer: small cell lung cancer (SCLC) and non-small cell lung cancer (NSCLC). NSCLC represents 85% of the lung cancer cases [9]. NSCLC is further divided into 3 main subtypes; squamous cell lung carcinoma (SCC), adenocarcinoma (AC) and large cell carcinoma with SCC and AC being the most common. SCC comprises approximately 30% of lung cancers and generally arises centrally within the lungs inside a large bronchus. AC, represents almost 30% of invasive lesions, tends to occur in more peripheral locations arising from the smaller airways but they can be found centrally in a main bronchus. In other words, regardless to its histology most lung tumors seem to allocate in the airways [9-10]. A possible reason is that inhaled carcinogens primarily come in contact with the epithelial lining of the lung airways resulting in molecular changes and genetic mutations within these cells leading to inflammatory responses in this area followed by progressive proliferative epithelial reactivity. The resulting epithelial lesions grow over time from hyperplasia to advanced preneoplastic lesions, and finally to AC and SCC [11]. Since the late 1990s, NSCLC has been commonly staged according to the fifth edition of the TNM classification system, which measures the size of the primary tumor (T), the extent of lymph node involvement (N), and the presence of distant metastases (M). **Figure 2** summarizes the classification system [12].

2. Chemotherapy in NSCLC:

Accurate staging of lung cancer according to TNM staging is essential for deciding appropriate therapy [13]. Till this moment, surgical resection is considered as the most successful and consistent option for lung cancer diagnosed patients. However, this option is limited by the feasibility of cancer being resectable, and the tolerability of patient to the proposed surgical intervention, making surgery only possible for patients with stages I-II[13] or I-III[14]. However, almost 70% of lung cancer patients at the time of diagnosis show up with locally advanced disease rendering surgery inappropriate [13]. Even in cases where surgery is a valid option, about 50% of the patients experience recurrence within 5 years after tumor resection [14]. For such reason adjuvant chemotherapy is generally accepted for patients with resectable stage IIA-III A NSCLC [13-14] and is thought to increase survival rates and reduce recurrence. Neoadjuvant, or induction, chemotherapy

administered preoperatively has also been proposed since it may render inoperable tumors resectable and improve the success of surgery by reducing tumor size and the occurrence of residual micrometastases [14].

3. Drawbacks of intravenously (I.V.) administered chemotherapy:

Several chemotherapeutic drugs are suggested for the use in NSCLC including cisplatin, etoposide, mitomycin C, vindesine, vinorelbine, vinblastine, and ifosfamide. There seems to be a consensus on the use of cisplatin based therapy in NSCLC; a series of trials conducted between 1991-2007 all have included cisplatin in their regimens [15-21]. Cisplatin is a platinum-containing anticancer drug which was discovered by Michele Peyrone in 1845 has water solubility of 2.5 mg/ml and is renally excreted. It acts by crosslinking DNA via binding Pt^{2+} to the guanine bases of DNA interfering with cell division of cancer cells and elicit repair mechanism which will induce apoptosis of the cancer cells [22].

Although cisplatin-based chemotherapy reduces the risk of death from NSCLC by approximately 5%, considerable toxicity is unfortunately associated with platinum-based chemotherapy, which resulted in discontinuation of therapy in many patients [14]. Side effects include interstitial pneumonia, bone marrow suppression, hair loss, nephrotoxicity, myocarditis, and neurotoxicity all of which are a result of systemic dissemination of the drug following I.V. administration [9]. It is important to emphasize that the access of systemic intravenous drugs to tumors is surprisingly limited. Primeau et al.[23] utilized an immunofluorescent technique to assess the access of doxorubicin to tumors via the circulatory system. The authors found that an exponential reduction in the concentration of drug was visualized at a distance from tumor blood vessels; decreased to half the perivascular concentration within only 40–50 μm . Such findings raise several questions. Is it a delivery problem? Would chemotherapeutic drugs have a larger impact on survival rates if they actually reach the tumor? Would targeted delivery provide a higher therapeutic value with less systemic side effect?

4. NSCLC targeting; Endobronchial intratumoral chemotherapy (EITC):

Currently in the eyes of physicians, a benefit is granted by adjuvant chemotherapy that is equivalent to the cancer recurring risk; a higher risk cancer is more likely to have. The risk is reduced by chemotherapy to an extent that counterbalances the acute and chronic adverse effects of adjuvant chemotherapy. In other words, adjuvant chemotherapy is quiet beneficial but, its use is only hampered by its inability to reach its target and consequently cause intolerable systemic side effects. Such problems possibly ailed with the use of targeted delivery system, concentrating the drug and its actions to the tumor only, circumventing its distribution throughout the body and avoiding excruciating side effects.

Literature includes several attempts in localized chemotherapeutic drug application. Celikoglu et al. elegantly summarized advances in EITC where chemotherapeutic drugs are intratumorally injected into tumor tissue directly through a flexible bronchoscope by means of an ordinary needle-ended-catheter [9]. Precise cancer drugs delivery into the tumor is afforded by EITC, where complete lesion perfusion, increased intratumour drug concentrations, and most importantly decreased toxic side effects which normally occur with conventional systemic chemotherapy can be obtained [9].

Unfortunately EITC utilizes a bronchoscope rendering it an invasive technique. Though minimally invasive, the technique still mandates the availability of the patient in a bronchoscopy facility which makes the treatment modality far from convenient for patients and having a negative impact on patient compliance. Apart from that, bronchoscopy in particular is known to spike patient anxiety with sedating medicaments such as midazolam usually prescribed pre- procedure, making the treatment modality far less appealing for such patients [24]. In simpler words for efficient treatment a cancer patient would have to visit the EITC facility several times a month (possibly a week) and go through an invasive, discomfoting procedure on a regular basis for a long time. Patients also complain from, sensation of nausea, moderate chest pain, and a moderate fever after the procedure [9], though not quiet problematic, all of which are trivial forms of pain and discomfort that could be spared by a cancer patient.

It is true that EITC initially delivers large amounts of chemotherapeutic drug into the tumor, however the drug seems to diffuse of from the injection site [9]. A prolonged high

intratumoral drug concentration from few hours to several days is desirable for more effective treatment. In attempt to do so several researchers have tried intratumoral injection of gel containing drugs [25-26] and microspheres [27]. Such attempts though ail the drug diffusion problem, show no improvement of the drawbacks of the bronchoscopy based technique.

5. NSCLC targeting; Oral chemotherapeutic drugs?

An efficient targeted delivery platform is therefore required to deliver chemotherapeutic drugs to lung tumors in the most comfortable and convenient way. Compared to systemic administration and bronchoscopy based procedures, the oral route is more patient friendly. A patient interview conducted on 103 patients showed that the oral route was preferred by the majority of patients (90%), mainly due to greater convenience (57%), intravenous access problems such as fear of needles (55%) or medicament administration at better environment (i.e., the home setting) [28]. However for chemotherapeutic drugs the oral route does not present itself as the most efficient. Apart from concerns about drug absorption, bioavailability and general random pharmacokinetics, orally administered chemotherapeutic drugs ultimately reach the blood and are distributed systemically with minimal amounts reaching the lung in general and the tumor in particular. Thus, only solving the problem of impracticality but not the intolerable side effects and low target accessibility [29].

6. NSCLC targeting; Inhaled nanoparticle (NP)/microparticle (MP) based chemotherapy:

Inhalation was believed to be the optimal route of administration in the case of NSCLC chemotherapy and that use of the creatively engineered inhalable particulate carriers may in fact hold the solution to the current dilemma. Inhalation offers a non-invasive route for chemotherapeutic drug delivery lacking the undesirable attributes of I.V. and bronchoscopy based approaches. The use of particulate carriers affords specific tumor targeting and a tailored drug release profile. Moreover, it provides a non-invasive method for targeted delivery of chemotherapeutic drugs to the lungs, with minimal systemic side effects and patient inconveniency. Since most of NSCLC are AC and SCC and most of which seem to

allocate in the airways [9-10], the development of NP/MP carrier system capable of delivering chemotherapeutic drugs to airway tumors is a valid approach. To further elaborate on how airway targeting could be achieved, first light is needed to be shed on the in-vivo fate on inhaled NP/MPs.

6.1. In-vivo fate of inhaled particulate carriers:

The fate of inhaled NPs and MPs depends on where they initially deposit in the lungs and how they are cleared, the latter is being greatly dependant on the former and both are being a function of the particle's physico-chemical properties and lung anatomy [30-32]. The epithelium in the trachea and bronchial area is protected by a ciliated mucus layer. Therefore, rapid clearance of particles depositing in the upper airways by the cilia results within the mucus layer, moving them to the throat, where they are swallowed and metabolized eventually [30-31]. Deposition of inhaled particulate system in the lung is achieved by any of the following mechanisms; inertial impaction, gravitational sedimentation and Brownian diffusion [31]. Deposition mechanism followed by the particulate system depends on its aerodynamic diameter (AD); a parameter greatly dependant on particle density, material of synthesis, geometrical diameter, and shape [32-33]. By inertial impaction particles with ADs larger than 5 μm mainly deposit in the large airways and oropharynx, in which they will most likely be cleared through mucocillary clearance instead of reaching the lung [32]. Those with ADs ranging from 1-5 μm deposit by gravitational sedimentation and diffusion deeper into the lungs [31-32, 34-35]. As for NPs most of them will be exhaled as a result of their small size, however they can still be delivered to the lung by being incorporated into larger particles with appropriate AD or nebulization [32, 36]. Though hard to sediment in the lungs, it has been demonstrated by several studies that small NPs are able to overcome steric inhibition possessed by the dense mucin fiber mesh [37-38], moving into the mucus layer where they interact with the non-phagocytic cells of the epithelium and their endocytosis will be regulated by clarithin coated pits, caveolae and scavenger receptors, allowing them to gain access into the pulmonary interstitium [31]. Particle deposition is also highly influenced by surface electrostatic charge; higher deposition efficiencies is achieved by the charged NPs rather than neutral ones [31]. In other words charged NPs have a greater chance in allocating into airway cells

and in this case in NSCLC cells, they do however lack the desirable AD for deposition in the airways.

6.2. The Proposed Formulation: Nanoparticle embedded in microparticles (NEMs) for airway tumor delivery:

The formulation of chitosan NPs (CS NPs) encapsulating a chemotherapeutic drug and magnetic NPs (MNPs) all enclosed in Maltodextrin (MD)-based MPs (CS-MNPs-MPs) and CS NPs encapsulating a chemotherapeutic drug only enclosed in MD MPs (CS NPs-MPs) (**Figure 3**) was proposed.

6.2.1. Why CS NPs?

CS is obtained from deacetylation of chitin which is the main component of crustaceans' shells. It is a linear polysaccharide composed of randomly distributed β -(1-4)-linked N-acetyl-D-glucosamine and D-glucosamine. As a result of its water solubility, biocompatibility and biodegradability it has been used in various biomedical applications. Molecular weight and degree of deacetylation of CS affect its properties whether chemical or biological and classify commercially available CS into high, medium and low molecular weight CS with molecular weight and degree of deacetylation are decreasing respectively. Since molecular weight and degree of deacetylation of CS affects NPs degradation, therefore medium molecular weight CS was preferred for moderate degradation and drug release for the sustained release purpose aimed by synthesized CS NPs for continuous supply of chemotherapeutic drug to lung cancer cells. Sustained drug delivery together with the mucoadhesive property of CS that allows prolonged contact time with cell surface for continuous drug release, render CS NPs as the optimum type of NP for chemotherapeutic drug delivery in NSCLC [39].

6.2.2. Why MNPs?

MNPs have been recently used in various biomedical applications such as magnetic hyperthermia, drug targeting, MRI enhanced imaging and cell separation [40]. For these biomedical applications it is preferred for MNPs to possess superparamagnetic characteristic to avoid aggregation in organs or vascular system resulting in unwanted side effects after the removal of externally applied magnetic field. Toxicity of MNPs depends on several

factors among which are the shapes, size, materials used for synthesis and degradation byproducts of MNPs. Therefore, green synthesis method that is devoid from any organic solvents is important to reduce cytotoxicity of MNPs. The use of small sized MNPs (< 20 nm) for superparamagnetic behavior will ensure rapid renal clearance of MNPs from the body after their use as a result of their small size, thus accumulation of MNPs in the body will be avoided. Knowing that MNPs are made up of iron which is the main component of hemoglobin, byproducts from MNPs degradation can be stored in the liver to be used later for red blood cells production [41].

6.3. Route and method of administration:

CS-MNPs-MPs and CS NPs-MPs are to be co-administered using a dry powder inhaler.

6.4. Deposition in the lung:

MPs with AD 1-5 μm deposit by gravitational sedimentation and diffusion deeper into the lungs [31-32, 34-35]. MD MPs developed with mean AD ranging from 1-5 μm will allow deposition in the airways. MD is a soluble sugar and upon contact with lung lining fluids the MPs will dissolve liberating the cationic CS NPs. Similar attempts utilizing NEMS proved success of the concept with the use of lactose [42] and mannitol [43] for MP synthesis.

6.5. Specific targeting and entry into tumor cell:

CS is a biodegradable non-toxic cationic polymer [44] yielding positively charged hydrogel NPs [45]. Since charged NPs are more readily up taken by airway cells than neutral larger particles then CS NPs are a valid approach. To further augment cellular entry and increase specificity to tumor cells CS NPs are to be conjugated with a targeting moiety.

From the tyrosine kinase ErbB family, epidermal growth factor receptor (EGFR) is abnormally activated in many epithelial tumors (**Figure 4**) [46]. EGFR was found to be over-expressed in samples and cell lines of NSCLC, and associated with increased tumor proliferation, higher incidence of metastases to lymph nodes, poor differentiation, and a worse prognosis [47]. Surface conjugation of an EGFR specific ligand would further facilitate tumor localization into NSCLC cells by receptor mediated endocytosis.

6.6. Drug release and theranostic potential:

One of advantages of EITC is its ability to deliver a large bolus of drug into the tumor. Instantly after cytotoxic drug solution injection, the tumor shrinks to a smaller volume. It is assumed that these rapid effects result from direct contact of malignant cells to extremely high concentration of anticancer drug. It is believed that a transient super-dose spike of a few minutes in the tumor have more tumoricidal effect than tolerable doses of I.V. drugs [9]. However as mentioned earlier with EITC the drug diffuses from the injection site [9], making the technique incapable of the desirable continuous supply of chemotherapeutic drug. The importance of the latter made quite obvious by the continued efforts to develop chemotherapeutic drug sustained release dosage forms [48-49].

Co-administration of our proposed formulations CS-MNPs-MPs and CS NPs-MPs would provide an initial bolus dose, followed by a sustained release of the chemotherapeutic. CS-MNPs-MPs provide the initial bolus in the response to alternating magnetic field while CS NPs-MPs provide the sustained supply of drug (**Figure 5**). Physical stimuli (such as; ultrasound, temperature, light, magnetic and electrical fields) induce polymer response by directly modulating the energy level of the polymer/solvent system to critical energy level [50]. When CS-MNPs released from CS-MNPs-MPs are subjected to an alternating magnetic field, heat is produced either by hysteresis loss or by Néel (spin rotation) and Brownian (particle rotation) relaxations based on the material of enclosed MNPs [51]. This property is measured in terms of specific loss power (SLP) which depends on nanoparticles size (i.e. core radius, r), saturation magnetization (M_s), magnetic anisotropy constant (K) and solution volume [51-52]. This released heat can result in the swelling, collapse or degradation of temperature-responsive hydrogel NPs [50] and rapid release of the encapsulated drug; initial bolus. In addition to rapid drug release, the elevated temperature may actually participate in tumor cell ablation; magnetic hyperthermia [52]. Enhanced relaxivity coefficient (r_2) possessed by MNPs may also add the advantage for CS-MNPs-MPs to serve as contrast agents for imaging modalities such as magnetic resonance imaging (MRI) [52]. An image-guided drug release triggering with the provision of information regarding the anatomical location of the carrier system would be allowed by MNPs incorporation. By this means diagnostic feature or in this case theranostic feature can be

imparted. Co-administered MNPs-free CS NPs-MPs provide a sustained release of chemotherapeutic drug complementing the targeted bolus dose supplied by CS-MNPs-MPs.

7. State of the art:

Lung cancer targeting has been addressed previously in different studies where various biodegradable NP/MP drug delivery platforms were developed as summarized in **Table 1**. In this section the short comings of the published delivery devices that are addressed by our proposed formulation will be highlighted.

Although the above formulations offer improved therapy, they lack the advantages provided by the use of MNPs; the initial bolus release of chemotherapeutic drug in addition to the possible extra tumoricidal benefit due to magnetic hyperthermia and diagnostic/prognostic benefits. Except for studies performed by few authors (Sadhukha, T., et al [64], Nejati-Koshki, K., et al [65], and McBride, A.A., et al [69]) in which the use of MNPs was included however, they did not assess MNPs cytotoxicity on normal cells.

Some studies showed the potential of formulating inhalable formulations. They were administered using either aerosolizers or nebulizers, this is limited by the suspension and storage of NPs in liquid suspensions which will cause (1) Drug release and deactivation in aqueous media (2) Particle degradation or swelling [53-54, 70, 77]. Study performed by Kaminskas, L.M., et al [55], showed delivery platform to be administered via intratracheal instillation. Beside possessing same limitations as aerosolizers and nebulizers in suspending and storing NPs in liquid medium this route of administration is considered to be invasive. Other reports utilizing NP based platforms have also been reported, however they mostly utilize the IV route and therefore are thought to hold all the undesirable attributes mentioned earlier [60-62, 66-67, 73-75]. In some of them cytotoxicity of the formulation was not evaluated to determine tumor-platform specificity. Few studies have developed dry powder inhalable platforms such as our proposed formulation [56, 68-69, 76].

Authors in some of their studies also did not assess drug release profile of NPs to determine therapeutic efficacy of the developed platform [53, 55, 63, 66, 68, 76]. Even if it is known that polymer used will exhibit a sustained drug release profile, only one part of the desired drug supply regimen will be fulfilled with insufficient bolus dose of chemotherapy.

In some studies NPs were prepared using toxic chemicals such as glutaraldehyde [54, 75] which is considered to be unattractive for in-vivo administration of the therapeutic platform. For lung tumor-targeted delivery, EGF ligand was used as a targeting moiety in one of the studies [54, 77]. However, this could be associated with the risk of cancer growth induction.

Thesis Scope and Objectives

The main aim for this study was to develop a non-invasive, patient convenient platform for the targeted delivery of chemotherapeutic drugs to NSCLC. The delivery platform should be able to provide an initial high dose of chemotherapeutic drug that is controllable in response to external stimulation followed by a sustained supply of the drug in the tumor, all whilst providing a diagnostic edge; allowing physicians to actually see the tumor, which does not only assure success of delivery but may be of prognostic value. Therefore the formulation and optimization of CS NPs encapsulating a chemotherapeutic drug and MNPs all enclosed in MD MPs (CS-MNPs-MPs) and CS NPs encapsulating a chemotherapeutic drug only enclosed in MD MPs (CS NPs-MPs) was proposed.

The proposed delivery platform;

- Utilizes the inhalation route; non-invasive, convenient and could be administered at home, which in turn increases patient compliance.
- Specifically targets airway NSCLC cells, minimizing systemic side effects, lowering the overall dose and ultimately reducing patient expense.
- Exhibits a desirable drug release profile; initial bolus followed by a sustained supply of chemotherapeutic drug.
- May have an increased effect on tumor cell destruction by action of the MNPs; magnetic hyperthermia.
- Provides an idea about tumor size, location making it a diagnostic and therapeutic platform; theranostic. Could also be used to monitor tumor shrinkage and prognosis, giving an idea about patient response to the administered drug and possibility of regimen modification/ tailoring.
- Is expected to show minimal toxicity since it is formulated utilizing a green synthetic method devoid of any organic solvents and with biocompatible, biodegradable polymers.

The intended delivery platform was obtained in this thesis by achieving the following milestones:

1. Preparation and characterization of Chitosan Nanoparticles.
2. Preparation and characterization of Magnetic Nanoparticles.
3. Preparation and characterization of Drug-loaded Chitosan Nanoparticles and Chitosan-Magnetic Nanoparticles.
4. Tagging Nanoparticles with epidermal growth factor-antibody.
5. Nanoparticles in-vitro uptake by lung cancer cells.
6. Characterization of incorporated Nanoparticles in Microparticles.

Chapter 2: Materials and Methods

1. Materials:

Medium molecular weight chitosan (**CS**) (190-310 kDa) was purchased from Bio Basic Inc. (Ontario, Canada). Sodium Tripolyphosphate (**TPP**) was bought from Mistral (Northern Ireland, UK). Glacial acetic acid was purchased from El-Gomhouria Co. (Cairo, Egypt).

Iron (III) Chloride Hexahydrate (**FeCl₃·6H₂O**), Sodium Bicarbonate (**NaHCO₃**), and L-ascorbic acid/Vitamin C (**Vit C**) were supplied by Sigma-Aldrich (Munich, Germany).

N-acetyl-L-cysteine (**NAC**), sodium phosphate dibasic dihydrate, Ellman's reagent, FL, and sodium hydroxide (**NaOH**) were supplied from Sigma-Aldrich (Munich, Germany). Disodium Ethylenediaminetetraacetate (**EDTA**) was purchased from Fisher Scientific (Waltham, MA, USA). Spectra/Por Float-A-Lyzer G2 (MWCO 100 kDa) was supplied from Spectrum Laboratories Inc. (Schwerte, Germany).

Anti-mouse IgG (whole molecule) - Fluorescein isothiocyanate (**IgG-FITC**), monoclonal anti-epidermal growth factor receptor antibody (**EGFR-Antibody or Ab**), and N-(3-Dimethylaminopropyl)-N'-ethylcarbodiimide hydrochloride (**EDC**) were purchased from Sigma-Aldrich (Munich, Germany).

Phosphate buffered saline (**PBS**), RPMI 1640 with L-Glutamine, Pen-Strep, L-Glutamine, and Trypsin EDTA were purchased from Lonza (Basel, Switzerland). Fetal Bovine Serum (**FBS**), Hoechst 33258, Pentahydrate (bis-Benzimide) and Wheat Germ Agglutinin, Alexa Fluor 488 Conjugate (**WGA-AF**) were supplied by Life Technologies (Carlsbad, CA, USA). 6 Well Cell Culture Plate, sterile, F-bottom with lid, 96 Well Half-Area Black Microplate, clear F-bottom with lid, 96 Well Microplate, U-bottom without lid, 96 Well Cell Culture Plate, sterile, F-bottom with lid and T25 and T75 tissue culture flasks were from Greiner Bio-One (Monroe, NC, USA). 3-(4, 5-dimethylthiazolyl-2)-2, 5-diphenyltetrazolium bromide (**MTT**), Dimethyl sulfoxide (**DMSO**), Cis-Diammineplatinum

(II) Dichloride (**Cisplatin**), and methanol were purchased from Sigma-Aldrich (St. Louis, MO, USA). Trypan Blue Solution was from Fluka (St. Louis, MO, USA). A549 and L929 cell lines were obtained from Vacsera Holding Company (Cairo, Egypt) and the American Type Culture Collection (Manassas, VA, USA); respectively.

Maltodextrin (**MD**) and Polyvinylpyrrolidone (**PVP**) were bought from Sigma-Aldrich (St. Louis, MO, USA).

2. Methodology:

2.1. Nanoparticles (NPs) formulation and characterization:

2.1.1. Chitosan Nanoparticles (CS NPs):

The nanoparticles (NPs) were prepared by the ionotropic gelation of chitosan (CS) and tripolyphosphate (TPP). CS and TPP of different concentrations (0.1, 0.3, & 0.5 % w/v for CS and 0.04, 0.08 & 0.1 % w/v for TPP) and pH (3, 4 & 5 for CS and 5 & 8 for TPP) were prepared. CS was dissolved in 1 % acetic acid, while TPP in de-ionized (DI) water. For each formulation, 2 ml of TPP solution were added directly to 5 ml of CS solution. The mixture was stirred for 30 min at 400 rpm at room temperature using magnetic stirrer (VWR Scientific, PA, USA). CS NPs formation was determined initially through the appearance of obtained solution. Opalescent solution indicates the formation of CS NPs, otherwise either clear solution lacking CS NPs or aggregate is obtained [78].

The NPs morphology and size of different formulations were first determined using Field Emission-Scanning electron microscope (**FE-SEM**), (SUPRA 55, ZEISS, Jena, Germany). A drop from the NPs was placed on a SEM silicon wafer and left to dry. Then the samples were examined using FE-SEM. NP's hydrodynamic diameter and zeta potential were then evaluated using Dynamic Light Scattering (**DLS**) and Laser Doppler Electrophoresis (**LDE**); respectively (Zeta sizer nano series (Nano ZS), Malvern Instruments Ltd., Worcestershire, UK). For DLS 1 ml of freshly prepared formulation was used and 1 ml of purified NPs (centrifuged and re-suspended in DI water) was used for LDE. To validate reproducibility triplicate samples were analyzed and the S.D. value of the three was adopted. Atomic Force Microscope (**AFM**), (Nanoscope IIIa, Veeco, NY, USA)

was used for further assessment. Sample for AFM was diluted in 1:10 ratio using DI water. A drop from diluted sample was placed on a clean microscopic glass slide and left to dry in the air. Samples were observed by AFM in tapping mode.

2.1.2. Magnetic Nanoparticles (MNPs):

The MNPs were synthesized via chemical reduction of $\text{Fe}(\text{OH})_3$ using L-ascorbic acid (i.e. Vitamin C) to obtain water-dispersible, biocompatible ultrasmall superparamagnetic iron oxide nanoparticles (USPIONS) of 2-5 nm. To obtain biocompatible USPIONS, different formulations were tried out with varying parameters such as autoclaving time (4 & 6 hrs) and temperature (150 & 200°C), $\text{FeCl}_3 \cdot 6\text{H}_2\text{O}$ concentration (0.1 & 0.3 M) and $\text{FeCl}_3 \cdot 6\text{H}_2\text{O}$: Vit C molar ratio (6:1, 1:6, 1:1 & 2:1) to reach NPs with optimal characteristics. Aqueous solutions of $\text{FeCl}_3 \cdot 6\text{H}_2\text{O}$, NaHCO_3 and Vit C were prepared in DI water.

For each formulation, 20 ml of 0.45 M NaHCO_3 were added drop wise to 10 ml of $\text{FeCl}_3 \cdot 6\text{H}_2\text{O}$ to change soluble FeCl_3 into $\text{Fe}(\text{OH})_3$ precipitate. The mixture was stirred for 1 hr at 400 rpm at room temperature. Subsequently, 5 ml of Vit C were added drop wise and the whole mixture was left to stir for further 20 min. Following this 30 ml of the mixture was transferred into a 50-ml steel-lined Teflon autoclave tube. The Teflon tube was then placed in the autoclave after adjusting its temperature and timing. After the synthesis, the MNPs were washed with DI water and ethanol three times each and were collected by centrifugation eventually at 11 000 rpm (Centrifuge 5804, Eppendorf, Hamburg, Germany). The obtained precipitate was easily re-dispersed in DI water by ultrasonication (Ultrasonic Sonicator, SONOREX, BANDELIN electronic, Bandelin, Germany). After re-dispersion, external magnet was applied to confirm MNPs synthesis.

NPs hydrodynamic diameter was initially assessed by DLS. The NPs surface charge was determined by LDE. For both DLS and LDE, 1 ml of ultrasonicated 0.357 mg/ml stock solution of MNPs in DI water was used. Samples were analyzed in triplicates to validate the formulation's reproducibility. The morphology and actual size of the optimum formulation was examined using Scanning Transmission Electron Microscope (STEM), (CM300 FEG/UT, Philips, Eindhoven, Netherlands). A drop of MNP concentration used for DLS and LDE was placed on a carbon coated film 300 mesh copper grid, and left to dry at room

temperature. The transformation of $\text{FeCl}_3 \cdot 6\text{H}_2\text{O}$ and Vit C into iron oxide NPs capped with oxidized Vit C (dehydroascorbic acid, DHAA) has been analyzed by Fourier Transform-Infrared Spectrometer (**FT-IR**), (PerkinElmer, MA, USA). MNPs were then examined by Vibrating Sample Magnetometer (**VSM**), (7410, Lake Shore Cryotronics Inc., IL, USA) (0.05 g) and X-ray Diffractometer (**XRD**), (XPERT-PRO, PANalytical, Almelo, Netherland) (0.1 g) to determine MNPs magnetic properties and crystalline structure respectively.

2.1.3. Void MNPs-loaded CS NPs (CS-MNPs):

Different amounts of MNPs as a percentage of the CS mass were encapsulated in CS NPs. Since MNPs were negatively charged, thus different amounts of MNPs (0.5, 1 and 2 mg which were equivalent to 10, 20, and 40 % of CS mass; respectively) were added to 5 ml 0.1 % CS solution (pH 5). Then 2 ml of 0.1 % TPP solution (pH 5) were added directly to the CS solution containing MNPs. The mixture was stirred for 30 min at 400 rpm at room temperature.

Obtained NPs hydrodynamic size, zeta potential and morphology were examined using DLS, LDE and High Resolution Transmission Electron Microscope (**HR-TEM**), (2100, JEOL-JEM, Herts, UK) respectively as detailed earlier. For DLS and LDE samples were analyzed in triplicates and results were presented as mean \pm S.D.

2.2. Drug loading and its effect on NPs physicochemical properties:

2.2.1. Encapsulation Efficiency % (EE %) of CS NPs:

N-acetyl-L- cysteine (NAC) and fluorescein (FL) were chosen as model drugs (**Figure 6**) due to ease of quantification using sulfhydryl detection reagents and ease of cellular uptake evaluation for NPs; respectively. Similarly as CS NPs, drug-loaded NPs were formulated using ionotropic gelation.

For drug-loaded NPs; NAC/FL was initially added to 5 ml 0.1% CS solution (pH 5). To CS-drug solution, 2 ml 0.1% solution of TPP (pH5) were added all at once and stirred using magnetic stirrer for 30 min at 400 rpm at room temperature. NPs synthesis was confirmed by opalescent appearance. Different concentrations of NAC (7, 10 & 12 mg/ml) and 100 μl of FL (2 mg/ml in 0.01 M NaOH) were used to evaluate NPs EE %. For each sample

duplicates were analyzed and the S.D. of each duplicate was adopted to validate EE %'s reproducibility of the CS NPs.

EE % was determined indirectly for NAC; NP suspension was purified by centrifugation at 14000 rpm for 30 min. Un-encapsulated drug was quantified in the supernatant and accordingly the amount of encapsulated drug determined using **equation 1**.

$$EE\% = \frac{\text{Total Amount of Drug-Free Drug}}{\text{Total Amount of Drug}} \times 100 \quad (1)$$

On the other hand, FL EE % was determined directly where the centrifuged pellet was reconstituted in 1 ml of DI water. EE% was determined based on FL fluorescence using microplate fluorometer ($\lambda_{\text{ex}} = 490 \text{ nm}$, $\lambda_{\text{em}} = 519 \text{ nm}$). For NAC, Ellman's reagent (also known as DTNB) was used for quantification. DTNB is a water-soluble compound for quantitating free sulfhydryl groups in solution. DTNB reacts with a free sulfhydryl group to yield a mixed disulfide and 2-nitro-5-thiobenzoic acid (TNB). TNB is colored and has a high molar extinction coefficient in the visible range [79]. Accordingly absorbance of the resultant TNB at $\lambda = 412 \text{ nm}$ could be used to quantify NAC based on its sulfhydryl content (**Figure 7**).

To determine un-encapsulated and encapsulated concentration of NAC and FL; respectively, a calibration curve was constructed using standard solutions prepared in DI water (for NAC: 0.30, 0.25, 0.20, 0.15, 0.10, 0.050, 0.030, 0.020, 0.015, 0.010 mg/ml and for FL: 0.028, 0.020, 0.010, 0.005, 0.003, 0.002, 0.001, 0.0005 mg/ml). For NAC, DTNB reaction protocol was optimized for use in 96-well U-bottom microplate. In each well, 27 μl of sample or standard solution were added to mixture of 268 μl reaction buffer (0.1 M sodium phosphate, pH 8.0, containing 1 mM EDTA) and 6 μl DTNB. Absorbance was measured at $\lambda = 412 \text{ nm}$ for both samples and standards. For FL, fluorescence of 50 μl of standard solutions and samples were measured using the microplate fluorometer (FLUOstar Optima Microplate Fluorometer, BMG LABTECH, Ortenberg, Germany) and 96-well clear, F-bottom half-area black microplate at $\lambda_{\text{ex}} = 490 \text{ nm}$ and $\lambda_{\text{em}} = 519 \text{ nm}$. Sample concentration was calculated from the corresponding standard curve.

As for cisplatin (**Figure 8**), stock solution (2 mg/ml) was prepared in DI water. 200 μ l of stock solution were added to 2 ml of 0.1 % TPP solution (pH 5). Then to 5 ml 0.1% CS solution (pH 5) cisplatin-containing TPP solution was added all at once and the mixture was stirred for 30 min using magnetic stirrer at 400 rpm at room temperature to obtain cisplatin-loaded CS NPs and CS-MNPs respectively. Afterwards, the mixture was centrifuged for 30 min at 14000 rpm and EE % of cisplatin was determined indirectly similar to NAC. Absorbance of un-encapsulated cisplatin was determined using Flame Atomic Absorption Spectrometer (**FAAS**) (240 AA, Agilent Technologies Inc., CA, USA) with the aid of platinum standard curve prepared in DI water (5, 20, 40, 60, and 80 mg/L) at $\lambda=265.9$ nm. Triplicates for each type of NP were analyzed and the arithmetic mean for each triplicate was adopted to ensure EE % reproducibility.

2.2.2. Determining the effect of drug encapsulation on the physicochemical properties of CS NPs:

The effect of drug encapsulation on the CS NPs size and surface charge was evaluated. FE-SEM was used to evaluate the drug-loaded CS NPs morphology. DLS and LDE were used to determine size and surface charge of drug-loaded CS NPs respectively. Samples for FE-SEM, DLS and LDE were prepared similar to CS NPs samples mentioned before. Triplicates for optimum drug-loaded CS NPs were analyzed for size and surface charge. The arithmetic mean value of the three was adopted.

2.2.3. Determination of MNPs encapsulation's effect on drug-loaded CS NPs size, surface charge and EE %:

0.5 mg of MNPs were added to 5 ml drug-containing 0.1 % CS solution (pH 5) (this is incase of NAC and FL, but for Cisplatin it is dissolved in TPP). 2 ml of 0.1 % TPP solution (pH 5) were added directly to the CS solution containing MNPs. The mixture was stirred for 30 min at 400 rpm at room temperature. Triplicate for the sample was analyzed and the S.D. and arithmetic mean were adopted to ensure formulation's EE % reproducibility. For obtained NPs hydrodynamic size and zeta potential were examined using DLS and LDE; respectively as detailed earlier. For DLS and LDE samples were analyzed in triplicates and results were presented as mean \pm S.D.

2.3. Drug Release:

2.3.1. Determination of drug release profile from drug-loaded NPs:

NAC and FL release rate from NPs was determined. NPs were purified and re-suspended in 1 ml DI water. Purified NPs were placed inside spectra/por float-a-lyzers (MWCO=100 KDa). Float-a-lyzers were soaked in 6 ml PBS maintained at 37 °C while shaking at 100 rpm (**Figure 9**), at assigned time intervals (0.5, 1, 2, 4, 8, 12, 24, 48, 72, 96, 120, 144 and 168 hrs) aliquots were withdrawn from the release compartment and analyzed for the released drug. For NAC, Ellman's reagent was used and for FL fluorescence was determined directly using fluorometry. However, to avoid fluorescence of released FL being lower than the minimum detection limit of device, two batches of FL-loaded NPs were re-suspended in 1 ml DI water and placed in a float-a-lyzer. The same amount of free NAC and FL were dissolved in 1 ml DI water and placed in float-a-lyzers as controls and analyzed similarly to their corresponding samples. Duplicates of sample and control were run together and results were presented as mean \pm standard deviation (S.D).

2.3.2. Determination of MNPs effect on drug release upon the application of high frequency magnetic field (HFMF):

MNPs and FL-loaded CS NPs (FL-loaded CS-MNPs) were used to determine the effect of magnetic field application on drug release profile in comparison to FL-loaded CS NPs. 0.5 mg of MNPs were added to 5 ml of FL-containing 0.1 % CS solution (pH 5). To FL-containing CS solution 2 ml of 0.1 % TPP solution (pH 5) were added all at once and the mixture was stirred for 30 min at 400 rpm at room temperature.

In preliminary experiments, it was found that the temperature in the samples (measured using an Opsens IR-sensor OTG-A-62), independent from its composition, levels quickly to about 32 °C under the HFMF treatment employed. For comparison reasons, the release profiles of the samples were compared under a constant temperature of 32 °C (thermostat) and under the periodic influence of a HFMF. Each experiment was carried out twice in order to ensure reproducibility.

1st Experiment: Release profiles at 32°C (without HFMF):

500 µl of FL-loaded samples (CS NPs and CS-MNPs) were put in the sample holder of the float-a-lyzer. The exterior was filled with 6 ml of PBS solution, and the temperature of water bath was adjusted at 32 °C in which the float-a-lyzer was placed. Ever 20 min, samples were taken from the buffer reservoir, and employed for the fluorescence measurement after 1:1 dilution with PBS. This procedure was repeated over a period of 8 hours.

2nd Experiment: Release profiles under influence of HFMF:

The magnetic heating experiments were performed using a high frequency (**HF**) induction generator (AIXO T5, Hüttinger Electronic Inc., GmbH, Freiberg, Germany) at $f = 273$ kHz and a power of 5.0 kW, using a water cooled copper induction coil with 5 winds, an inner diameter of 35 mm and a length of 50 mm. Similar procedure was performed as in the 1st experiment, but this time float-a-lyzers were placed inside the induction coil to be exposed to alternating magnetic field (AMF). Magnetic field was switched on for 10 min, and paused for 10 min in order to prevent overheating of the sample. After this period of 20 min, samples were taken from the buffer reservoir, and employed for the fluorescence measurement after 1:1 dilution with PBS. Similarly this procedure was repeated over a period of 8 hours.

Normalized FL concentration ($C_{fl}/C_{fl, \text{theo}}$) was used to represent the release rate, where the theoretical FL concentration ($C_{fl, \text{theo}}$) is the theoretical fluorescence concentration at equilibrium, i.e. assuming all FL of the sample as obtained from the initial concentration measurement (FL $C_{fl, 0}$) was isotropically distributed throughout the sample. For each time point, $C_{fl, \text{theo}}$ is thus accessible by **equation 2**.

$$C_{fl, \text{theo}} = \frac{n_{fl}}{V_{\text{total}}} = \frac{C_{fl, 0} \times V_0}{V_0 + V_b + NV_s} \quad (2)$$

With n_{fl} : molar amount of FL present in the system, V_{total} : total volume in the system.

V_0 : sample volume placed in the inner sample holder of the float-a-lyzer, V_b : buffer volume in the reservoir, N : number of aliquots taken at the present data point, V_s : volume of the aliquot replaced.

For the determination of the time constant τ ; characteristic for the respective release rate, **equation 3** was applied.

$$Cfl = Cfl, \text{theo} \left(1 - e^{-\frac{t}{\tau}} \right) \quad (3)$$

With t : release time. This can be linearized to:

$$\log \frac{Cfl, \text{theo} - Cfl}{Cfl, \text{theo}} = -\frac{1}{\tau} \times t \quad (4)$$

By plotting the logarithmic term against time, τ was determined for the respective system.

2.4. NPs modification:

2.4.1. Tagging of EGFR-antibody to CS NPs surface:

CS-NPs and CS-MNPs (MNPs-loaded CS NPs) were initially tagged with IgG-FITC antibody to easily quantify the amount of antibody attached to NPs via fluorometry. To tag an antibody to CS, 1-ethyl-3-(3-dimethylaminoisopropyl) carbodiimide (EDC) was used. EDC is a an amine-COOH cross linker that is used to create covalent links between CS NPs amine- and IgG's carboxyl groups as shown by **Figure 10**.

From initial IgG-FITC stock (10-20mg/ml), 2 ml of 1mg/ml IgG-FITC were prepared in cold DI water (4°C). EDC (1 mg/ml) was also prepared in cold DI water (4°C). To an eppendorf tube 0.25 ml of 1mg/ml IgG-FITC was added; to which 10 μ l of 1mg/ml EDC were added. The mixture was vortexed (Vortex V1 plus, BOECO, Hamburg, Germany) for 1 min at maximum speed. Then 0.75 ml of either CS-NPs or CS-MNPs were added directly to the mixture. Finally, the whole mixture was shaken for 3 hours at room temperature.

2.4.2. Quantification of tagged EGFR-antibody:

The conjugated antibodies were quantified using fluorometry. Serial dilutions in DI water (0.1, 0.05, 0.03, 0.01, 0.005 & 0.0025 mg/ml) were used to construct a calibration curve. IgG-FITC tagged CS NPs and CS-MNPs were centrifuged at 14000 rpm for 30 min, supernatant was discarded and pellet was re-suspended in the same initial volume. FITC emission of re-suspended pellets is measured and tagged IgG were quantified accordingly. For each sample triplicates were analyzed and the arithmetic mean was adopted to validate reproducibility of tagging technique.

2.5. NPs-cell interaction:

2.5.1. Cellular cultivation:

A549 and L929 cells were cultivated in phenol red free RPMI 1640 with L-Glutamine media supplemented with 10 % FBS and 1 % Pen-Strep antibiotic in 5 % CO₂-incubator (AutoFlow NU-5510 Direct Heat CO₂ Incubator, NuAire, SC, USA) at 37°C.

2.5.2. Extent of NP uptake determination; effect of NP:

2.5.2.1. MTT assay:

For MTT toxicity assay, A549 and L929 cells were plated in separate 96-well F-bottom cell culture plates. For both types of cells 20x10³ cells/ well were plated. Different concentrations of CS NPs (250, 500, 1000 & 2000 µg/ml), CS-MNPs (250, 500, 1000 & 2000 µg/ml) and MNPs (25, 50, 100 & 200 µg/ml) were added. Quintuplets were assigned for each NP concentration and the arithmetic mean was eventually adopted. Untreated cells were used as controls and absorbance values at $\lambda= 570$ nm for those cells were considered as 100 % viability. Cells were incubated with particles for 24 hrs. Following incubation, cells were washed with PBS and MTT of concentration 0.5 mg/ml was added and followed by 2 hrs of incubation. MTT was then replaced with DMSO and the plate was thoroughly mixed in a shaking incubator for 1 hr. Finally, absorbance of wells was measured using microplate fluorometer at $\lambda= 570$ nm. Cell viability for each NP concentration was then determined relative to control.

2.5.2.2. Effect of NPs concentration and modification on the cells' uptake magnitude:

Tagged and non-tagged CS NPs and CS-MNPs loaded with FL were used to study NP cellular uptake in A549 cells. EGFR-antibodies were used to tag FL-loaded CS NPs and CS-MNPs. To one batch of NPs re-suspended in 0.5 ml of DI water, 30 μ l of EGFR-antibody (equivalent to 30 μ g/ml) were added to cells. Simultaneously, non-tagged NPs were prepared. Both tagged and non-tagged NPs were used to determine the uptake of A549 cells. For this purpose cells were seeded at a density of 10^5 cells/well. Different concentrations of tagged and non-tagged CS NPs and CS-MNPs (150 & 250 μ g/ml) were added to A549 cells and incubated for 24 hrs. After 24 hrs, cells were washed with PBS. Amount of uptaken NPs were determined by fluorometry (λ_{ex} : 495 nm and λ_{em} : 519 nm) with the help of a NP calibration curve in DI water (CS NPs and CS-MNPs in PBS: 0.1, 0.5, 1.0, 3.0, 5.0, 7.0, 10.0, 15.0, 20.0 & 25.0 μ g/ml).

2.5.2.3. NPs Uptake confirmation by CLSM:

In 6-well F-bottom plate 10^5 cells/ well were seeded on coverslips. For cellular uptake, 400 μ g/ml of purified FL-loaded CS NPs were added to well. Cells were incubated for 24 hrs. After incubation, cells were washed with PBS then 1 ml of 1 μ l/ml Hoechst (λ_{ex} : 352 nm and λ_{em} : 461 nm) was added to each well and incubated in the dark for 15 min at room temperature. Cells were then washed twice with PBS. Subsequently, 1 ml of 15 μ g/ml WGA-AF (λ_{ex} : 495 nm and λ_{em} : 519 nm) was added and cells were incubated for 5 min at 4°C in the dark. Cells were then washed twice with PBS and fixed with ice cold methanol at -20°C for 15 min. Finally, the coverslips are flipped on clean glass slides after being washed with PBS. Glass slides were incubated at 4°C overnight then was examined using Confocal Laser Scanning Microscopes (CLSM), (710, ZEISS, Jena, Germany).

2.5.3. Efficiency of Cisplatin-loaded NPs via MTT assay:

After determining encapsulated amount of cisplatin in both types of NPs, un-modified NPs were prepared. MTT assay was conducted as previously detailed (section 2.5.2.1), to determine the effect of cisplatin-loaded NPs on cell viability. Different concentrations of cisplatin (10 & 40 μ g/ml) encapsulated in CS NPs and CS-MNPs were added. Free cisplatin in DI water was assigned as control to evaluate loading of cisplatin into NPs. Percentage of

cisplatin that should have been released supposedly for both NPs after 24 hrs (which was higher than the minimum effective concentration of cisplatin (1 µg/ml) for all concentrations and NPs added) was added from cisplatin stock solution to determine the efficacy of amount released. Quadruplicates of each cisplatin concentration were analyzed and the arithmetic mean and S.D. of each quadruplicate were adopted.

2.6. Spray freeze drying (SFD) and evaluation of Lung deposition by next generation impactor (NGI):

2.6.1. Incorporation of NPs in Polyvinylpyrrolidone (PVP): Maltodextrin (MD) microparticles (MPs):

CS NPs and CS-MNPs were formulated and suspensions were SFD in the presence of cryopreservatives (5% (w/v) of 1:1 mixture of PVP: MD). The use of PVP:MD mixture was the most suitable for CS NPs encapsulation with the absence of aggregation based on several trials. SFD is a three step process: droplet formation, freezing, and freeze drying [80], **Figure 11** provides a description of the SFD device. For droplet formation, a drop jet nozzle (2 fluid nozzle, Microdrop Technologies GmbH, Norderstedt, Germany) with a nozzle diameter of 0.5 mm was placed at the top of the spray tower. To adjust the stimulation frequency of the drop jet nozzle a control panel was used, by pressurized air the feed solution (FL-loaded CS NPs and CS-MNPs suspensions) is transported to the nozzle. The jet was adjusted at an approximate velocity of 10 m/s, where a constant Rayleigh drop dispersion was achieved after leaving the nozzle, stimulated by a piezoelectric pulse. Within a cooled, stainless steel spray tower encased by liquid nitrogen-containing cooling jacket, the freezing process was performed. To avoid cooling losses, the cooling chamber was heavily insulated. In operation, the system was cooled to temperatures below $-90\text{ }^{\circ}\text{C}$. Particles froze instantaneously within the tower. They were then collected in a cooled and isolated beaker at the bottom of the tower. Then the frozen particles were transferred into a freeze dryer and subsequently dried under a vacuum for at least 36 h. Following SFD, NPs were reconstituted in de-ionized water and NP size and morphology was determined using SEM.

2.6.2. Evaluation of aerodynamic properties of MPs using NGI:

The aerodynamic properties of the prepared powders were determined using a Next Generation Impactor (NGI) (Copley Scientific, Nottingham, UK) (**Figure 12**). When vacuum is turned on, particles flow with the air stream passing by eight consecutive stages where they will impact based on their aerodynamic size cutoffs. Attached to the NGI was the HandiHaler DPI device (Boehringer Ingelheim, Germany) via a mouthpiece adaptor. All stages before each run were coated with 1% w/v silicon oil in n-hexane to reduce bouncing of particles between stages. Manually five capsules (size 3) were filled with 5–7 mg powder. They were discharged into the NGI into the DPI. The airflow rate was adjusted to 45 L/min for 5.3 s with the aid of a critical flow controller (Copley Scientific, UK); to mimic 4 L of air drawn per breath in human inhalation. For stages 1-7, the effective cut-off aerodynamic diameters for each stage are 9.1, 5.2, 3.3, 1.9, 1.1, 0.6, and 0.4 μm ; respectively at rate of 45 L/min. The contents of the following; capsules, DPI, mouthpiece adaptor, induction port, pre-separator, stages 1–7 and the micro-orifice contactor (MOC) after operation were washed with DI water into volumetric flasks and volume was adjusted. Spectrophotometrically the fluorescence intensities of the solutions were measured (λ_{es} : 485 nm and λ_{em} : 535 nm) using Multilabel counter (Wallac 1420 Victor3, PerkinElmer). Each powder was tested and analyzed in triplicate. Using data analysis the recovered dose (RD; all powder collected starting from the capsules to the MOC), the emitted fraction (EF; the powder fraction that left the inhaler with respect to the recovered dose) and the fine particle fraction (FPF; fraction of the recovered dose with cut-off AD $\leq 5.2 \mu\text{m}$) were calculated. Cumulative percentage undersize was plotted versus effective cut-off diameter. From this plot the mass median aerodynamic diameter (MMAD) was determined.

2.7. Statistical analysis:

Statistical analysis of data was performed with one-way analysis of variance (ANOVA) using Design-Expert® Software (Stat-Ease, Inc., USA). *P*-values less than 0.05 were considered significant.

Chapter 3: Results

1. NPs formulation and characterization:

1.1. CS NPs:

1.1.1. Morphology and size:

CS NPs synthesized with various parameters have developed three types of particles: microparticles, aggregates and small NPs (**Figure 13** and **Table 2**) via SEM measurement. After SEM examination it seemed that formulas 9-11 fall in the desired size range, and were therefore subjected to further analysis. DLS was used for further analysis of formulas 9-11 for size and size distribution. Results are summarized in **Table 3**. The smallest diameter was provided by formula 11, thus it was considered as the optimal. Two more samples of formula 11 were prepared and analyzed with DLS to confirm formula's reproducibility. The mean size for CS NPs was determined to be 63.0 ± 3.0 nm. In concurrence with SEM and DLS, AFM was used to confirm formula 11 as being the most suitable formulation by possessing smallest size as presented by **Figure 14**.

1.1.2. Surface charge measurement with LDE:

Zeta Potential was determined for three different samples of formula 11 by LDE technique. The obtained CS NPs showed surface charge of 28.6 ± 0.6 mV. This indicates that CS NPs were positively charged thus, ensuring formula 11 as the optimal with smallest size and relatively high positive charge.

2. MNPs:

Among various formulations prepared with varying parameters, only some of the developed MNPs were attracted to magnet when applied across the vial externally. Results are summarized in **Table 4**.

2.1. Morphology, size and surface charge:

2.1.1. DLS and LDE Measurement:

DLS and LDE were used to determine the size and surface charge respectively of MNPs synthesized with varied parameters. Results are summarized in **Table 5**. Formula 8 has provided the smallest diameter with highest surface charge, thus was considered as the optimal. Two more samples of formula 8 were prepared and analyzed with DLS and LDE to confirm formula's reproducibility. The mean size and surface charge for MNPs were 27.4 ± 2.8 nm and -26.6 ± 4.6 mV; respectively.

2.1.2. STEM Measurement:

Further characterization was performed for formula 8 using STEM to determine the actual size for the synthesized MNPs rather than the hydrodynamic diameter provided by the DLS. This is to ensure that the particles obtained are superparamagnetic since these nanoparticles should be ≤ 20 nm. The actual size of formula 8 MNPs is shown in **Figure 15** to be 5.5 ± 0.7 nm. This indicates that obtained MNPs are USPIONs.

2.2. Functional groups determination with FT-IR:

The functional groups of obtained MNPs for formula 8 were examined using FT-IR (**Figure 16**). The functional groups of MNPs are represented in **Figure 16(a)**, while the relationship of these functional groups to precursors from which MNPs are synthesized ($\text{FeCl}_3 \cdot 6\text{H}_2\text{O}$ and Vit C) is shown in **Figure 16(b)**.

The chemical transformation of $\text{FeCl}_3 \cdot 6\text{H}_2\text{O}$ and Vit C into iron oxide NPs capped with dehydroascorbic acid (DHAA) has been analyzed by FT-IR. In **Figure 16b** the characteristic absorption bands for stretching $\text{C}=\text{O}$ of the five membered lactone ring of Vit C were shown at 1755 cm^{-1} and stretching vibrations of $\text{C}=\text{C}$ coupled with neighbouring vibrations were visualized at 1656 cm^{-1} [81-82]. In **Figure 16a** the strong band visualized at 553 cm^{-1} in the spectrum of the prepared MNPs is due to the Fe-O vibrations characteristic for iron oxide NPs. However, the stretching $\text{C}=\text{O}$ bands in Vit C were absent in the prepared MNPs, indicating the presence of a coordination bond between the carbonyl group's O atom and the Fe center on the surface of NPs [83-85]. The presence of new absorption band at 1611 cm^{-1} confirmed the coordination. The bands at 1356, and 1048, 1100 cm^{-1} are assigned

to the C-O and C-O-C stretches of the lactone ring [82] in the as-prepared γ -Fe₂O₃-DHAA conjugate, suggesting that no interaction is taking place between lactone ring O atoms and the NPs. Moreover, the presence of hydroxyl groups on the surface of the prepared MNPs was confirmed by the strong OH stretching mode at 3241 cm⁻¹.

2.3. Magnetic properties measurement using VSM:

VSM was used to determine the magnetic properties of synthesized MNPs (formula 8). As shown by **Figure 17**, the hysteresis loop of MNPs is sigmoid in shape with negligible hysteresis. The VSM chart (**Figure 17**) showed that these MNPs present magnetic saturation (Ms), coercivity (Hc) and retentivity (Mr) of 48.4 Am²/Kg, 9.9x10⁻⁴ T and 0.5 Am²/Kg; respectively.

2.4. Determination of MNPs crystallography using XRD:

XRD was used to determine the crystal structure of MNPs (formula 8) as shown in **Figure 18**. Peaks provided were related to cubic γ -Fe₂O₃ (JCPDS-ICDD Card No. 24-0081).

3. Void CS-MNPs:

3.1. Morphology, size and surface charge:

3.1.1. DLS and LDE Measurement:

Formula 1 (CS-MNPs) possessed a size and surface charge of 104.3±9.9 nm and 40.8±0.2 mV; respectively. For the aim of obtaining better drug release upon the application of alternating magnetic field (AMF), the encapsulation of more MNPs was tried. Thus, 1 and 2 mg of MNPs were incorporated into CS-NPs. Both formulas showed aggregation and irreproducibility in synthesis with regards to size. This aggregation was significantly visualized for formula 3. Thus, these formulas were excluded.

3.1.2. HR-TEM:

Characterization of formula 1 (CS-MNPs) using HR-TEM was performed to ensure MNPs encapsulation within the CS NPs with the preservation of the spherical morphology. **Figure 19** showed that each CS NP was encapsulating several MNPs, providing CS NPs

with homogeneously dispersed magnetic multi-cores. Obtained CS-MNPs were spherical in shape.

4. Drug loading and its effect on NPs physicochemical properties:

4.1. Determining the effect of drug encapsulation on the physicochemical properties of CS NPs:

4.1.1. EE % of CS NPs:

CS NPs zeta potential and size were assessed after drug incorporation to evaluate the drug's influence on NPs physicochemical properties. For NAC, different concentrations were used to determine NPs EE% and encapsulation reproducibility. NAC concentration of 10 mg/ml has provided the most reproducible EE% (**Table 6**). Thus, this concentration was used later for evaluation of drug release profile of CS NPs.

For FL and Cisplatin, NPs entrapped the following concentrations: 23.9 ± 1.1 and 498.02 ± 0.002 $\mu\text{g/ml}$; respectively.

4.1.2. Morphology, size and surface charge:

Size of NPs after drug incorporation was measured using DLS. Fortunately, no significant alteration of size was visualized for added concentrations of drugs (63.4 ± 6.5 nm, 60.4 ± 2.4 nm and 62.5 ± 7.8 nm, for AC, FL and Cisplatin; respectively). To further confirm NP formation in the presence of drug, drug-loaded CS NPs were analyzed by SEM (**Figure 20**). SEM image showed that NPs preserved their spherical morphology with same size range as void CS NPs.

4.2. Determination of MNPs encapsulation's effect on drug-loaded CS NPs size, surface charge and EE %:

Using Formula 1, the incorporation of MNPs reduced the amount of entrapped drugs in CS NPs to 29.7 ± 1.6 %, 13.0 ± 0.1 and 412.2 ± 0.0008 $\mu\text{g/ml}$ for NAC, FL and Cisplatin; respectively. The incorporation of MNPs also have resulted in the increase of hydrodynamic size of NAC, FL and cisplatin-loaded CS-MNPs significantly by 1.5-2 folds (93.6 ± 4.0 , 122.4 ± 0.0 , 128.8 ± 1.5 nm; respectively) (un-paired t-test).

5. Drug Release:

5.1.Determination of drug release profile from drug-loaded CS NPs:

Release profile of CS NPs was determined for NAC versus control of free NAC as shown in **Figure 21**. Free NAC has shown to provide higher release rate than CS NPs, but the release profile was rather erratic and not reproducible. The reason for such unexpected results was attributed to the nature of NAC quantification as will be discussed in **Chapter 4-section 2.1**. Further experiments with NAC loaded NPs were therefore halted and only FL-loaded CS NPs were used for further evaluation of NPs release profile.

5.2.Determination of drug release profile from drug-loaded CS NPs and CS-MNPs:

Figure 22 shows the FL release profile from FL loaded NPs. Only 5 and 25 % of FL was released from CS NPs and CS-MNPs; respectively after 168 hrs compared to the control that provided 100 % release during the same period. By visualizing the obtained chart, for CS-NPs an initial burst of FL is seen where 2 % is released in 1 hour followed by a slow, steady increase in the percent of FL released from NPs. For CS-MNPs the initial burst is absent. The percentage of FL released from CS-MNPs was significantly higher than that of CS NPs.

5.3.Determination of MNPs effect on drug release upon the application of HFMF:

For FL-loaded CS NPs and CS-MNPs, release profile with and without HFMF application was performed. From **Figure 23** it can be visualized that there is significant difference in the rate of release for FL-loaded CS-MNPs upon the application of AMF. From the constructed logarithmic charts, τ was obtained for both types of NPs either exposed or non-exposed to HFMF (**Figure 24**). τ values for CS NPs in the absence and presence of HFMF were not significantly different (917 ± 77 and 762 ± 83 min without, and with HFMF application; respectively ($P > 0.05$, $n=3$)). As for CS-MNPs τ values were rather significantly different (258 ± 11 and 150 ± 14 min, without and with HFMF application; respectively ($P < 0.001$, $n=3$)) indicating that a stimulus responsive release is only seen in CS-MNPs.

6. Quantification of EGFR-antibody used to modify the surface of drug and MNP-loaded CS NPs:

Figure 25 shows the IgG-FITC calibration curve from 0.05mg/ml to 0.0025mg/ml. From the curve equation the concentration of tagged IgG-FITC was determined for CS NPs and CS-MNPs. Using this curve's equation concentration of tagged IgG-FITC was 0.024 ± 0.002 and 0.018 ± 0.001 mg/ml for CS NPs and CS-MNPs; respectively.

7. NPs-cell interaction:

7.1. Extent of NP uptake determination; effect of NP:

7.1.1. MTT assay:

The cytotoxicity of CS NPs, CS-MNPs and MNPs were evaluated for A549 and L929 cell lines using MTT assay as shown in **Figure 26**. From **Figure 26** it can be seen that at high concentrations for CS NPs and CS-MNPs (2000 μ g/ml) preferential cytotoxicity towards cancer cells is observed. Whereas, at high concentration of MNPs (200 μ g/ml) cytotoxicity was visualized on both cell lines.

7.1.2. Effect of NPs concentration and modification on the cell's uptake magnitude:

After tagging NPs with EGFR-antibody, the cellular uptake of tagged and non-tagged NPs were evaluated using A549 cell lines as represented by **Figure 27**. From the chart it can be determined that the cellular uptake increased with increased NPs concentration while modification of NPs with ABs has lowered the cellular uptake significantly.

7.1.3. NPs Uptake confirmation by CLSM:

By the aid of CLSM the uptake of FL-loaded CS NPs by A549 cell lines were confirmed. **Figure 28** represents CLSM images of A549 cell lines in which **Figure 28(a)** shows untreated cells. Red fluorescence is attributed to labeling with WGA-AF, which in the absence of CS-NPs labels cell membranes and some organelles. **Figure 28(b)** shows NP treated cells; green FL is attributed to FL loaded NPs, which appear to be inside the cell in the perinuclear area. **Figure 28(c)** shows overlap of red (WGA-AF) and green (FL) fluorescence. Since WGA-AF and FL-CS-NPs are co-localized this indicates that green FL

seen in Figure 27 (b) is in fact owed to NPs rather than noise or released FL since WGA shows preferential affinity to chitosan.

7.1.4. Efficiency of Cisplatin-loaded NPs via MTT assay:

MTT assay was used to determine cisplatin efficacy on A549 cells after being encapsulated in developed NPs (**Figure 29**). For free cisplatin it can be visualized that increasing the concentration of drug, cell viability is significantly lowered. As for CS-loaded cisplatin decrease in cell viability is not significantly different from void NPs.

8. SFD and evaluation of Lung deposition by NGI:

8.1. Incorporation of NPs in PVP: MD MPs:

After SFD, MPs were examined by SEM (**Figure 30**). As seen, MPs obtained for both types of NPs are spherical in shape and nearly of the same size $\sim 3 \mu\text{m}$.

8.2. Evaluation of aerodynamic properties of MPs using NGI:

Figure 31 shows the NGI dispersion results for CS NPs and CS-MNPs. For both NPs, a very small amount seems to be retained in the capsule and similarly in the mouth as indicated by amount in capsules in mouth piece. Inhaled percentage of dose (passed the throat) is $\sim 37\%$ for both NPs. However, $\sim 50\%$ were deposited past the trachea. Both types of particles have also possessed fine particle fraction ($\text{FPF} \leq 5.2 \mu\text{m}$) of $\sim 40\%$ indicating successful delivery to deep lung tissue. Processing the NGI data also allowed the determination of the MMAD which corresponded to $6.1 \mu\text{m}$ for CS-MNPs and $5.1 \mu\text{m}$ for CS NPs.

Chapter 4: Discussion

1. NP formulation and characterization:

1.1. CS NPs:

CS NPs synthesis was performed via ionotropic gelation process. This procedure is very mild; devoid of the usage of organic solvents (which are crucial to the popular emulsion based NP formulation methods). The method involves the addition, of alkaline TPP solution (pH=7–9) onto an acidic CS solution (pH=4–6). NPs are formed instantaneously upon mixing of the two phases through intra and intermolecular crosslinking between TPP negatively charged phosphate and CS positively charged amino groups (**Figure 32**). By varying concentrations, pH and added volumes of CS and TPP, NPs with varying characteristics can be obtained [86].

While formulating the NPs, the aim was to obtain NPs optimal for cell uptake; positively charged and less than 150 nm in diameter. Positively charged NPs are attracted to the negative cell surface enhancing cellular entry by endocytosis [87]. Studies have also showed that smaller NPs (less than 150 nm) show higher cell uptake than larger ones [88]. Since CS NPs will later encapsulate drug and MNPs which may possibly lead to an increase in particle size, therefore the optimal formula should initially have the smallest size. To do so varying formulation parameters were initially tried out to reach NPs with optimal characteristics and initial assessment was based on visual observations, where opalescent samples were regarded as colloidal suspensions and subjected to further examination by SEM visualization. **Table 2** summarizes the results.

1.2. MNPs:

While formulating the MNPs the aim was to obtain biocompatible MNPs that are negatively charged and 5 nm in diameter or less. Negatively charged MNPs were preferred to be easily encapsulated within positively charged CS NPs through electrostatic interaction. Small sized MNPs (less than or equal 5 nm i.e. USPIOs), ensure absence of aggregation upon the removal of external magnetic field [89-91], to avoid blockage of vascular system and toxicity due to aggregation within a tissue or organ.

MNPs were prepared via hydrothermal method in which Vit C acted as both reducing and capping agent for the resulting NPs. This redox reaction allowed synthesis of NPs to be performed in one step in the absence of any organic solvents [92].

Different formulations were tried out with varying formulation parameters to reach NPs with optimal characteristics. Initial assessment was performed by DLS for formulations summarized in **Table 5** (i.e. those showed magnetic attraction to externally applied magnet). Analysis by SEM was difficult due to particles' agglomeration on silicon wafer as a result of Van der Waal forces between them [93]. In addition to the difficulty of identifying the size of individual particles due to inability of imaging using high magnification to prevent detector damage. SEM imaging is based on the transmission of electron beam to the specimen's surface to provide a topological image for the specimen's surface. To focus the beam of electrons on the examined specimen electromagnetic lenses are used. To obtain high resolution image in-lens detectors are preferred to focus the back scattered electrons. The presence of this high magnetic field results in the magnetization of MNPs accelerating them towards the detector. Thus, other than distorting the obtained images, detector malfunctioning may result especially at high magnification since the magnetic field will increase as more focusing will be required [94-95]. LDE measurement was performed to assess MNPs stability based on their surface charge.

The average hydrodynamic size of MNPs is provided by DLS, actual core size was determined using both XRD and STEM. Assessment of MNPs (formula 8) with XRD confirmed the production of cubic $\gamma\text{-Fe}_2\text{O}_3$ (JCPDS-ICDD Card No. 24-0081). Using Debye-Scherrer formula (represented as **equation 5**), the average crystallite size of the individual maghemite NPs was calculated to be 5.6 nm from XRD peak broadening.

$$T = \frac{K\lambda}{\beta \cos \theta} \quad (5)$$

With K : shape factor of value of 0.9, λ : x-ray wavelength, β : line broadening at half the maximum intensity and θ : Bragg angle.

STEM confirmed that spherical NPs with homogenous size distribution of an average size of 5.5 ± 0.7 nm is achieved (**Figure 15**). This size is harmonious with the crystallite size,

calculated from the XRD data. The formation of NPs was also confirmed by FT-IR (**Figure 16**). FT-IR also proved the presence of terminal hydroxyl groups as indicated by the strong OH stretching at 3241 cm^{-1} [92]. These terminal hydroxyls explain why the overall MNP charge is negative and are quite favorable as they increase the MNPs water dispersibility and may serve as potential for further functionalization for the intended biomedical application.

The magnetic properties of prepared iron oxide NPs were measured using VSM at room temperature with magnetic field of 3.1 T. The synthesized MNPs magnetic properties were all of comparable values to previously synthesized iron oxide NPs in accordance with their size [91, 96-97]. Low coercivity and remanence values indicate that MNPs possess superparamagnetic behavior. Thus, complications that may result from agglomeration of MNPs after withdrawal of externally applied magnetic field will be avoided [98].

1.3. Void CS-MNPs:

Several amounts of MNPs were added to CS. However with amounts larger than 0.5mg aggregation was observed. The latter could be attributed to increased NPs size simultaneously with increased MNPs encapsulation, this is due to interference of negatively charged MNPs with TPP-CS crosslinking; weakening it resulting in aggregate formation [99].

2. Drug loading and its effect on NPs physicochemical properties:

2.1. Determining the effect of drug encapsulation on the physicochemical properties of CS NPs:

Since NAC and FL are negatively charged at pH 5, they will electrostatically interact with positively charged CS [100-101]. Thus, during drug-loaded CS NPs synthesis, both types of drug were first added to CS before NP formation. For NAC, when EE% for NPs prepared with 12 and 7 mg/ml were compared to the initial batches prepared with 10mg/ml, changes in EE% were not statistically significant (unpaired t test). However synthesis with 10mg/ml showed highest reproducibility and therefore further tests were conducted with NP batches prepared with 10 mg/ml NAC.

The CS NPs showed an EE% of 41% for 10 mg/ml added NAC using Ellman's reagent. Although 41% seems to be small, for a small molecule (low molecular weight) such as NAC in NPs of such size is acceptable [102-104]. CS NPs are hydrogel NPs where drugs are encapsulated into their matrix and may exit by diffusion. Diffusion rates are generally higher for smaller molecules than for proteins and other macromolecules, for such reason higher EE% is seen for larger molecules while lower EE% for smaller ones as seen in **Table 7**. Moreover EE% increases with the increase in NP size, however a smaller size allows for better cell uptake. Since formulated NPs were prepared for drug delivery purpose into cancer cells, compromising cell uptake by increasing EE% at the expense of NP size was not desirable, especially that CS-NPs do not exhibit toxic effects on non-cancer cells at very high concentrations (up to 2 mg/ml) and therefore a larger concentration of NPs could always be used to compensate for the rather low EE%.

2.2. Determination of MNPs encapsulation's effect on CS NPs size, surface charge, morphology and drug loading:

Negatively charged MNPs were added to CS solution with NAC or FL during synthesis to electrostatically interact with positively charged amino groups of CS before the addition of TPP. The addition of 0.5 mg MNPs provided NPs with good dispersibility, but resulted in the entrapment of 30% of the drug instead of 40% obtained with void CS NPs. This is considered to be normal since the MNPs have displaced some drug molecules as both are aiming to form electrostatic bonds with positively charged amine groups of CS. This competition resulted in the decrease of loaded drug by almost 10% and increase of NPs size from 63 to 93 nm.

3. Drug Release:

3.1. Determination of drug release profile from drug-loaded NPs:

NAC release profiles (**Figures 21**) obtained from duplicated runs were not reproducible and drug levels in the release compartment seems to fluctuate which is quite unusual. A possible reason for such abnormal results is the method of NAC quantification. NAC quantification using Ellman's reagent depends on NAC's sulfhydryl content. NAC thiol group is nucleophilic and easily oxidized, resulting in dimer formation, interfering with Elman's reagent detection [79, 105]. It can be spotted that across time, fluctuations in

release percentage is obvious as a result of increasing NAC concentration in PBS with time, increasing the tendency of dimer formation. Thus, a decline in the release percentage is seen using Ellman's reagent detection technique. For such reason new NPs were formulated using another model drug; FL.

3.2. Determination of drug release profile from FL-loaded NPs in the absence of magnetic field:

When NAC was substituted by FL, the problem of complicated drug quantification was solved giving an improved release profile for free FL (control), FL-loaded CS NPs and FL-loaded CS-MNPs. It is quite obvious from the chart (**Figure 22**) that encapsulation of FL into chitosan NPs retarded their release with only 5 % and 25 % of encapsulated FL released after 168 hours from CS NPs and CS-MNPs respectively compared to the control that provided 100 % release during the same period. A sustained drug release profile is very desirable since it allows for continuous exposure of cancer cells to drugs [106]. Release of surface adsorbed drug, diffusion of drug through a swollen rubbery matrix and release of drug upon surface erosion are the usual release mechanisms followed by polymeric particulate systems. Either one mechanism or more are followed [39, 107]. By visualizing the obtained chart, for CS-NPs both mechanisms seem to exist; an initial burst of FL is seen where 2 % is released in 1 hour followed by a slow, steady increase in the percent of FL released from NPs. For CS-MNPs the initial burst is absent indicating a lower prevalence of surface adsorbed drug.

The percentage of FL released from CS-MNPs was significantly higher than that of CS NPs. This was believed to be due to increased CS hydrogel porosity size as a result of multi-core MNPs, the latter might be attributed to the interaction of MNP hydroxyls with chitosan amines, making them less available for TPP binding and accordingly yielding NPs with looser crosslinking and wider pores [99]. This contradicts the conclusion drawn by recent studies (Alexandre T Paulino, 2011 and Feng Xu, 2012) [108-109], however the size of FL-loaded NPs showed a significant increase from 60 to 122 nm with MNPs incorporation, this suggests that encapsulation of MNPs affected CS NPs crosslinking. As a consequence the pore size of NP may have enlarged too resulting in faster release of FL from CS-MNPs.

3.3. Determination of MNPs effect on drug release upon the application of magnetic field:

In preliminary experiments all samples showed a slow increase of the temperature after AMF exposure, resulting in an average temperature of 32 – 34 °C. This raise in temperature is mainly due to joule heating of the electrolyte solution [110]. Thus, the release profiles of FL-loaded CS NPs and FL-loaded CS-MNPs were compared among each other, and to those unexposed to HFMF, but maintained at constant temperature of 32°C. **Figure 23a** represents the logarithmic presentation for FL-loaded CS NPs, in which there is no significant difference in FL release upon the absence or presence of HFMF treatment is obvious. However, for FL-loaded CS-MNPs the logarithmic presentation (**Figure 23b**) showed that there is clear impact of the HFMF irradiation. The release of FL was faster under field influence. This was confirmed by calculated time constants (τ) (**Figure 24**) for both samples (FL-loaded CS NPs and CS-MNPs) and treatments (with and without HFMF) in which FL release was accelerated under field influence by a factor of 1.7, well beyond the experimental error. This indicates that MNPs played a role in accelerating drug release successfully. It can be explained as a result of magnetically induced stress where the oscillatory movement of MNPs within the CS NPs upon the application of an oscillating magnetic field resulted in the expansion of polymer chains; accelerating FL release [111-113]. At the same time, it is verified that the sample temperature is ~ 32 °C in all performed experiments, thus ruling out a global thermal effect. thus, from this experiment, it can be determined that incorporation of MNPs will help in obtaining bolus release of drug; desired release profile for cancer treatment [9]. In addition, tailoring drug delivery will be possible for each patient by controlling drug release with magnetic field.

4. NP modification:

Cancer therapeutic device's effectiveness is measured by its ability to eliminate tumor without deteriorating healthy tissue. Thus, targeted delivery of chemotherapeutic drug is essential in the success of the therapeutic device. Targeting will aid in increasing the specificity and internalization of the therapy thus, enhancing its efficiency while lowering the associated serious side effects always experienced by cancer patients. NP systems offer the quality of specificity and delivery of chemotherapeutic drugs, however active targeting can enhance this quality with cellular internalization. Active targeting involves the external

conjugation of targeting moieties to nanoparticles as represented by **Figure 33** [114]. Knowing that 40-80% of non-small lung cancer (NSCLC) tissues overexpress epidermal growth factor receptor (EGFR), it proposed that the optimal targeting moieties for NSCLC will be either EGF or EGFR-antibody [114-115]. EGFR is a protein tyrosine kinase receptor from ErbB family that plays an essential role in signal transduction pathways that regulate key cellular functions such as proliferation and survival. Thus, targeting this receptor will be better using antibody as cell proliferation may be enhanced rather than inhibited by an free unbound or liberated EGF ligand [116].

For efficient active targeting, the use of EDC as a cross-linker was considered as the convenient method for the reason that both types of NPs (CS NPs and CS-MNPs) expose CS's amino groups [117]. Based on EDC's mechanism of action it will induce amide bond formation specifically binding activated carboxylic group of IgG-FITC to CS's amino group based on previously mentioned procedure. Since, the amount of IgG-FITC binding to NPs depend on number of amino groups, the concentration of tagged IgG-FITC differs for CS NPs and CS-MNPs as seen in **Chapter 3-section 4**. This suggests that CS content or available amines are lower in CS-MNPs than CS NPs. This supports the proposed hypothesis as to why drug loading of CS-MNPs was lower than that of CS NPs and FL release from CS-MNPs (in the absence of HFMF) is faster than with CS-NPs. For hypothesis confirmation, further quantification of CS yield can be performed in the future.

5. NP-cell interaction:

NP uptake begins with the initial adsorption of the NPs on to the cell membrane. This is followed by mostly an energy-dependent uptake process, which allows the NPs to be internalized into the cell and further trafficked to different subcellular locations [118]. Several studies have been conducted to determine the rate and extent of NP internalization into cells and its dependency on NP size, physicochemical properties and concentration [119-121] as well as the mechanisms involved in such process [119, 121-125]. Established techniques involve inductively coupled plasma (ICP) spectroscopies such as ICP mass spectrometry, fluorescence activated cell sorting/scanning (FACS), and methods employing fluorometric analysis of intact or lysed cells [126].

5.1. MTT assay:

The effect of synthesized nanoparticles on cell viability and proliferation is an essential study of cellular response to external factors. A widely accepted and reliable method to examine cell proliferation is via tetrazolium salts reduction. Metabolically active cells reduce yellow tetrazolium MTT into purple formazan. These formazan crystals are found intracellularly and can be released and solubilized by the addition of DMSO. The solubilized formazan is then quantified spectrophotometrically. For dead cells the absorbance of formazan will be lower than that for viable cells. Thus, the linear relationship between signal produced and cell number for each cell type is established. Therefore, an accurate quantification of changes in the rate of cell proliferation was allowed [127].

Figure 26 shows that CS NPs have a significant cytotoxic effect on lung cancer cells at concentration 2000 $\mu\text{g/ml}$ where cell viability reached $\sim 70\%$; while at the same concentration fibroblast viability was $\sim 90\%$. This proves that CS NPs specifically possess cytotoxicity towards cancer cells and that they are biocompatible and non-toxic for normal cells [128-132]. This is due to that cancer cells possess highly negative surface in contrast to normal cells, thus accordingly increased cell membrane binding and uptake from cationic NPs for cancer cells will be visualized [126, 133]. MNPs showed to possess significant cytotoxicity at concentration of 200 $\mu\text{g/ml}$ for both cell types. As mentioned by Caixia Fan (2011), this could be due to DNA damage, lipid and protein peroxidation, induced by reactive oxygen species developed as a result of free iron ions release [134]. However, this is not considered as a threat since sufficient cellular uptake was obtained at lower MNPs concentrations. Their cytotoxicity has additionally been evidently lowered through CS encapsulation. Therefore, the possibility of using the obtained formulation (CS-MNPs) for targeted delivery of chemotherapeutic drugs in-vivo is strongly supported since naked MNPs are not the intended therapeutic formulation.

5.2. Extent of NP uptake determination; effect of NP:

The extent of NP uptake in A549 lung cancer cells was studied as a function of NP concentration and Ab modification. Based on the Ab's structure presented in **Figure 34** it was important to perform EGFR-Ab-NP linkage at Fc region of the Ab, to ensure high cancer tissue specificity and minimal uptake of NPs by normal tissues; leaving the antigen-

binding site (Fab region) free for EGFR interaction in cellular uptake. This was achieved through following the tagging methodology mentioned above in **Chapter 2-section 2.4.1**. Tagging Ab through Fc region was conducted by several studies [135-136]. Trials such as (Sarbari Acharya, 2009 and Petra Kocbek, 2007) [137-138] involved crosslinking between Abs' amino groups and NPs carboxylic groups risking interference with Ab active binding site [138-139].

Figure 27 shows that increasing the NPs concentration added, increases NPs concentration uptaken significantly for both CS NPs and CS-MNPs whether non-tagged or tagged with Ab. However, the uptake of non-tagged NPs is significantly higher than corresponding tagged NPs. The incorporation of Ab reduced the uptake of CS NPs by 0.4 and 0.7 folds for concentrations 150 and 250 $\mu\text{g/ml}$; respectively. As for CS-MNPs the incorporation of Ab reduced uptake by 0.5 folds for both concentrations. This could be a consequence of increased NPs size via high molecular weight Ab; from 60 to 122 nm and from 122 to 255 nm for FL-loaded CS NPs and CS-MNPs; respectively. Abs are large molecules, increase in NP's size with Ab tagging has been repeatedly reported [135, 140-141]. In addition to size increase, a change in the nature of protein corona formed around the NPs due to presence of Ab, might be limiting cellular uptake of NPs [142-144] since the nature of adsorbed serum proteins depends greatly on the NP surface chemistry [145]. Single chain EGFR-Abs fragments (known as single chain variable fragment, scFv) are of size range 25 to 28 kDa that is 80 % smaller in size from intact Abs (150 kDa). They usually consist of light and heavy chain variable domains joined with peptide linker. Thus, maintaining high binding affinity and cancer cell specificity [146]. scFv are highly recommended for future NPs targeting because not only is the NP uptake enhanced as a result of their low molecular weight, small size and high specificity in cancer cells targeting (due to absence of Fc region), but they are also of lower cost than whole antibodies [115, 147-148]. Furthermore, significantly higher cellular uptake was attained by CS NPs in comparison to CS-MNPs. Cellular uptake of NPs are affected by several factors including: NPs size, charge, and concentration. Since they are both positively charged, then the uptake difference can be attributed to CS-MNPs size enlargement as a result of MNPs incorporation [149-151].

To further confirm unmodified NP uptake, CLSM was used (**Figure 28**). The control cells, in absence of NPs show WGA labelling (red) of their cell membranes. (**Figure 28a**). As seen by **Figure 28b** NPs have escaped lysosome encapsulation preferentially exhibiting perinuclear co-localization as expected which is essential for the delivery of anti-cancer therapeutics [149, 151-152]. WGA-AF is a cationic dye with high affinity to sialic acid and N-acetylglucosaminyl residue therefore, used to label cell membranes [153-154]. However, in the presence of chitosan, WGA preferentially labels chitosan NPs[126]. Since fixation was performed with ice cold methanol, cells were also permeabilized enabling the WGA-AF to go into the cell and label CS NPs present intracellularly (**Figure 28c**) [126]. Thus, in **Figure 28c** in the presence of WGA only labels CS NPs showing a rather different pattern than that seen in **Figure 28(a)**. It is quite important to note that green fluorescence from FL-loaded NPs seems to completely co-localize with WGA red fluorescence indicating that green dots seen are actually internalized NPs rather than noise.

5.3. Efficiency of Cisplatin-loaded NPs via MTT assay:

Figure 29 shows lower cytotoxicity of cisplatin loaded in NPs in comparison to free cisplatin of the same concentrations. This can be owed to sustained release profile characteristic for hydrogel NPs where small concentrations were released. Despite equivalent amount of cisplatin that should have been released after 24 hr from each NP represented cytotoxic effect, release of cisplatin from NPs within the cell could be actually quite different than the in-vitro release experiment. In-vitro experiments are generally conducted to prove the ability of formulation to release the drug, however actual release profiles are not exact replica due to different condition in the cell that could have not been simulated in in-vitro experiment.

6. SFD and evaluation of Lung deposition by NGI:

6.1. Incorporation of NPs in PVP: MD MPs:

SFD technique is used for the development of uniformly sized microparticles. This technique is favored in contrast to most commonly used techniques; dry powder coating, oppositely charge NPs flocculation, spray drying fluidized bed granulation and spray drying as it does not expose the drug to harsh synthetic procedures that may adversely affect its therapeutic efficiency [155]. In **Figure 30**, the SEM images of both CS NPs and CS-MNPs

show that both of them are spherical in shape with nearly the same size of approximately 3 μm . Obtaining microparticles of the same size was due to the SFD technique itself, since size of particles depend mainly on the size of the nozzle from which droplets are released and less on the initial size of the particle [156-157].

6.2. Evaluation of aerodynamic properties of MPs using NGI:

NPs represented different MMAD values. A possible reason for the higher MMAD for CS-MNPs is the higher density imposed by the MNPs, since MMAD is greatly affected by density [158]. Particle deposition is a function of its AD. Particles with ADs $> 5\mu\text{m}$ deposit mainly in the large airways and oropharynx by inertial impaction, where they will be probably cleared via mucociliary clearance rather than reaching the lung [32]. Particles with ADs ranging from 1-5 μm deposit by gravitational sedimentation and diffusion deeper into the lungs [31-32, 34-35] making the formulated NPs suitable drug delivery candidates to the lung.

For both NPs, a very small amount seems to be retained in the capsule and similarly in the mouth as indicated by amount present in capsules and in mouth piece from the recovered dose in **Figure 31**. Approximately 37 % of the inhaled dose for both NPs was deposited in the trachea. However, ~50 % were deposited past the trachea where the majority of NSCLC occurs [159]. This ensures the minimum systemic delivery of drug due to lack of deposition of NPs in the alveolar region. Particles have also possessed fine particle fraction ($\text{FPF} \leq 5.2 \mu\text{m}$) of ~40 % indicating successful delivery to deep lung tissue.

Conclusions and Future Perspectives

In conclusion, lung cancer is the deadliest solid tumor among all types of cancer. The number of cases and deaths caused cancer is exponentially increasing by time. This is due to poor diagnosis and exposure of the largest surface area of the body to carcinogenic substance through inhalation route. Despite the development of various chemotherapeutic drug delivery platforms, still the optimum formulation has not been achieved. The optimum route of chemotherapeutic drug delivery was thought to be inhalation since it lacks systemic toxicity and invasiveness experienced by I.V. route as well as patient inconvenience with endobronchial route. The combination of initial spike dose of chemotherapy followed by sustained supply of the drug was thought to provide an efficient therapeutic platform for tumor eradication and recurrence prevention. Thus, based on these thoughts a non-invasive, patient convenient platform for the targeted delivery of chemotherapeutic drugs to cancer in deeper lung tissue was developed and studied. The formulation consisted of inhalable MD-based MPs obtained by SFD. These MPs were either encapsulating CS NPs loaded with MNPs and a chemotherapeutic drug or chemotherapeutic drug only. MNPs prepared were USPIOs of size 5 nm. They have enhanced drug release by 1.7 fold in response to external magnetic field. CS possessed sustained drug release profile in which only 5 and 25% of loaded FL were released in one week from CS NPs and CS-MNPs; respectively. CS NPs showed preferential toxicity to tumor cells (A549) in comparison to cultured fibroblasts (L929). Modification of CS NPs with Abs hindered their uptake by the cells in comparison to un-modified NPs due to enlargement of NPs size associated with Ab labeling. The prepared SFD powders had fine particle fraction ($FPF_{\leq 5.2 \mu m}$) of ~40 % w/w and MMAD of 5-6 μm as determined by the NGI. The targeted delivery to the lung cancer using the developed formulation seems to be a promising approach.

For future studies, release profile of NPs for cisplatin should be examined to determine whether release profile is dependent or independent on type of drug encapsulated. Application of bolus drug release using HFMF induction generator with cisplatin-loaded NPs in-vitro on lung cancer cells (A549) should be tested to study the effect of exposure to spike drug concentrations on cells. Imaging properties of MNPs should be determined for

diagnostic purposes. Targeted delivery of NPs using whole Abs versus Ab fragments should be studied and compared. The effect of cisplatin-loaded NPs (with and without magnetic field) on tumor growth inhibition and recurrence prevention in-vivo on tumor A549 cell tumor bearing mouse should be examined. Optimization of MNPs content for efficient bolus delivery of drug, MRI imaging and deep lung deposition (since AD depends on the particle's density) should be essentially evaluated. Stability of dry MPs powder and NPs should be studied to investigate the long-term effect on the stability of the biodegradable materials. Long-term effects of MNPs on animals should be tested to ensure minimized cytotoxicity in-vivo.

Tables

Table 1: Recently developed biodegradable NP/MP drug delivery platforms used in lung cancer targeting.

References	Formulation	Route of administration	Formulation Evaluation	Findings
Choi, S.H., et al [53]	Self-assembled DOX-conjugated albumin NPs containing apoptotic TRAIL proteins	Inhalation- Aerosolizer	<ul style="list-style-type: none"> - In-vitro H226 uptake of NPs - In-vivo uptake in an H226 cell tumor-bearing mouse model. 	<ul style="list-style-type: none"> - Synergistic anti-cancer efficacy in-vitro and in-vivo due to DOX and TRAIL. - New inhalable approach for treating resistant lung cancer.
Long, J.T., et al [54]	EGF-modified gelatin NPs (EGNP) loaded with DOX.	Inhalation - Nebulization	<ul style="list-style-type: none"> - In-vitro A549 and H226 uptake of NPs. - In-vivo uptake in an A549 cell tumor-bearing mouse model. 	<ul style="list-style-type: none"> - EGF-modified NPs possessed high targeting and cytotoxicity towards lung cancer cells in-vitro and in-vivo.
Kaminskas, L.M., et al	PEGylated dendrimers loaded	Intratracheal -Instillation	<ul style="list-style-type: none"> - In-vitro MAT 13762 IIIB uptake 	<ul style="list-style-type: none"> - Efficiently potent inhibitory of cell and tumor growth in-vitro and in-vivo.

[55]	with DOX.		of dendrimers. - In-vivo uptake in a MAT 13762 IIIB cell tumor-bearing mouse model.	
Guo, X., et al [56]	2-ME-loaded PLGA NPs coated with Chitosan	Inhalation- Dry powder	- In-vitro A549 and SPC-A1 uptake of NPs.	- Spray-freeze dried NPs possessed desirable inhalation properties (high fine particle fraction and rough surfaces). - Significantly high antitumor efficiency was achieved by proposed platform compared to free drug combination or drug-free NPs. - Deposition to deep lung tissue was achieved with absence of irritation.
Xu, H., et al [57]	Tet-loaded PVP-b-PCL NPs	Not mentioned	- In-vitro A549 uptake of NPs.	- Inhibition of cell growth, migration and invasion was enhanced through NPs in contrast to free Tet.
Sun, Q., et al [58]	Gelatin/DHA and HA/DHA NPs aggregates	Not mentioned	- In-vitro A549 uptake of NPs.	- Cancer cell death was significant after 2 days.
Zhao, T., et al [59]	(PTX-loaded (PGA-co-PCL)c-	Intratumoral	- In-vitro A549 uptake of NPs. - In-vivo uptake in an	- Drug release enhanced by the incorporation of hydrophilic PCL. - Tumor and cell growth were more effectively

	<i>b</i> -TPGS _{2k} NPs)		A-549 cell tumor-bearing mouse model.	inhibited by (PGA- <i>co</i> -PCL)- <i>b</i> -TPGS _{2k} NPs in comparison to free Taxol.
Shen, J., et al [60]	Hollow mesoporous silica nanospheres (HMSNs) encapsulating Bortezomib	I.V.	<ul style="list-style-type: none"> - In-vitro H1299 uptake of NPs. - In-vivo uptake in a H1299 cell tumor-bearing mouse model. 	<ul style="list-style-type: none"> - Tumor and cell growth were more effectively inhibited by Bortezomib-loaded HMSNs in comparison to free Bortezomib.
Lv, S., et al [61]	mPEsG- <i>b</i> -PLG- <i>b</i> -PLL/DOCA NPs encapsulating DOX and PTX	I.V.	<ul style="list-style-type: none"> - In-vitro A549 uptake of NPs. - In-vivo uptake in an A549 cell tumor-bearing mouse model. 	<ul style="list-style-type: none"> - Significantly high antitumor efficiency was achieved by Co-NPs platform compared to free drug combination or single drug-loaded NPs with absence of side effects.
Li, M., et al [62]	DOX-loaded CMC NPs + Endostar	I.V.	<ul style="list-style-type: none"> - In-vitro A549 uptake of NPs. - In-vivo uptake in an A-549 cell tumor-bearing mouse model. 	<ul style="list-style-type: none"> - Surface functionalized CMC NPs for stealth purpose were prepared by simple procedure. - High DOX loading. - Efficient delivery and inhibitory effect of NPs in-vitro and in-vivo. - Synergistic effect was achieved with co-administered endostar.

Maya, S., et al [63]	Chitosan cross-linked (γ -PGA) NPs loaded with DTXL and decorated with CET	Not mentioned	<ul style="list-style-type: none"> - In-vitro A549 uptake of NPs. 	<ul style="list-style-type: none"> - Enhanced cancer cell death by targeted NPs was determined by cytotoxicity assays as a result of DTXL selective delivery in comparison to non-targeted NPs and normal cell lines (NIH3T3).
Sadhukha, T., et al [64]	EGFR-targeted, SPIO NPs (\approx AD 1.1 μ m)	Inhalation-Aerosolizer	<ul style="list-style-type: none"> - In-vitro A549 uptake of NPs. - In-vivo uptake in Metastatic Lung Cancer Model in SCID-bg Mice. 	<ul style="list-style-type: none"> - EGFR-targeting enhances tumor retention of SPIO NPs. - Significant inhibitory effect to tumor growth in-vivo was achieved via magnetic hyperthermia. - Efficient therapeutic concentration was successfully delivered to the lung.
Nejati-Koshki, K., et al [65]	Cisplatin-loaded Fe ₃ O ₄ NPs modified with PLGA-PEG6000 copolymers	Not mentioned	<ul style="list-style-type: none"> - In-vitro A549 uptake of NPs. 	<ul style="list-style-type: none"> - Therapeutic potency was achieved in-vitro.
Karra, N., et al [66]	Antibody-tagged PLGA NPs loaded with PTX Palmitate	I.V.	<ul style="list-style-type: none"> - In-vitro A549-luc-C8 uptake of NPs. - In-vivo uptake in Metastatic Lung 	<ul style="list-style-type: none"> - Surface functionalized PLGA NPs for antibody tagging were developed through simple procedure. - Efficient targeting and cytotoxicity to lung cancer cells in vitro was achieved through antibody

			Cancer Model in SCID-bg Mice.	labeling. - In-vivo therapeutic potential and tolerability was experienced.
Yordanov, G., et al [67]	Epirubicin-loaded PBCA NPs	I.V.	- In-vitro A549 uptake of NPs.	- Drug loaded efficiently (60-70 %). - NPs possessed significant cytotoxicity towards lung cancer cells in comparison to free drug.
Meenach, S.A., et al [68]	PEGylated phospholipid MPs loaded with PTX	Inhalation-Dry powder	- Next Generation Impactor (NGI)	- Platform suitable for PTX delivery to the middle and deep regions of the lungs in a targeted fashion.
McBride, A.A., et al [69]	Lactose MPs loaded with SPIO NPs and DOX	Inhalation-Dry powder	- NGI	- Spray-freeze dried SPIONs with very high saturation magnetization had the potential to be targeted to specific regions of the lung using an external magnet.
Patel, A.R., et al [70]	Celecoxib encapsulated Nanolipidcarriers + I.V. DTXL	Inhalation-Aerosolizer	- In-vivo uptake in an A549 cell tumor-bearing mouse model.	- Significant inhibitory effect on tumour growth was achieved via aerosolized Cxb-NLCs due to increase in lung residence time. - Aerosolized Cxb-NLC enhanced the therapeutic activity of Doc.
Srinivasan, A.R., et al [71]	Self-associated bevacizumab NPs	Not mentioned	- In-vitro A549 uptake of NPs.	- NPs have shown to possess high targeting specificity towards lung cancer cells.

Yin, H., et al [72]	(mPEG)–PCL NPs encapsulating curcumin	Not mentioned	<ul style="list-style-type: none"> - In-vitro A549 uptake of NPs. 	<ul style="list-style-type: none"> - Cancer cell death was more efficient for curcumin-loaded (mPEG)–PCL NPs in comparison to free curcumin.
Wang, P., et al [73]	Curcumin-loaded SLPs	Oral or I.V.	<ul style="list-style-type: none"> - In-vitro A549 uptake of NPs. - In-vivo uptake in an A549 cell tumor-bearing mouse model. 	<ul style="list-style-type: none"> - Inhibited cell and tumor growth was achieved more efficiently for curcumin-loaded SLPs in comparison to free curcumin.
Garg, N.K., et al [74]	Gemcitabine loaded PEG-chitosan NPs tagged with NSCLS specific anisamide	I.V.	<ul style="list-style-type: none"> - In-vitro A549 uptake of NPs. - In-vivo uptake in an A549 cell tumor-bearing mouse model. 	<ul style="list-style-type: none"> - Efficient targeting and inhibitory effect of NPs in-vitro and in-vivo towards cell and tumor growth.
Karthikeyan, S., et al [75]	Resveratrol loaded gelatin NPs	I.V.	<ul style="list-style-type: none"> - In-vitro NCI-H460 cells uptake of NPs. - In-vivo uptake in a NCI-H460 cell tumor-bearing mouse model. 	<ul style="list-style-type: none"> - Anti-tumor activity is enhanced by NPs in comparison to free Resveratrol with reduced side effects.

Roa, W.H., et al [76]	DOX in PACA NPs embedded in effervescent and non-effervescent MPs (\approx AD 3.4 μ m)	Inhalation- Dry powder	- In-vivo uptake in a H460 cell tumor-bearing mouse model.	- The formulation has the desired characteristics for airway targeting. - Significant anti-tumor effect was achieved through inhalation versus I.V with reduced side effects.
Tseng, C.-L., et al [77]	Gelatin NPs tagged with NSCLS EGF.	Inhalation- Nebulization	- In-vivo uptake in an EGFR-overexpressing cell tumor-bearing mouse model.	- Aerosol droplets of a suitable MMAD were formed and showed enhanced deep lung tissue deposition. - Targeted delivery of NPs was achieved through EGF adsorption.
<p>Abbreviations: NPs: Nanoparticles, MPs: Microparticles, TRAIL: Tumor necrosis factor (TNF)-related apoptosis-inducing ligand, PACA: Poly alkylcyanoacrylate, DOX: Doxorubicin, EGF: Epidermal growth factor, PEG: Poly ethylene glycol, PBCA: Poly(butyl cyanoacrylate), PEITC: Phenethyl isothiocyanate, CDDP: Cisplatin, SPIO: Superparamagnetic Iron Oxide, MMAD: Mass Median Aerodynamic Diameter, 2-ME: 2-methoxyestradiol, PLGA: Poly(lactic-co-glycolic acid), MNPs: Magnetic nanoparticles, γ-PGA: γ-poly(glutamic acid), DTXL: Docetaxel, CET: Cetuximab, PTX: Paclitaxel, PCL: Poly-ϵ-caprolactone, TPGS2k: D-α-tocopheryl polyethylene glycol 2000 succinate, mPEG: Methoxy poly(ethylene glycol), Tet: Tetrandrine, PVP: Poly(N-vinylpyrrolidone), HA: Hyaluronan, DHA: Dihydroartemisinin, DOCA: Deoxycholate, PLL: Poly(l-lysine), SLP: Solid Lipid Nanoparticles, CMC: Carboxymethyl Cellulose.</p>				

Table 2: Opalescent NP formulations with varied parameters and their assessment using SEM.

Protocol no.	Details	Observation	Figure
F1	0.1% CS at pH 3 + 0.04% TPP at pH 8	Microparticles	12A
F2	0.1% CS at pH 4 + 0.04% TPP at pH 5	Aggregates	12B
F3	0.1% CS at pH 4 + 0.04% TPP at pH 8		12C
F4	0.1% CS at pH 5 + 0.04% TPP at pH 8		12D
F5	0.3% CS at pH 3 + 0.04% TPP at pH 8		12E
F6	0.5% CS at pH 3 + 0.04% TPP at pH 5		12F
F7	0.5% CS at pH 3 + 0.04% TPP at pH 8		12G
F8	0.5% CS at pH 4 + 0.04% TPP at pH 5		12H
F9	0.1% CS at pH 5 + 0.04% TPP at pH 5		Small nanoparticles
F10	0.1% CS at pH 5 + 0.08% TPP at pH 5	12J	
F11	0.1% CS at pH 5 + 0.1% TPP at pH 5	12K	

Table 3: Further analysis of NPs (formulas 9-11) using DLS.

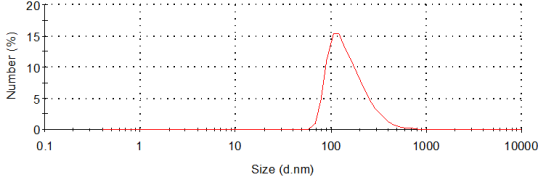
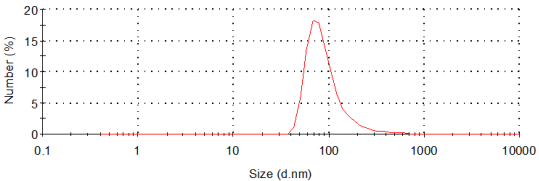
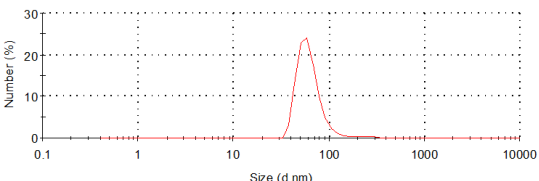
Protocol No.	Mean Size (nm)	DLS Chart (Size Distribution by Number)
9	160	 <p>A DLS chart for Protocol No. 9. The y-axis is labeled 'Number (%)' and ranges from 0 to 20 with major ticks every 5 units. The x-axis is labeled 'Size (d.nm)' and is on a logarithmic scale from 0.1 to 10000 with major ticks at 0.1, 1, 10, 100, 1000, and 10000. A single red peak is centered at 160 nm, reaching a maximum height of approximately 16%.</p>
10	97	 <p>A DLS chart for Protocol No. 10. The y-axis is labeled 'Number (%)' and ranges from 0 to 20 with major ticks every 5 units. The x-axis is labeled 'Size (d.nm)' and is on a logarithmic scale from 0.1 to 10000 with major ticks at 0.1, 1, 10, 100, 1000, and 10000. A single red peak is centered at 97 nm, reaching a maximum height of approximately 18%.</p>
11	65	 <p>A DLS chart for Protocol No. 11. The y-axis is labeled 'Number (%)' and ranges from 0 to 30 with major ticks every 10 units. The x-axis is labeled 'Size (d.nm)' and is on a logarithmic scale from 0.1 to 10000 with major ticks at 0.1, 1, 10, 100, 1000, and 10000. A single red peak is centered at 65 nm, reaching a maximum height of approximately 25%.</p>

Table 4: Various formulations for MNPs synthesized with varied parameters that were attracted by externally applied magnet.

Protocol no.	Details
F1	0.1 M FeCl ₃ .6H ₂ O + 0.45 M NaHCO ₃ + 0.0167 M Vit C Autoclave at 150°C for 4 hrs.
F2	0.1 M FeCl ₃ .6H ₂ O + 0.45 M NaHCO ₃ + 0.6 M Vit C Autoclave at 150°C for 4 hrs.
F3	0.1 M FeCl ₃ .6H ₂ O + 0.45 M NaHCO ₃ + 0.1 M Vit C Autoclave at 150°C for 4 hrs.
F4	0.1 M FeCl ₃ .6H ₂ O + 0.45 M NaHCO ₃ + 0.1 M Vit C Autoclave at 200°C for 6 hrs.
F5	0.3 M FeCl ₃ .6H ₂ O + 0.45 M NaHCO ₃ + 1.8 M Vit C Autoclave at 150°C for 4 hrs.
F6	0.3 M FeCl ₃ .6H ₂ O + 0.45 M NaHCO ₃ + 1.8 M Vit C Autoclave at 200°C for 6 hrs.
F7	0.3 M FeCl ₃ .6H ₂ O + 0.45 M NaHCO ₃ + 0.3 M Vit C Autoclave at 150°C for 4 hrs.
F8	0.3 M FeCl ₃ .6H ₂ O + 0.45 M NaHCO ₃ + 0.3 M Vit C Autoclave at 200°C for 6 hrs.
F9	0.3 M FeCl ₃ .6H ₂ O + 0.45 M NaHCO ₃ + 0.15 M Vit C Autoclave at 200°C for 6 hrs.

Table 5: Mean size and potential for different MNPs formulations.

Protocol no.	Details	Mean size (nm)	Mean potential (mV)
F1	0.1 M FeCl ₃ .6H ₂ O + 0.45 M NaHCO ₃ + 0.0167 M Vit. C Autoclave at 150°C for 4 hrs.	1266	-15.2
F2	0.1 M FeCl ₃ .6H ₂ O + 0.45 M NaHCO ₃ + 0.6 M Vit. C Autoclave at 150°C for 4 hrs.	45.7	-2.04
F3	0.1 M FeCl ₃ .6H ₂ O + 0.45 M NaHCO ₃ + 0.1 M Vit. C Autoclave at 150°C for 4 hrs.	61.04	-3.14
F4	0.1 M FeCl ₃ .6H ₂ O + 0.45 M NaHCO ₃ + 0.1 M Vit. C Autoclave at 200°C for 6 hrs.	2337	-0.08
F5	0.3 M FeCl ₃ .6H ₂ O + 0.45 M NaHCO ₃ + 1.8 M Vit. C Autoclave at 150°C for 4 hrs.	54.6	-1.28
F6	0.3 M FeCl ₃ .6H ₂ O + 0.45 M NaHCO ₃ + 1.8 M Vit. C Autoclave at 200°C for 6 hrs.	113.6	-4.23
F7	0.3 M FeCl ₃ .6H ₂ O + 0.45 M NaHCO ₃ + 0.3 M Vit. C Autoclave at 150°C for 4 hrs.	616.8	-5.04
F8	0.3 M FeCl ₃ .6H ₂ O + 0.45 M NaHCO ₃ + 0.3 M Vit. C Autoclave at 200°C for 6 hrs.	30.6	-29.9
F9	0.3 M FeCl ₃ .6H ₂ O + 0.45 M NaHCO ₃ + 0.15 M Vit. C Autoclave at 200°C for 6 hrs.	30.99	-0.83

Table 6: Different Concentrations of AC with their corresponding CS NPs EE %.

Concentration (mg/ml)	Samples	Entrapped Concentration (mg/ml)	Mean \pm S.D
7	1	3.22	2.9 \pm 0.5
	1'	2.51	
10	2	4.06	4.1 \pm 0.1
	2'	4.19	
12	3	4.69	5.6 \pm 1.2
	3'	6.42	

Table 7: EE% and size comparison between the developed formula and same formulas in different studies.

Drug	EE%	NP size	Ref.
N-acetylcysteine	41.3±0.9	63 ± 3 nm	Our Formula
Dextran-Doxorubicin complex	60-65	100±10 nm	[102]
5-fluorouracil	69.69±0.3	243±18 nm	[103]
	31.23±0.9	87±1 nm	
	29.98±0.8	69±1 nm	
Levofloxacin	24.91	140 nm	[104]

Figures

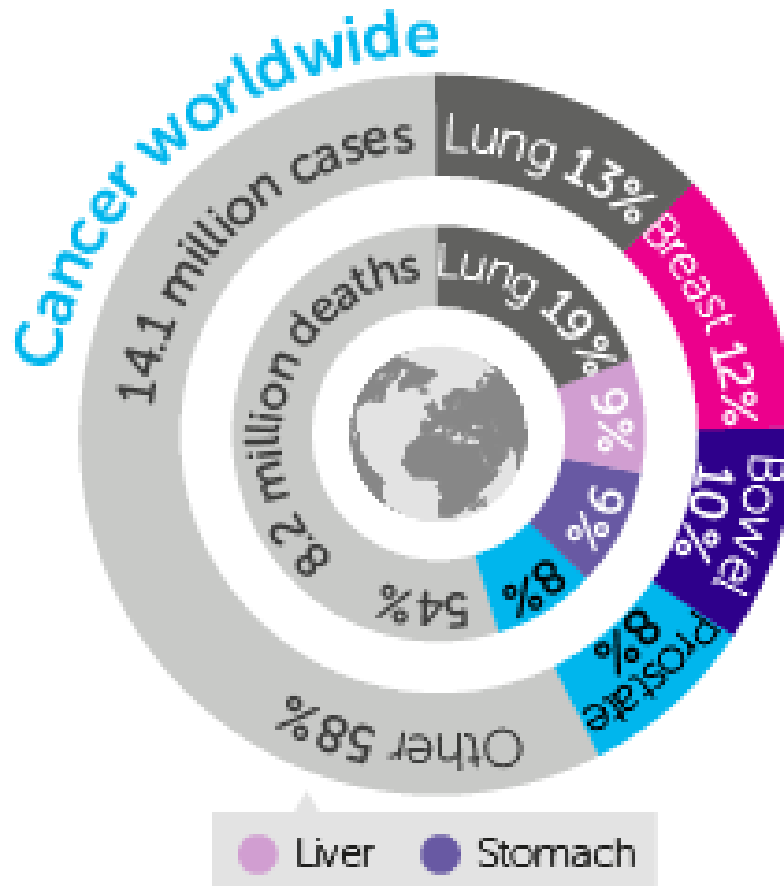


Figure 1: Cancer Worldwide- International Agency for Research on Cancer and Cancer Research UK. World Cancer Factsheet. Cancer Research UK, London, 2014.

Stage	Primary Tumor (T)	Regional Lymph Nodes (N)	Distant Metastasis (M)
IA	T1	N0	M0
IB	T2	N0	M0
IIA	T1	N1	M0
IIB	T2	N1	M0
IIIA	T3	N1	M0
	T1	N2	M0
	T2	N2	M0
	T3	N2	M0
IIIB	T4	N0	M0
	T4	N1	M0
	T4	N2	M0
	T1	N3	M0
	T2	N3	M0
	T3	N3	M0
	T4	N3	M0
IV	Any	Any	M1

Figure 2: TNM staging for NSCLC- “T1= ≤3 cm in greatest dimension; T2= 3 cm in greatest dimension; T3 = any size with invasion of the chest wall, diaphragm, mediastinal pleura or parietal pericardium, or a tumor in the main bronchus (<2 cm distal to the carina) but without involvement in the carina, associated atelectasis or obstructive pneumonitis of the entire lung; T4 = any size with invasion of the mediastinum, heart, great vessels, trachea, esophagus, vertebral body or carina, or tumor with a malignant pleural or pericardial effusion, or with satellite tumor nodule(s) within the ipsilateral primary tumor lobe of the lung; N0 = no regional lymph node metastasis; N1= metastasis to ipsilateral peribronchial and/or ipsilateral hilar lymph nodes, and intrapulmonary nodes involved by direct extension of the primary tumor; N2 = metastasis to ipsilateral mediastinal and/or subcarinal lymph nodes(s); N3= metastasis to contralateral mediastinal, contralateral hilar, ipsilateral or contralateral scalene, or supraclavicular lymph node(s); M0 = no distant metastasis; M1= distant metastasis present”- Carbone, D.P. and E. Felip, *Adjuvant therapy in non-small cell lung cancer: future treatment prospects and paradigms*. Clin Lung Cancer, 2011. 12(5): p. 261-71

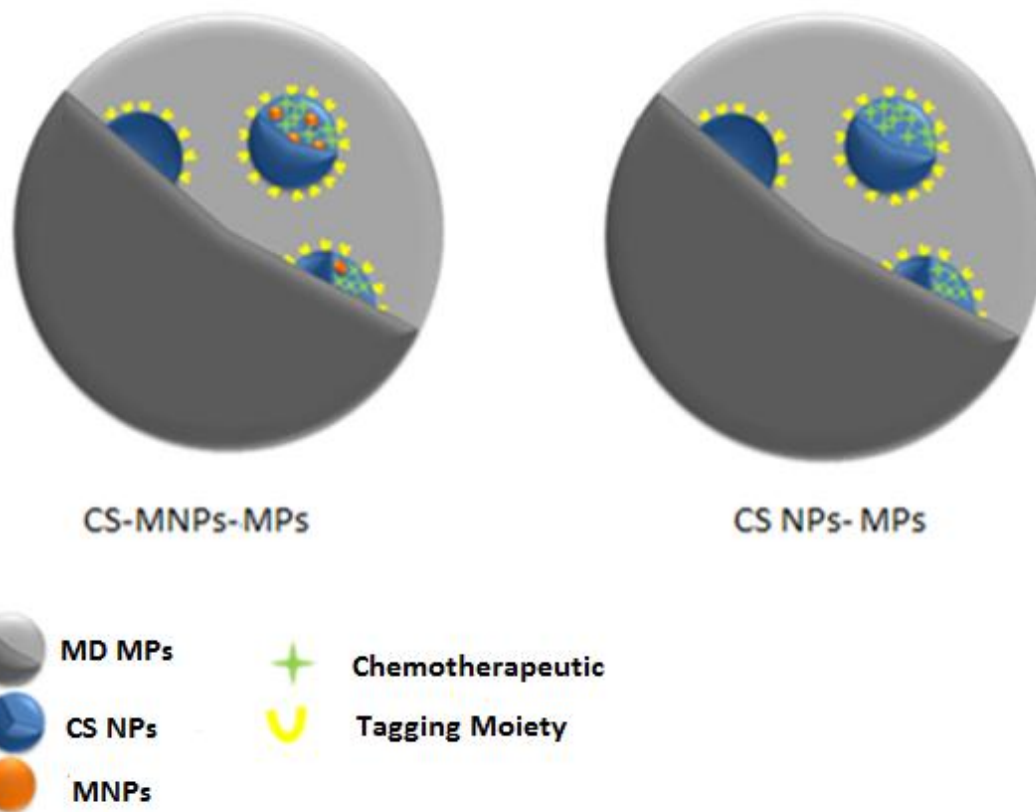


Figure 3: Nanoparticles embedded in microparticles (NEMs) for airway tumor delivery- CS NPs encapsulating MNPs and chemotherapeutic drug and CS NPs encapsulating chemotherapeutic drug only tagged with tagging moiety are encapsulated separately in MPs.

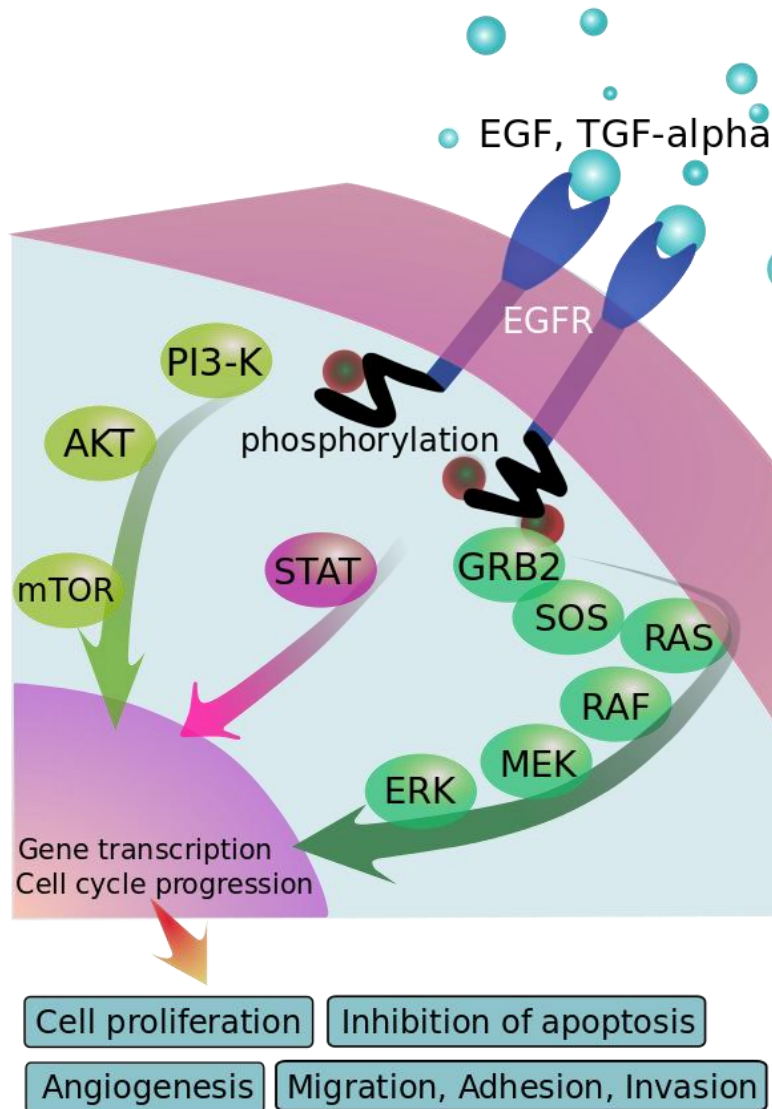


Figure 4: Role of EGFR in cell growth and division- Growth ligands such as epidermal growth factor (EGF) and tumor growth factor alpha (TGF α) bind to EGFR inducing signaling cascades within the cell to promote cell division and growth- Retrieved from www.en.wikipedia.org, January, 2015.

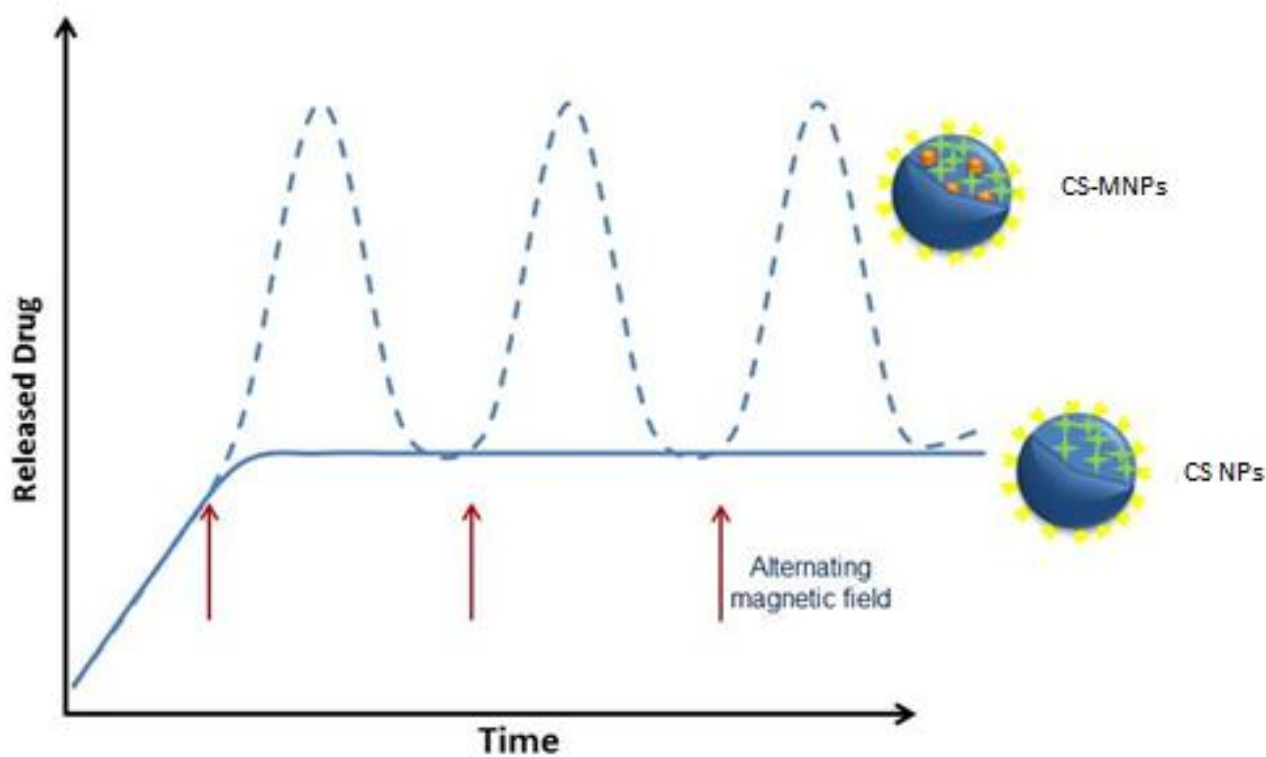
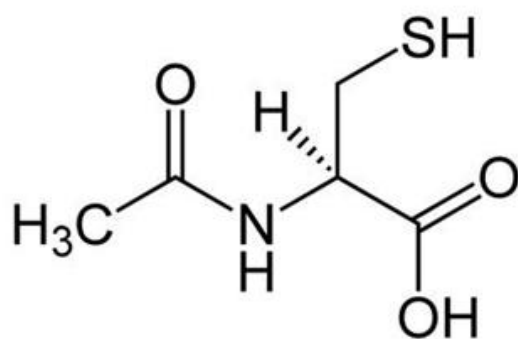


Figure 5: Desirable release profile of chemotherapeutic drug from proposed formulation- Spike doses of chemotherapeutic drug are released from CS-MNPs upon alternating HFMF application as a stimulus to which MNPs respond, followed by sustained supply of chemotherapeutic drug from CS NPs.

(a)



(b)

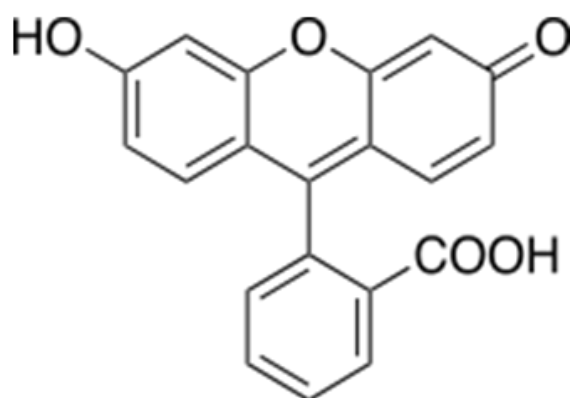


Figure 6: Model Drugs: (a) N-acetyl cysteine (NAC) and (b) Fluorescein (FL) –

Retrieved from www.wikimedia.org, June, 2014.

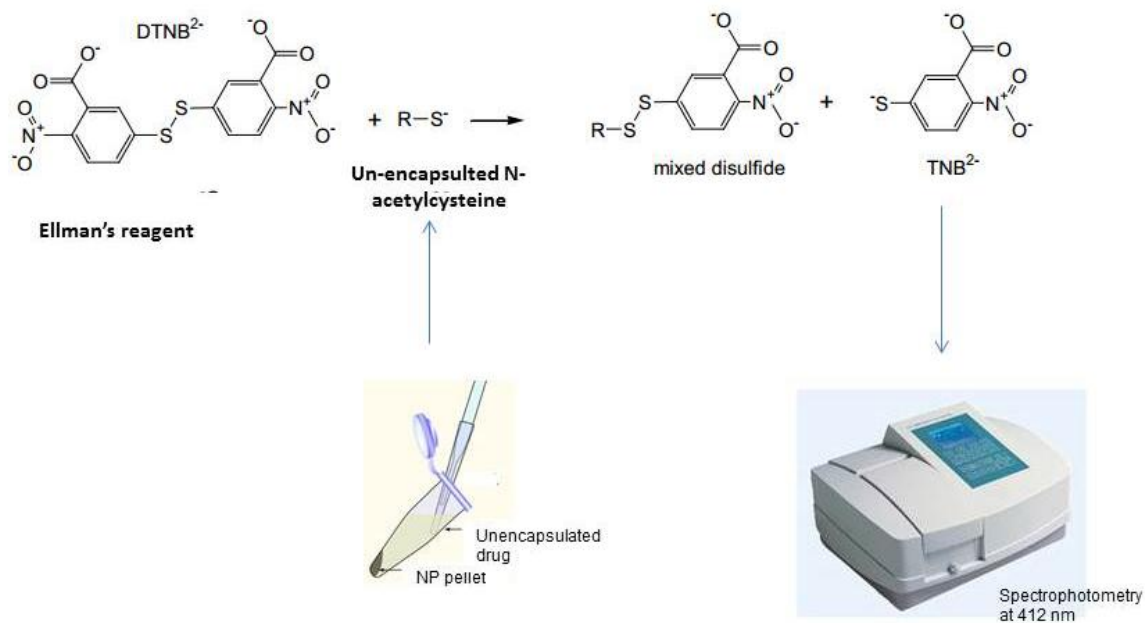


Figure 7: Indirect determination of N-acetyl cysteine (NAC) using Ellman's reagent- Ellman's reagent reacts with free sulfhydryl group of NAC to produce dimer molecule and nitro-thiobenzoic acid that can be detected spectrophotometrically in the visible range. The absorbance of nitro-thiobenzoic acid is proportional to NAC concentration.

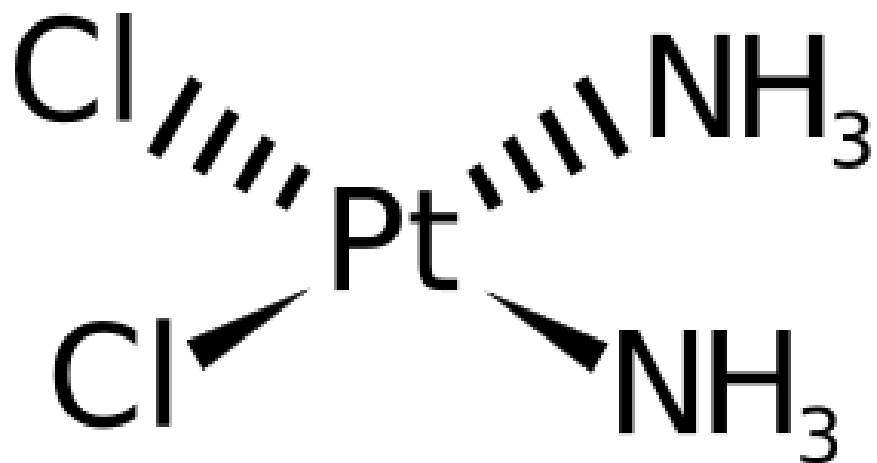


Figure 8: Cisplatin- Retrieved from www.wikimedia.org, December, 2014.

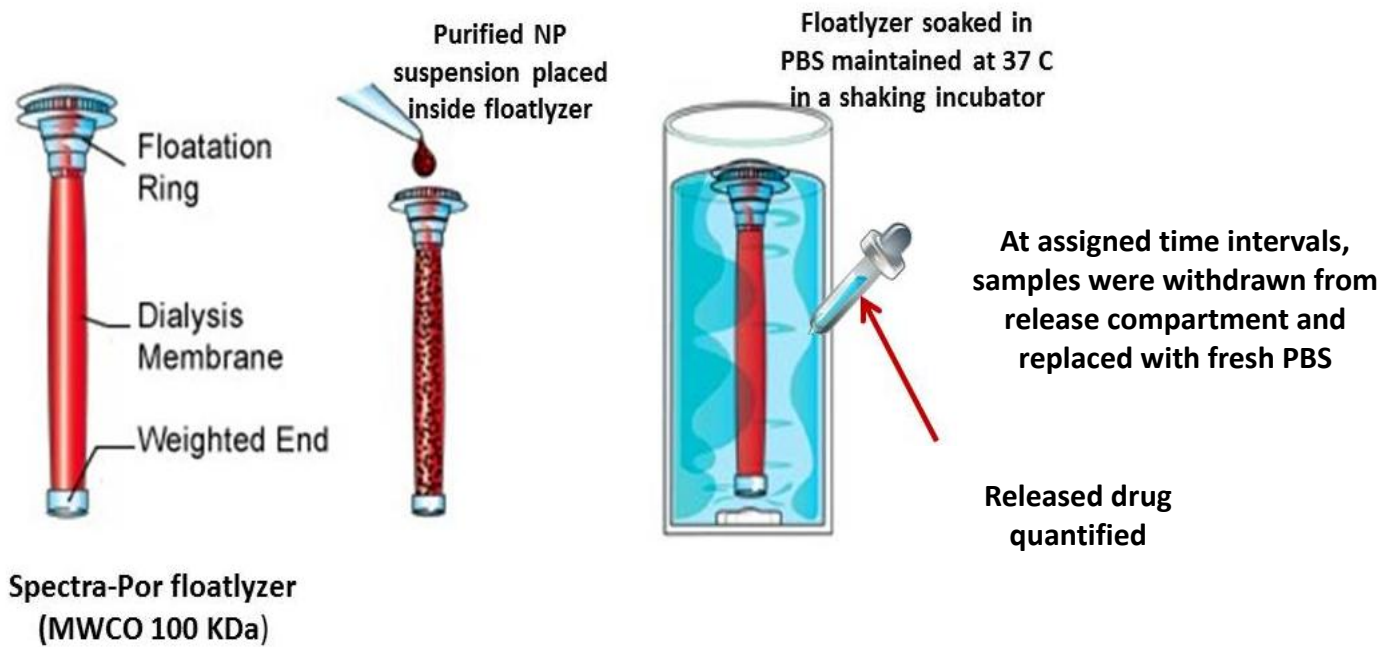


Figure 9: Drug release profile determination from Drug-loaded NPs- Experimental Design in which purified NPs are placed in the dialysis membrane of the float-a-lyzer which is then placed in PBS-containing compartment that is eventually placed in a shaking incubator at 37°C. At specified time intervals aliquots from PBS are taken where drug was released to be quantified.

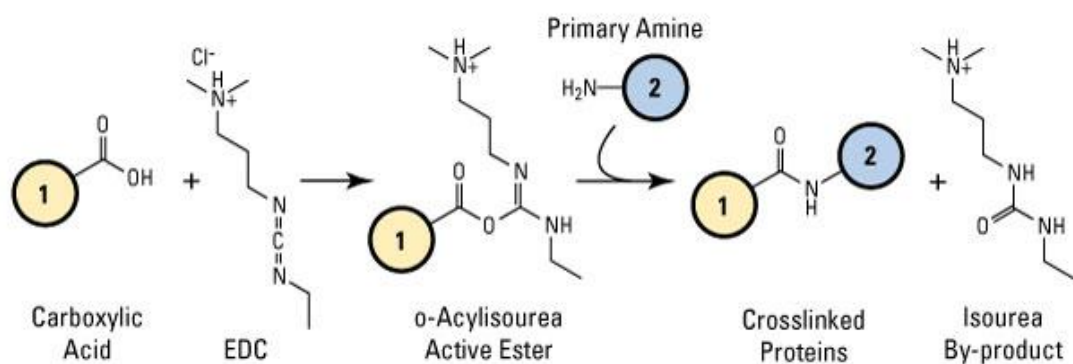


Figure 10: EDC (carbodiimide) cross-linking reaction scheme- EDC will work by activating carboxylic group of Ab forming active ester which upon NPs addition will allow the formation of amide bond between the carboxylic group of Ab and amino group of NPs- Hayworth, D. *Carbodiimide Crosslinker Chemistry*. Retrieved, August 2014.

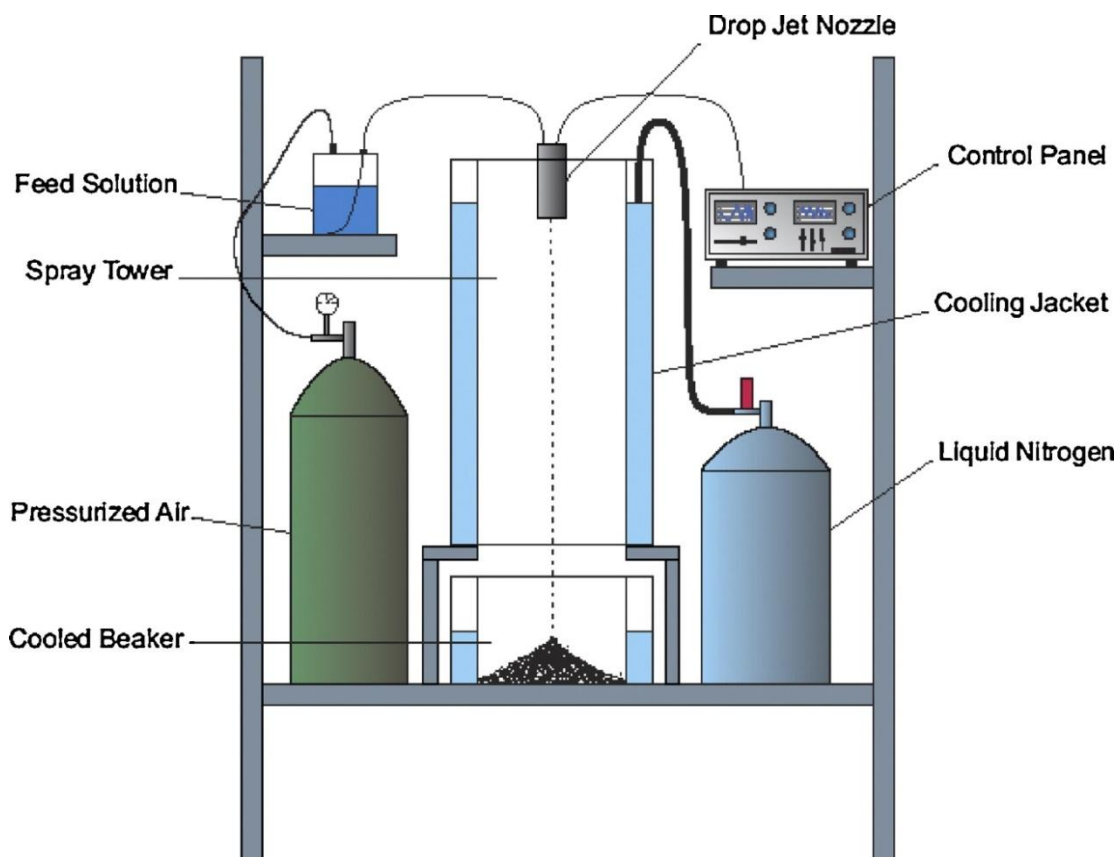


Figure 11: Spray Freeze Drying (SFD) apparatus [80]- CS NPs and CS-MNPs placed in PVP:MD solution are fed by pressurized air through 2-fluid nozzle into spray tower cooled by liquid nitrogen-containing jacket covering the spray tower. MPs formed are then collected at the end of the spray tower in a cooled beaker which will then undergo lyophilization.

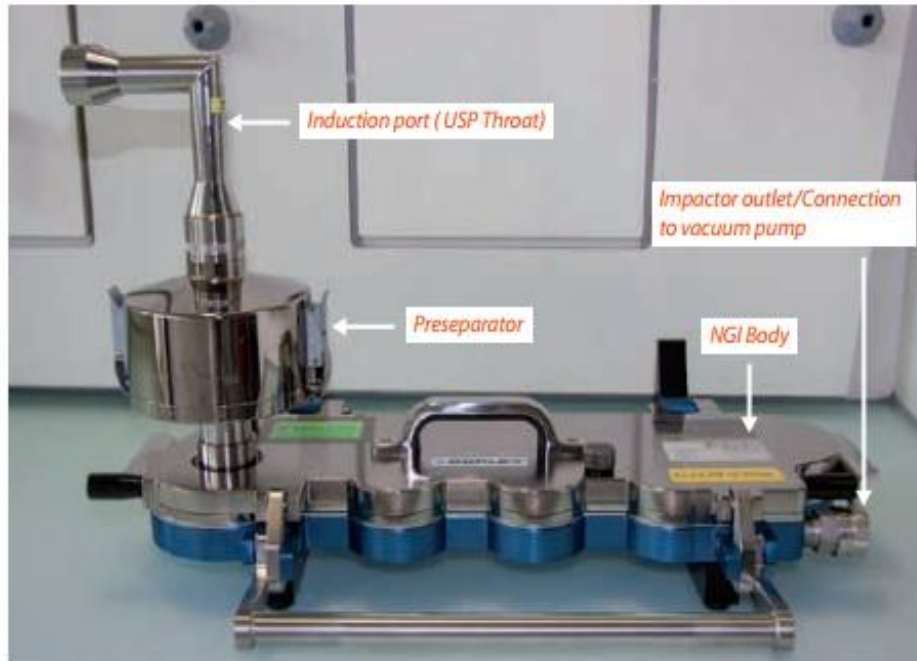


Figure 12: NGI Assembly (Induction port, Preseparator, Stages 1-7 and MOC) – Dry Powder will be moving from DPI placed at the mouth adaptor along the whole apparatus from the left to the right when vacuum is turned on. Particles will then deposit in different compartments of the NGI based on the AD cutoffs- Retrieved from www.solvias.com/sites/default/files/solvias_prospects_02_2012_web.pdf, December, 2014.

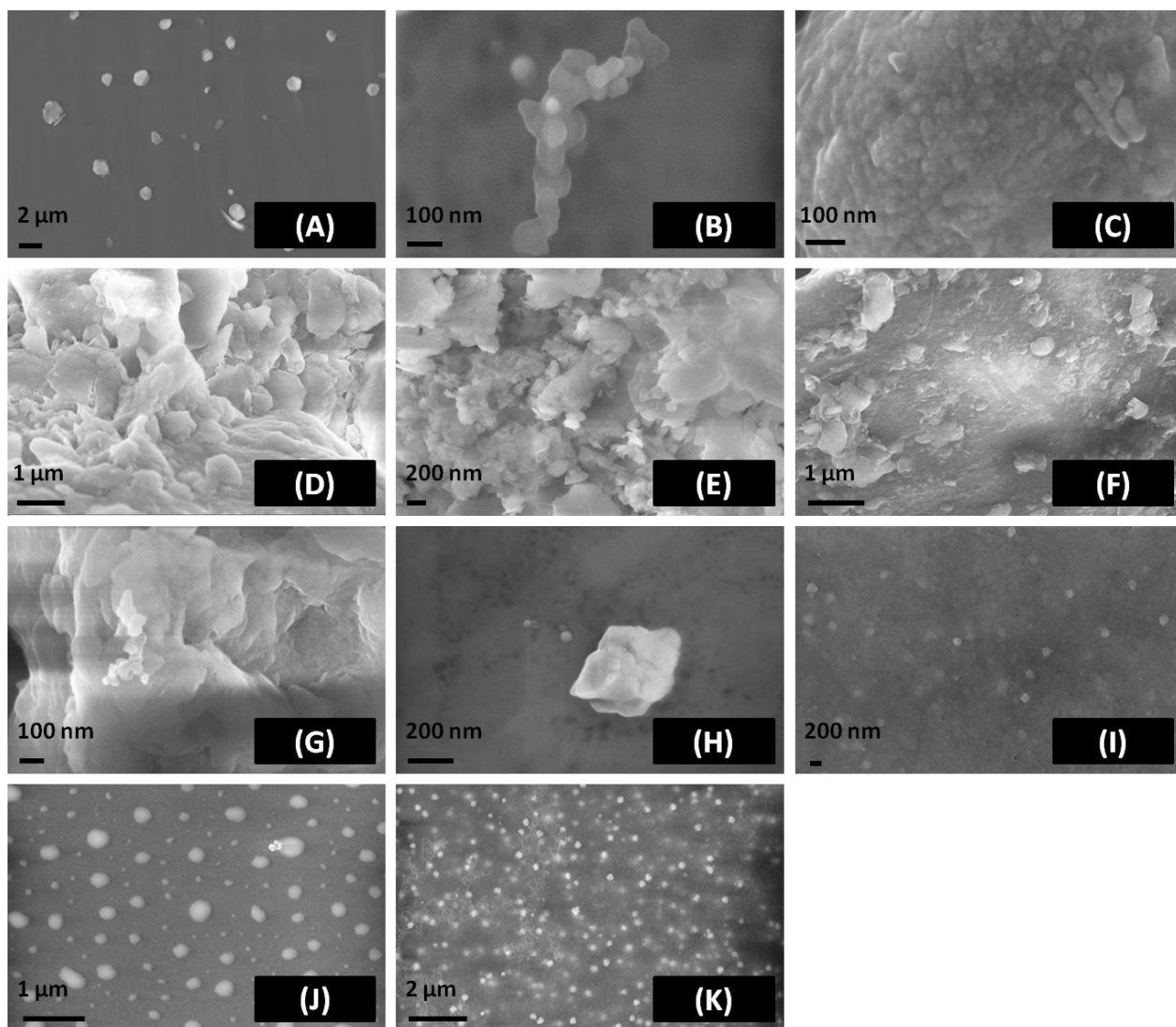


Figure 13: Initial assessment of formulated NPs using SEM (Magnifications: 12.34, 349.97, 372.49, 48.54, 71.86, 52.20, 243.21, 223.80, 67.52, 46.92 and 29.08 K X for A, B, C, D, E, F, G, H, I, J and K respectively)- Microparticles, aggregates and small-sized NPs are formed.

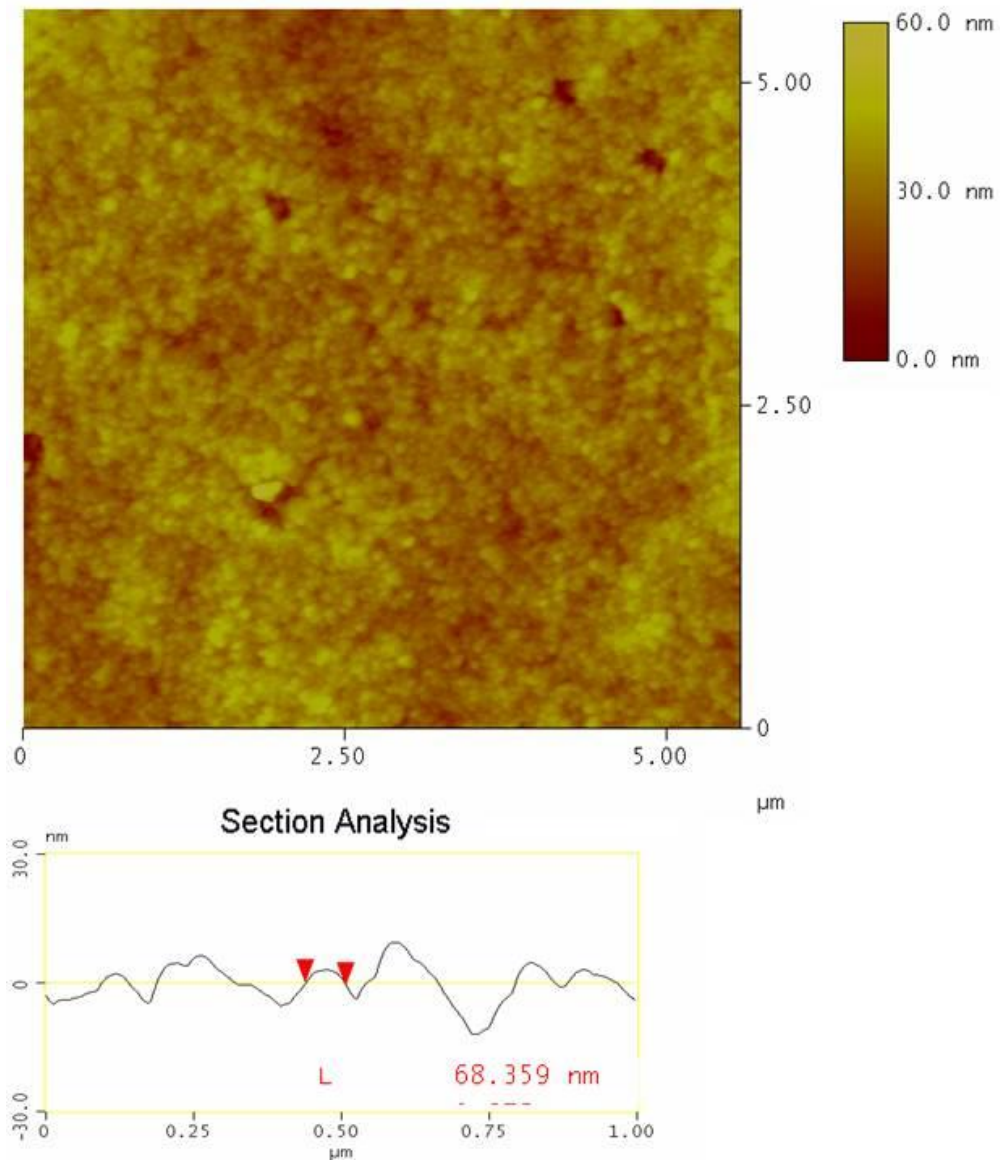


Figure 14: AFM analysis for formula 11 (CS NPs)- NPs size are determined by height and lateral dimensions measurement using AFM.

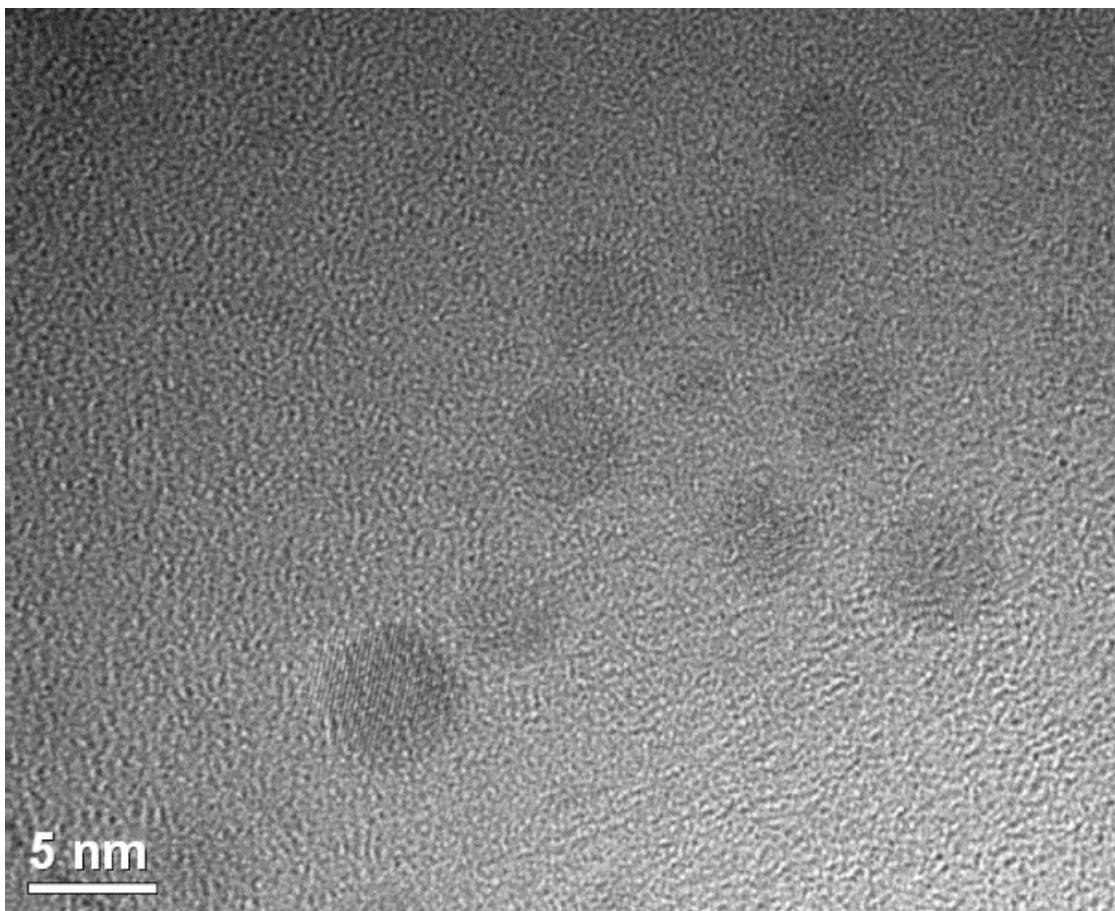


Figure 15: STEM image for prepared MNPs (formula 8) in DI water.

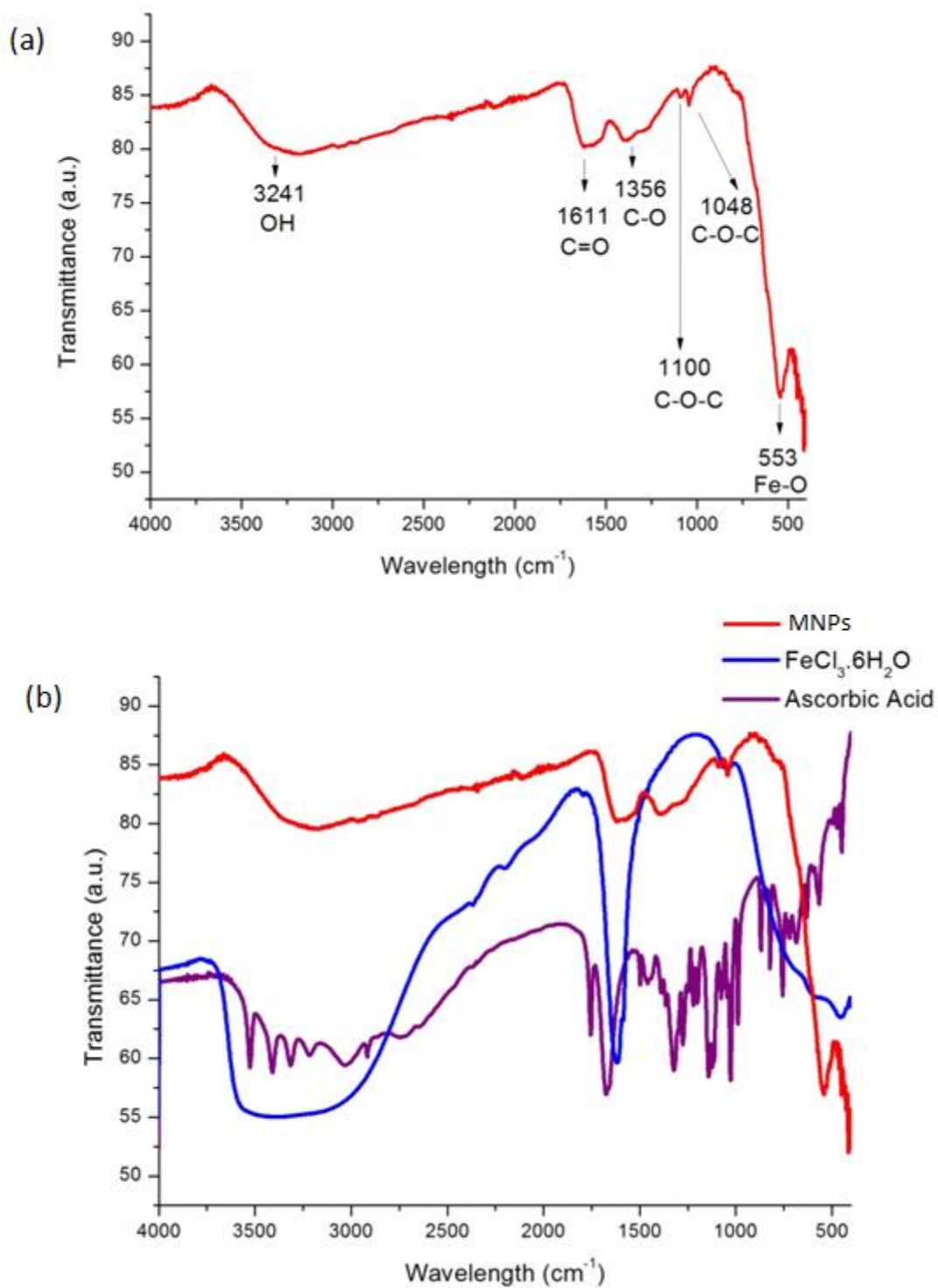


Figure 16: FT-IR of (a) MNPs and (b) Precursors (vitamin C and FeCl₃·6H₂O) with product (MNPs)-

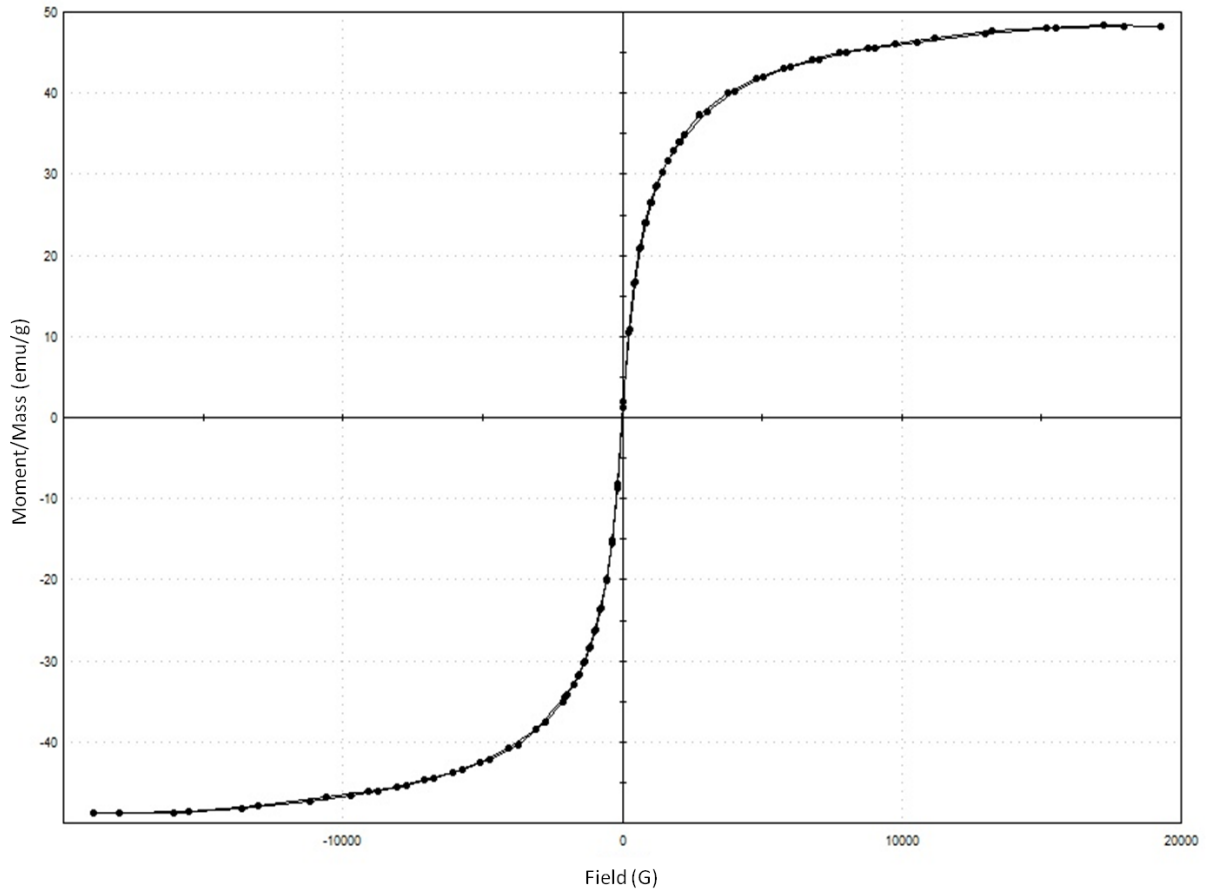


Figure 17: Hysteresis loop of prepared MNPs powder (formula 8) measured using VSM at room temperature.

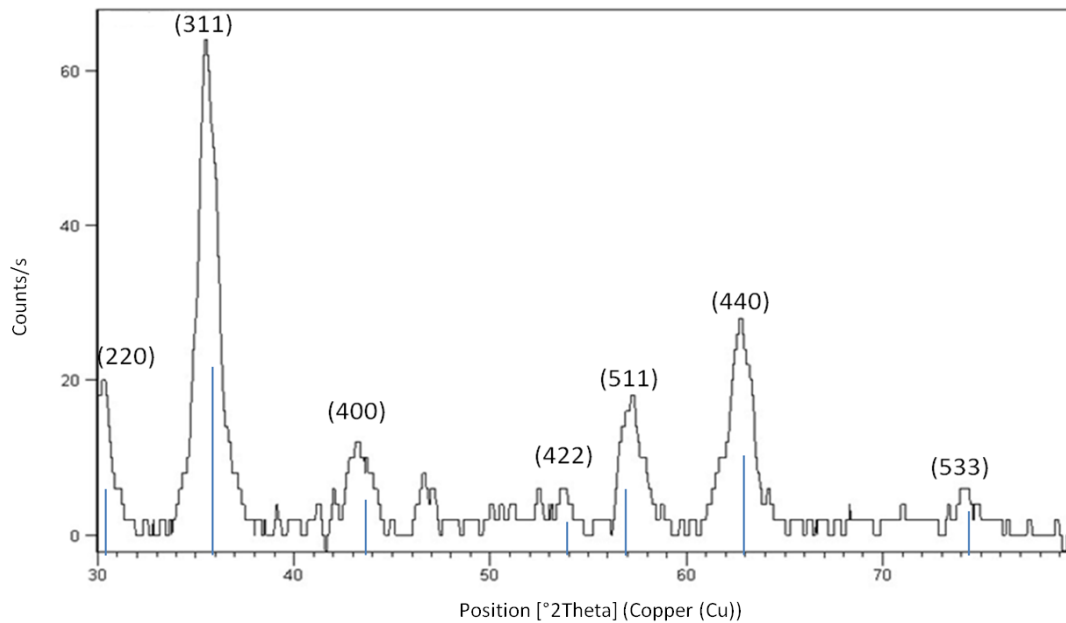


Figure 18: XRD chart showing the crystal structure of prepared MNPs (formula 8).
The lines correspond to the profile of the magnetic cubic phase (JCPDS-ICDD Card No. 24-0081).

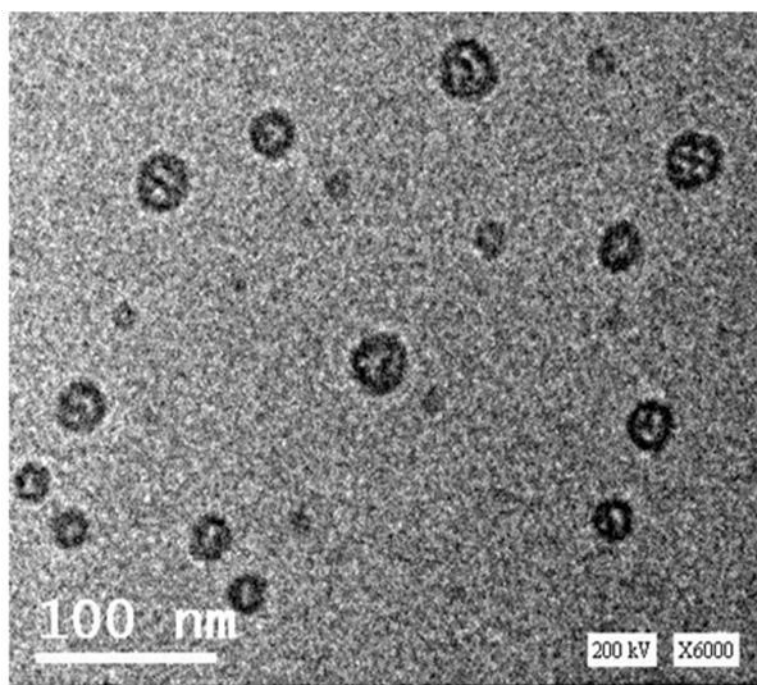
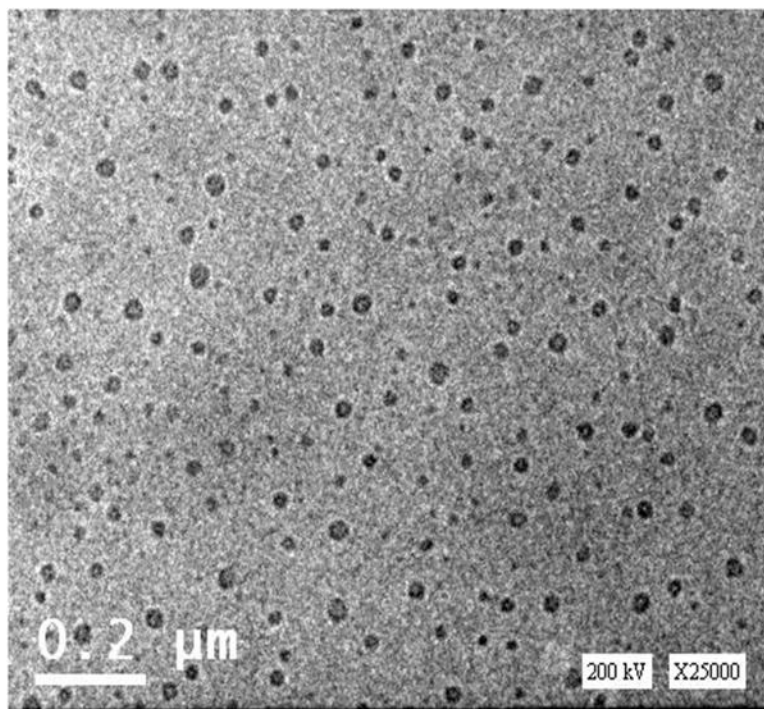


Figure 19: HR-TEM images for prepared MNPs-loaded CS NPs in DI water.

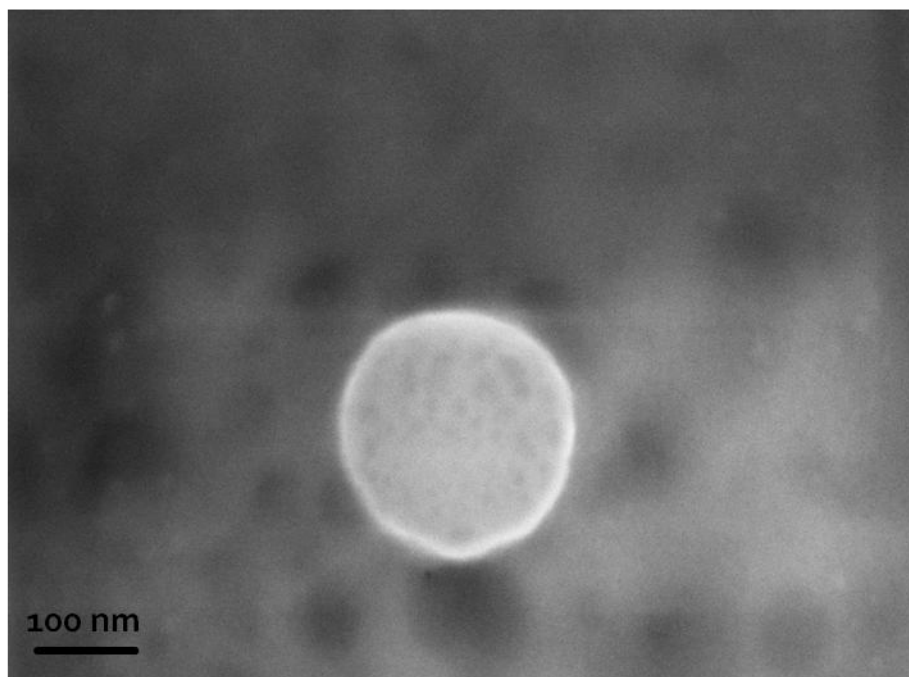


Figure 20: SEM images of drug-loaded CS NPs purified in DI water (Magnifications 37.43 and 420.85 K X; respectively).

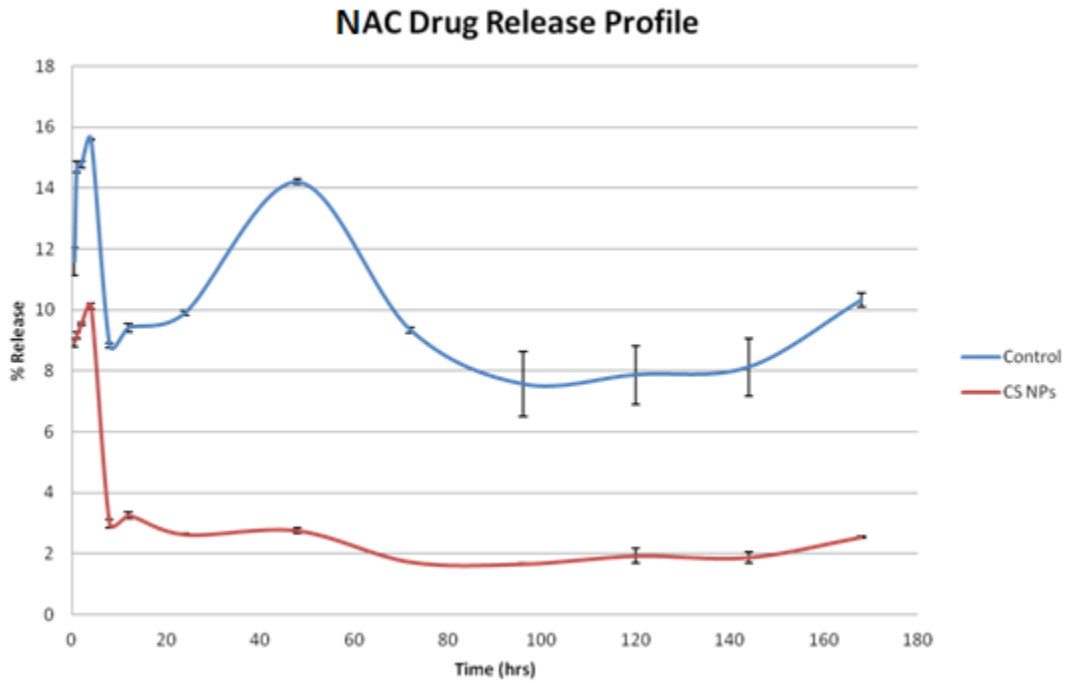


Figure 21: Figure 4- N-acetyl cysteine (NAC) drug release profile. There is a significant difference between the release of Control (free NAC) and NAC-loaded CS NPs ($P < 0.0001$, $n = 2$)

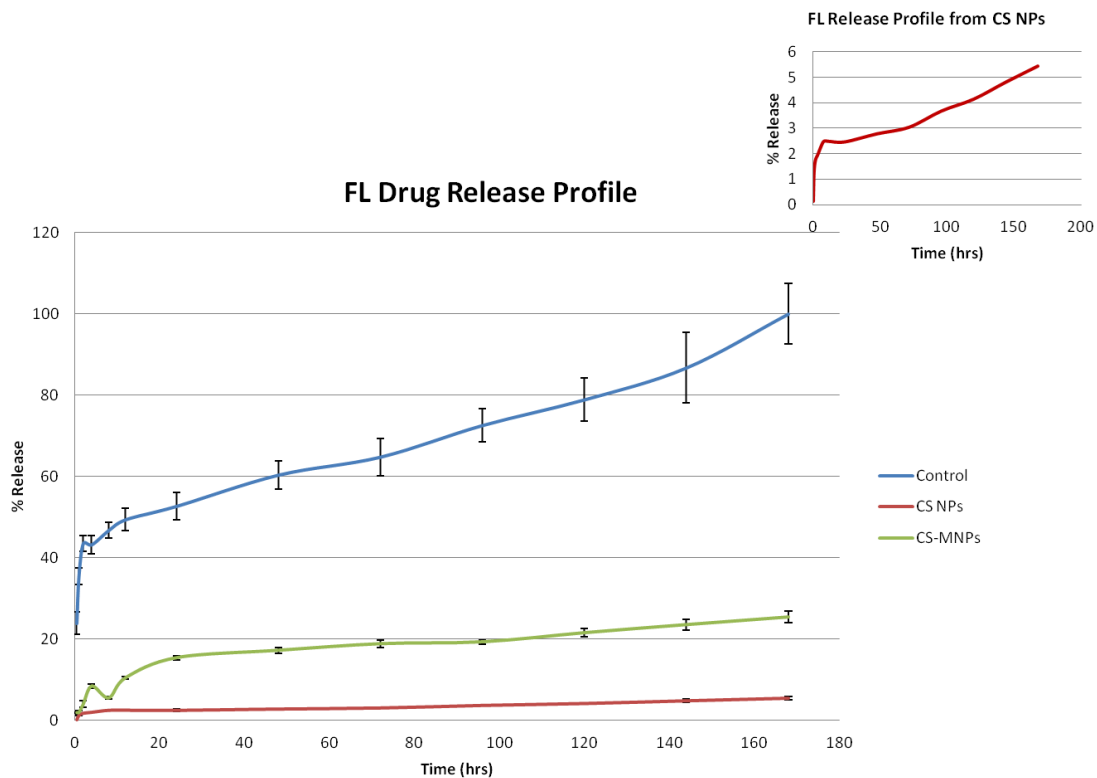


Figure 22: Fluorescein (FL) drug release profile. The release profiles of the three samples were normalized to total released amount of control. The release was significantly affected by the sample ($P < 0.0001$, $n = 2$).

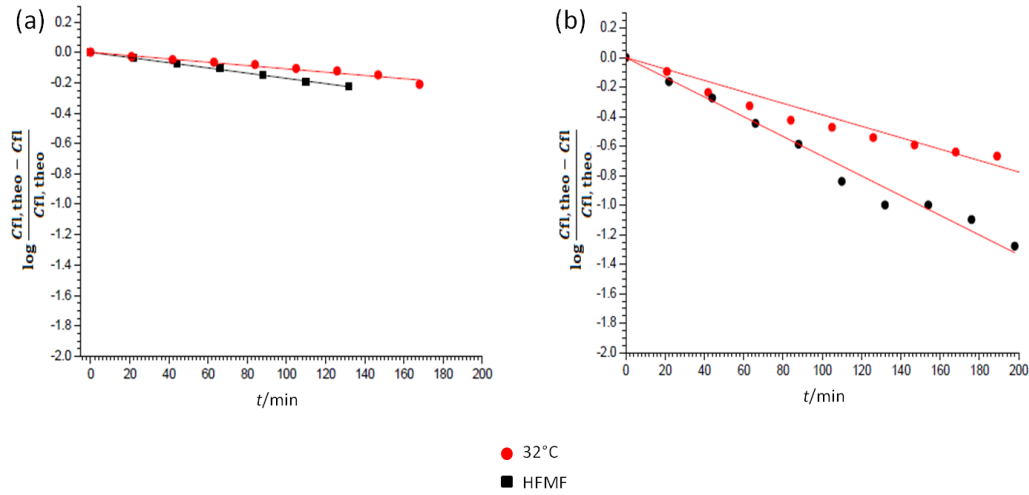


Figure 23: Logarithmic presentation for the release profile of a) FL-loaded CS NPs and b) FL-loaded CS-MNPs. Samples were taken from float-a-lyzers at 32°C and upon application of HFMF.

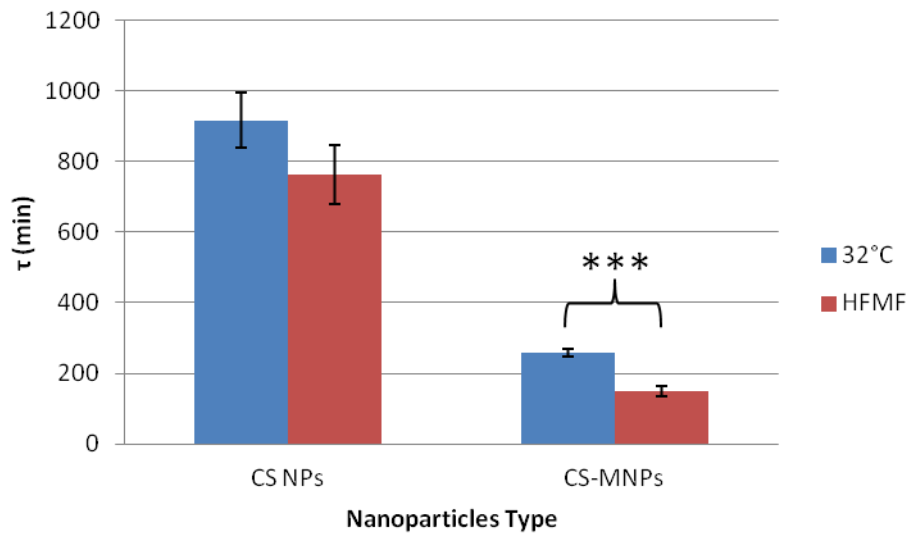


Figure 24: τ for CS NPs and CS-MNPs- At 32°C did not show any significance difference while τ for same NPs showed extremely significant difference (*) $P < 0.001$, $n=3$) upon the application of HFMF.**

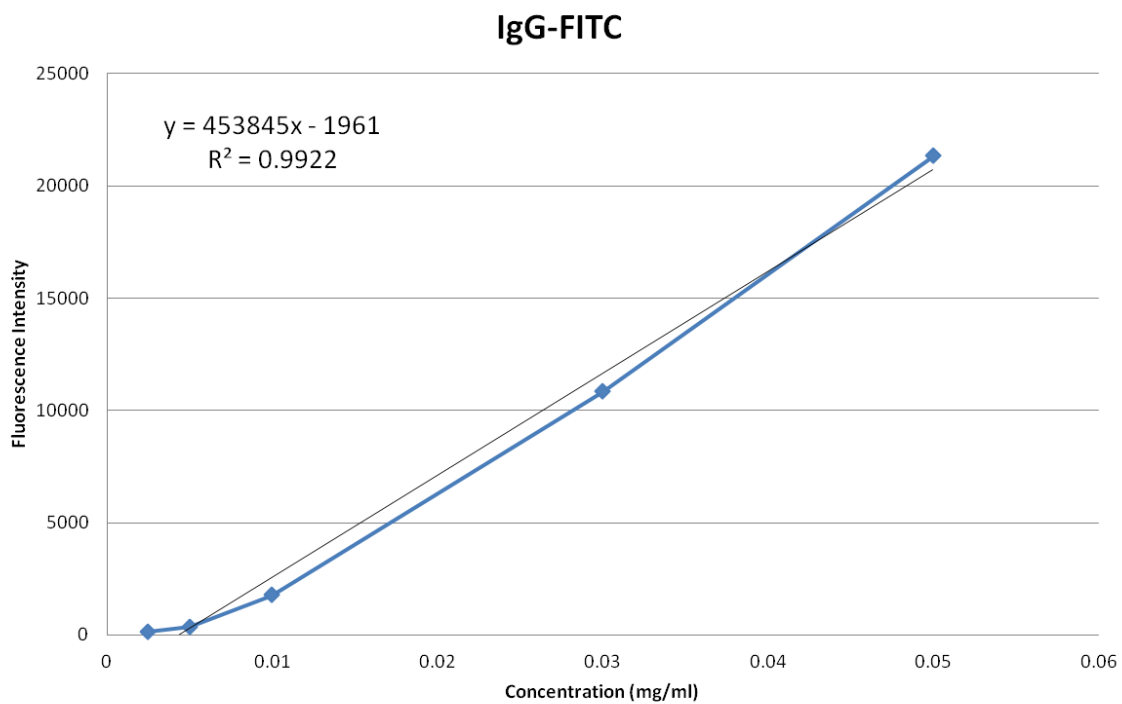


Figure 25: IgG-FITC calibration curve in DI water. From which the concentration of tagged IgG-FITC on CS NPs and CS-MNPs are determined.

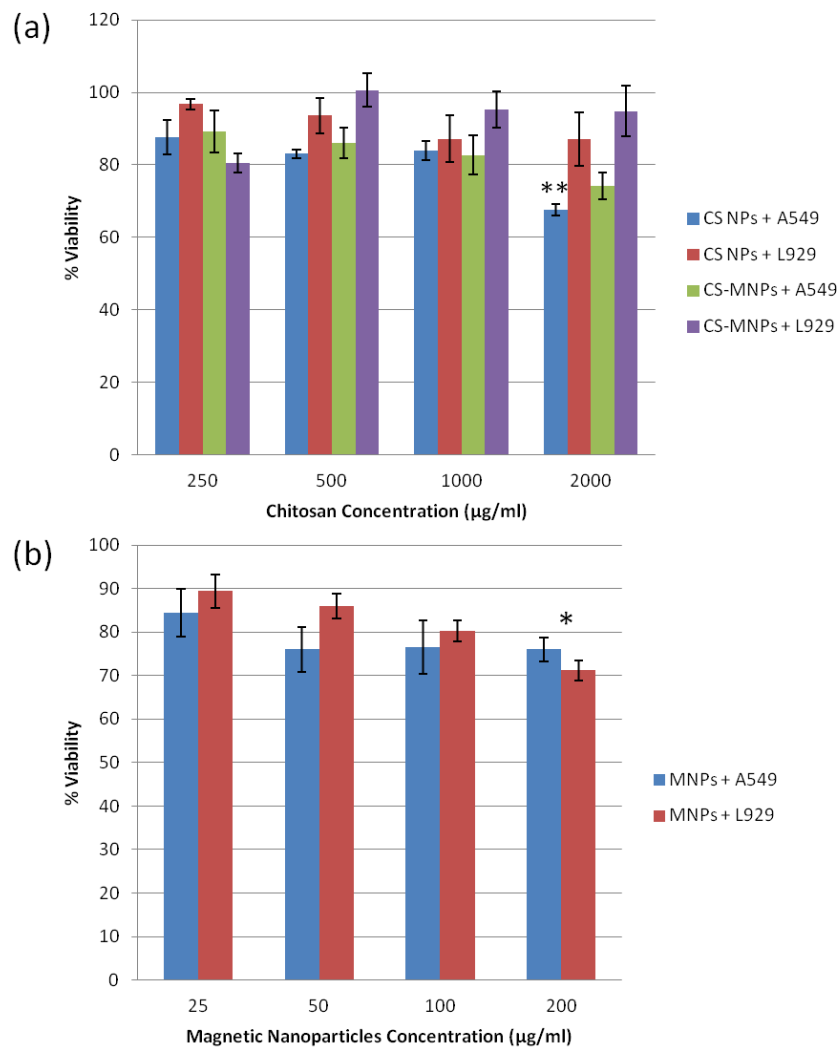


Figure 26: MTT assay for (a) CS NPs, CS-MNPs and (b) MNPs on A549 and L929 cell lines. The decrease of viability % with increasing the CS concentration is statistically significant (** $P < 0.01$ for $n = 6$) for A549 cell lines. For MNPs, significant decrease in % viability was observed at concentration = 200 µg/ml (* $P < 0.05$ for $n = 6$) in both types of cells.

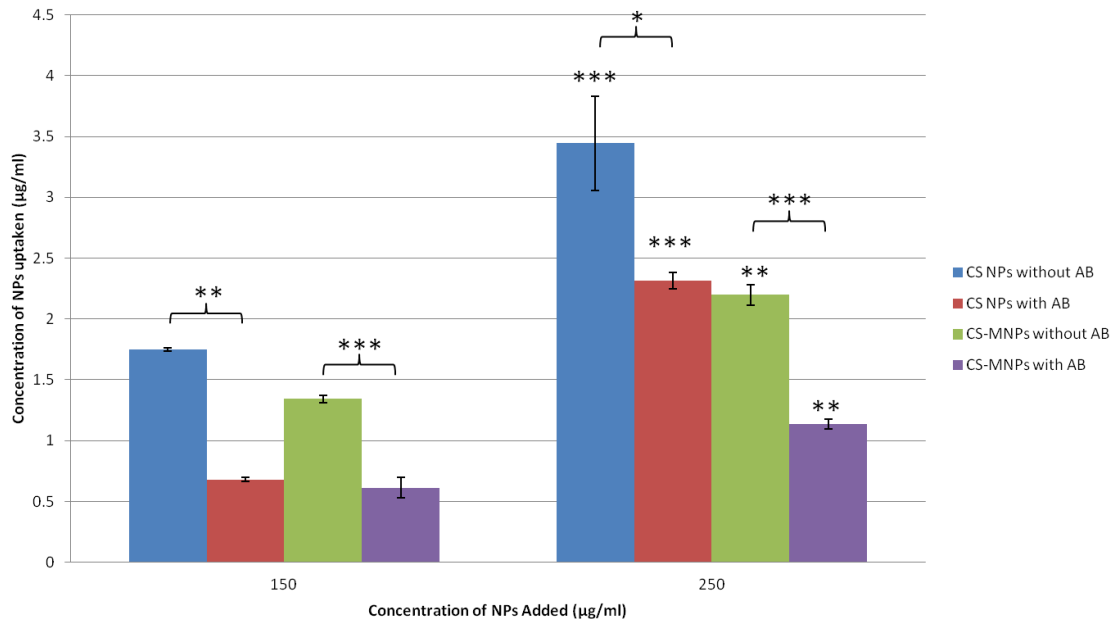


Figure 27: Cellular Uptake of tagged and non-tagged NPs for A549 cell lines. It is statistically significant that increasing the NPs concentration added, increases NPs concentration uptaken for both CS NPs and CS-MNPs whether tagged or not with AB ($***P < 0.001$ for $n=6$, $**P < 0.01$ for $n=6$ respectively). However, the uptake of non-tagged NPs is significantly higher than corresponding tagged NPs (CS NPs: $**P < 0.01$, $*P < 0.05$ for $n=6$ and CS-MNPs: $***P < 0.001$ for $n=6$)

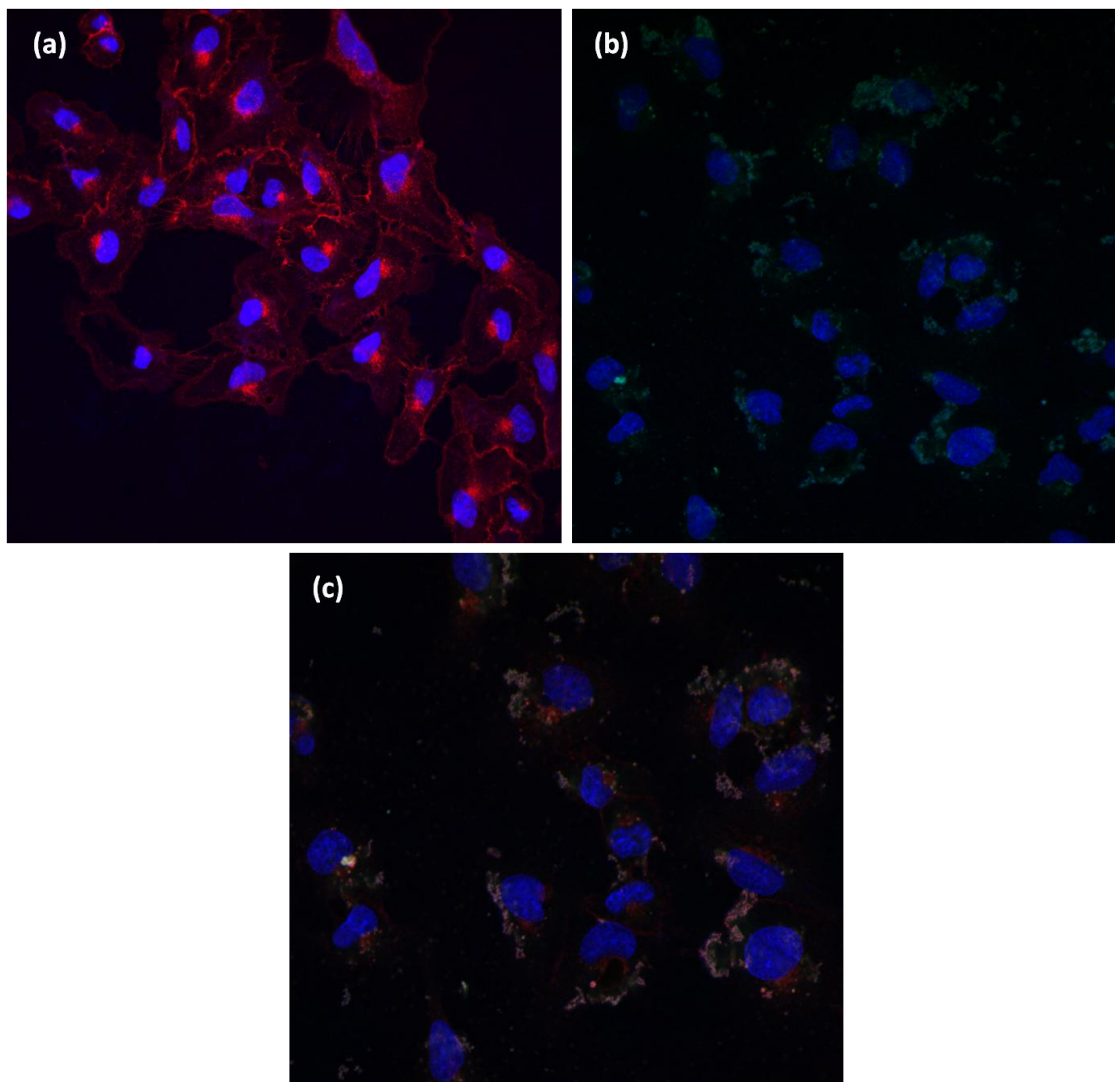


Figure 28: CLSM images for intact A549 cells (a) control cells; untreated with NPs and (b), (c) after uptake of unmodified FL-loaded CS NPs in 24 hrs incubation. Cell membrane, nucleus and nanoparticles were labeled with Hoechst (blue), WGA-AF (red) and FL (green) dyes; respectively.

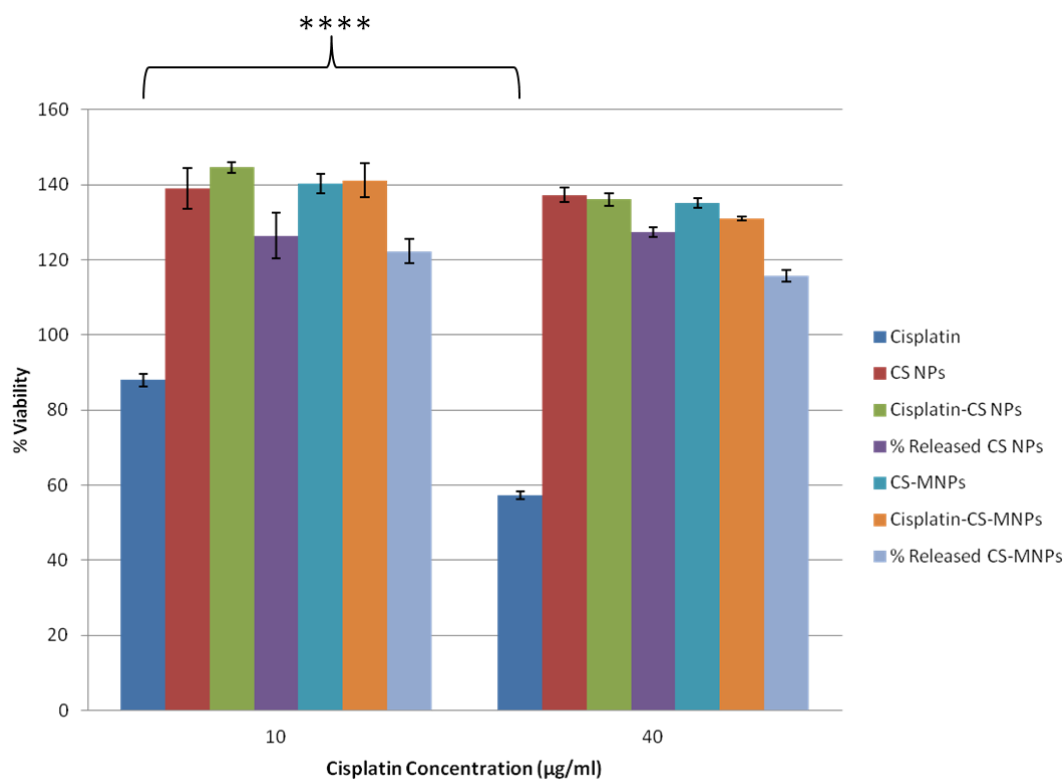


Figure 29: MTT assay for free cisplatin versus NPs-loaded cisplatin and cisplatin released correspondingly to each NP for both concentrations. Cell viability decreased significantly with increased free cisplatin concentration (** $P < 0.0001$, $n=4$).**

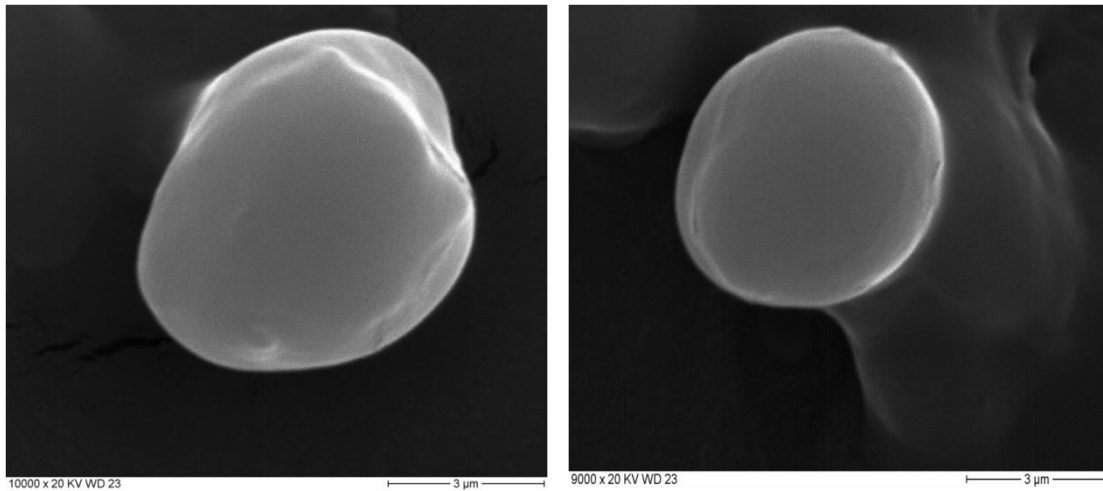


Figure 30: SEM images for SFD NPs.

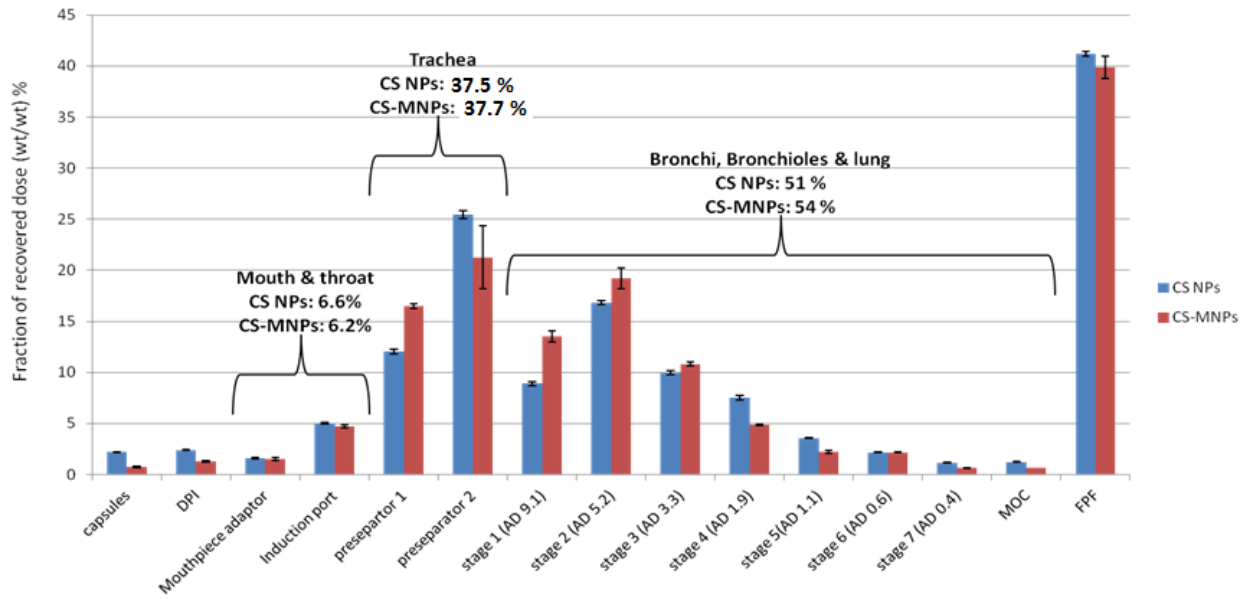


Figure 31: The NGI dispersion results for CS NPs and CS-MNPs in different compartments based on MPs AD. Data presented as mean \pm standard deviation (n = 3).

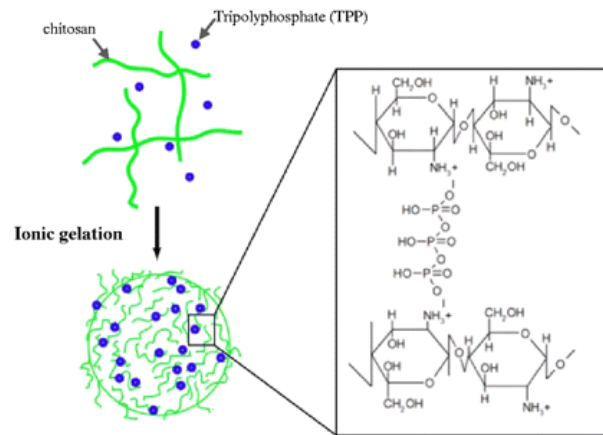


Figure 32: CS NPs preparation by Ionotropic Gelation- Inter and Intramolecular electrostatic interactions taking place between amino groups of CS and phosphate groups of TPP- Luis E. Chávez de Paz, et al., *Antimicrobial Effect of Chitosan Nanoparticles on Streptococcus mutans Biofilms*. APPLIED AND ENVIRONMENTAL MICROBIOLOGY, 2011. 77(11): p. 3892–3895.

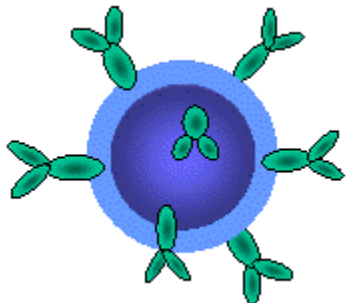


Figure 33: Active targeting moieties attached to the surface of nanoparticle- Retrieved from www.aparnabio.com/the-science/targetting, December, 2014.

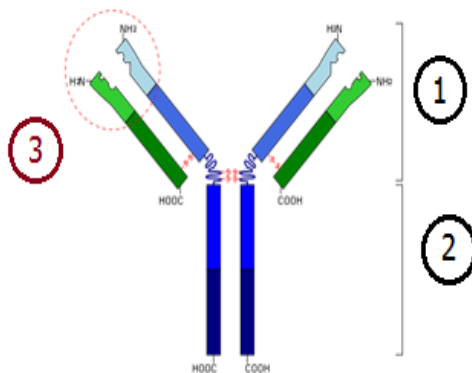


Figure 34: Schematic diagram of monoclonal antibody: 1) Fab region, 2) Fc region, 3) Antigen-binding site- Retrieved from www.en.wikipedia.org, December, 2014.

References

1. Pope-Harman, A. and M. Ferrari, *Medical Nanotechnology and Pulmonary Pathology*, in *BioMEMS and Biomedical Nanotechnology*, M. Ferrari, Desai, T., and Bhatia, S., Editors. 2007, Springer US. p. 193-212.
2. *World cancer factsheet*. 2014, International Agency for Research on Cancer and Cancer Research UK: London.
3. Mathers, C.D. and D. Loncar, *Updated projections of global mortality and burden of disease, 2002-2030: data sources, methods and results*. Geneva: World Health Organization, 2005.
4. Barros, J.A., G. Valladares, A.R. Faria, E.M. Fugita, A.P. Ruiz, A.G.D. Vianna, G.L. Trevisan, and F.A.M.d. Oliveira, *Diagnóstico precoce do câncer de pulmão: o grande desafio. Variáveis epidemiológicas e clínicas, estadiamento e tratamento*. *Jornal Brasileiro de Pneumologia*, 2006. **32**: p. 221-227.
5. Tyczynski, J.E., F. Bray, and D. Maxwell Parkin, *Lung cancer in Europe in 2000: epidemiology, prevention, and early detection*. *The lancet oncology*, 2003. **4**(1): p. 45-55.
6. Mühlfeld, C., B. Rothen-Rutishauser, F. Blank, D. Vanhecke, M. Ochs, and P. Gehr, *Interactions of nanoparticles with pulmonary structures and cellular responses*. *American Journal of Physiology-Lung Cellular and Molecular Physiology*, 2008. **294**(5): p. L817-L829.
7. Yang, W., J.I. Peters, and R.O. Williams III, *Inhaled nanoparticles—a current review*. *International Journal of Pharmaceutics*, 2008. **356**(1): p. 239-247.
8. Alberg, A.J., J.G. Ford, and J.M. Samet, *Epidemiology of lung cancer*: Accp evidence-based clinical practice guidelines (2nd edition)*. *CHEST Journal*, 2007. **132**(3_suppl): p. 29S-55S.
9. Celikoglu, F., S.I. Celikoglu, and E.P. Goldberg, *Bronchoscopic intratumoral chemotherapy of lung cancer*. *Lung Cancer*, 2008. **61**(1): p. 1-12.
10. Lam, B., S.Y. Lam, M.P. Wong, C.G.C. Ooi, D.Y.T. Fong, D.C.L. Lam, A.Y.K. Lai, C.-m. Tam, C.B.Y. Pang, M.S.M. Ip, and W.-k. Lam, *Sputum cytology examination followed by autofluorescence bronchoscopy: A practical way of identifying early stage lung cancer in central airway*. *Lung Cancer*, 2009. **64**(3): p. 289-294.
11. Blanco, D., S. Vicent, M.F. Fraga, I. Fernandez-Garcia, J. Freire, A. Lujambio, M. Esteller, C. Ortiz-de-Solorzano, R. Pio, F. Lecanda, and L.M. Montuenga, *Molecular*

- analysis of a multistep lung cancer model induced by chronic inflammation reveals epigenetic regulation of p16 and activation of the DNA damage response pathway.* Neoplasia, 2007. **9**(10): p. 840-52.
12. Carbone, D.P. and E. Felip, *Adjuvant therapy in non-small cell lung cancer: future treatment prospects and paradigms.* Clin Lung Cancer, 2011. **12**(5): p. 261-71.
 13. Molina, J.R., P. Yang, S.D. Cassivi, S.E. Schild, and A.A. Adjei, *Non-Small Cell Lung Cancer: Epidemiology, Risk Factors, Treatment, and Survivorship.* Mayo Clinic proceedings. Mayo Clinic, 2008. **83**(5): p. 584-594.
 14. Carbone, D.P. and E. Felip, *Adjuvant Therapy in Non-Small Cell Lung Cancer: Future Treatment Prospects and Paradigms.* Clinical Lung Cancer, 2011. **12**(5): p. 261-271.
 15. Winton, T., R. Livingston, D. Johnson, J. Rigas, M. Johnston, C. Butts, Y. Cormier, G. Goss, R. Inculet, E. Vallieres, W. Fry, D. Bethune, J. Ayoub, K. Ding, L. Seymour, B. Graham, M.-S. Tsao, D. Gandara, K. Kesler, T. Demmy, and F. Shepherd, *Vinorelbine plus Cisplatin vs. Observation in Resected Non-Small-Cell Lung Cancer.* New England Journal of Medicine, 2005. **352**(25): p. 2589-2597.
 16. Douillard, J.-Y., R. Rosell, M. De Lena, F. Carpagnano, R. Ramlau, J.L. González-Larriba, T. Grodzki, J.R. Pereira, A. Le Groumellec, V. Lorusso, C. Clary, A.J. Torres, J. Dahabreh, P.-J. Souquet, J. Astudillo, P. Fournel, A. Artal-Cortes, J. Jassem, L. Koubkova, P. His, M. Riggi, and P. Hurteloup, *Adjuvant vinorelbine plus cisplatin versus observation in patients with completely resected stage IB–IIIA non-small-cell lung cancer (Adjuvant Navelbine International Trialist Association [ANITA]): a randomised controlled trial.* The Lancet Oncology, 2006. **7**(9): p. 719-727.
 17. Keller, S.M., S. Adak, H. Wagner, A. Herskovic, R. Komaki, B.J. Brooks, M.C. Perry, R.B. Livingston, and D.H. Johnson, *A Randomized Trial of Postoperative Adjuvant Therapy in Patients with Completely Resected Stage II or IIIa Non-Small-Cell Lung Cancer.* New England Journal of Medicine, 2000. **343**(17): p. 1217-1222.
 18. Pignon, J.-P., H. Tribodet, G.V. Scagliotti, J.-Y. Douillard, F.A. Shepherd, R.J. Stephens, A. Dunant, V. Torri, R. Rosell, L. Seymour, S.G. Spiro, E. Rolland, R. Fossati, D. Aubert, K. Ding, D. Waller, and T. Le Chevalier, *Lung Adjuvant Cisplatin Evaluation: A Pooled Analysis by the LACE Collaborative Group.* Journal of Clinical Oncology, 2008. **26**(21): p. 3552-3559.
 19. Scagliotti, G.V., R. Fossati, V. Torri, L. Crinò, G. Giaccone, G. Silvano, M. Martelli, M. Clerici, F. Cognetti, M. Tonato, and F.t.A.L.P.I.E.O.f.R.T.o.C.L.C.C.G. Investigators, *Randomized Study of Adjuvant Chemotherapy for Completely Resected Stage I, II, or*

- IIIA Non-Small-Cell Lung Cancer*. Journal of the National Cancer Institute, 2003. **95**(19): p. 1453-1461.
20. Waller, D., M.D. Peake, R.J. Stephens, N.H. Gower, R. Milroy, M.K.B. Parmar, R.M. Rudd, S.G. Spiro, and o.b.o.a.B. participants, *Chemotherapy for patients with non-small cell lung cancer: the surgical setting of the Big Lung Trial*. European Journal of Cardio-Thoracic Surgery, 2004. **26**(1): p. 173-182.
 21. *Cisplatin-Based Adjuvant Chemotherapy in Patients with Completely Resected Non-Small-Cell Lung Cancer*. New England Journal of Medicine, 2004. **350**(4): p. 351-360.
 22. Trzaska, S. *Cisplatin*. 2005.
 23. Primeau, A.J., A. Rendon, D. Hedley, L. Lilge, and I.F. Tannock, *The Distribution of the Anticancer Drug Doxorubicin in Relation to Blood Vessels in Solid Tumors*. Clinical Cancer Research, 2005. **11**(24): p. 8782-8788.
 24. Viedma E, C., J. Pérez Pallarés, M. Martínez García, R. López Reyes, F. Sanchís Moret, and J. Sanchís Aldás, *A randomised study of midazolam for sedation in flexible bronchoscopy*. Arch Bronconeumol, 2010. **46**(6): p. 302-309.
 25. Smith, J.P., S. Kanekal, B. Montesa, M.B. Patawaran, and C.Y.J.e. al., *Drug retention and distribution after intratumoral chemotherapy with fluorouracil/epinephrine gel in human pancreatic cancer xenografts*. Cancer Chemother Pharmacol, 1999. **44**: p. 267–274.
 26. Monga, S.P.S., R. Wadleigh, A. Sharma, H. Adib, D. Strader, G. Singh, J.W. Harmon, M. Berlin, D.K. Monga, and L. Mishra, *Intratumoral Therapy of Cisplatin/Epinephrine Injectable Gel for Palliation in Patients With Obstructive Esophageal Cancer*. American Journal of Clinical Oncology, 2000. **23**(4): p. 386-392.
 27. Cheung, R.Y., A.M. Rauth, and X. Yu Wu, *In vivo efficacy and toxicity of intratumorally delivered mitomycin C and its combination with doxorubicin using microsphere formulations*. Anti-Cancer Drugs, 2005. **16**(4): p. 423-433.
 28. Liu, G., E. Franssen, M.I. Fitch, and E. Warner, *Patient preferences for oral versus intravenous palliative chemotherapy*. Journal of Clinical Oncology, 1997. **15**(1): p. 110-5.
 29. Bhattacharyya, G., *Oral systemic therapy: Not all "win-win"*. Indian Journal of Medical and Paediatric Oncology, 2010. **31**(1): p. 1-3.
 30. Sung, J.C., B.L. Pulliam, and D.A. Edwards, *Nanoparticles for drug delivery to the lungs*. Trends in biotechnology, 2007. **25**(12): p. 563-570.

31. Yang, W., J.I. Peters, and R.O. Williams Iii, *Inhaled nanoparticles—A current review*. International Journal of Pharmaceutics, 2008. **356**(1–2): p. 239-247.
32. Rytting, E., J. Nguyen, X. Wang, and T. Kissel, *Biodegradable polymeric nanocarriers for pulmonary drug delivery*. Expert Opinion on Drug Delivery, 2008. **5**(6): p. 629-639.
33. Martonen, T.B. and I.M. Katz, *Deposition Patterns of Aerosolized Drugs Within Human Lungs: Effects of Ventilatory Parameters*. Pharmaceutical Research, 1993. **10**(6): p. 871-878.
34. Azarmi, S., W.H. Roa, and R. Löbenberg, *Targeted delivery of nanoparticles for the treatment of lung diseases*. Advanced Drug Delivery Reviews, 2008. **60**(8): p. 863-875.
35. Chow, A., H. Tong, P. Chattopadhyay, and B. Shekunov, *Particle Engineering for Pulmonary Drug Delivery*. Pharmaceutical Research, 2007. **24**(3): p. 411-437.
36. Sham, J.O.H., Y. Zhang, W.H. Finlay, W.H. Roa, and R. Löbenberg, *Formulation and characterization of spray-dried powders containing nanoparticles for aerosol delivery to the lung*. International Journal of Pharmaceutics, 2004. **269**(2): p. 457-467.
37. SANDERS, N.N., S.C. DE SMEDT, E. VAN ROMPAEY, P. SIMOENS, F. DE BAETS, and J. DEMEESTER, *Cystic Fibrosis Sputum*. American Journal of Respiratory and Critical Care Medicine, 2000. **162**(5): p. 1905-1911.
38. Lai, S.K., Y.-Y. Wang, and J. Hanes, *Mucus-penetrating nanoparticles for drug and gene delivery to mucosal tissues*. Advanced Drug Delivery Reviews, 2009. **61**(2): p. 158-171.
39. Dash, M., F. Chiellini, R.M. Ottenbrite, and E. Chiellini, *Chitosan—A versatile semi-synthetic polymer in biomedical applications*. Progress in Polymer Science, 2011. **36**(8): p. 981-1014.
40. Neuberger, T., B. Schöpf, H. Hofmann, M. Hofmann, and B. von Rechenberg, *Superparamagnetic nanoparticles for biomedical applications: Possibilities and limitations of a new drug delivery system*. Journal of Magnetism and Magnetic Materials, 2005. **293**(1): p. 483-496.
41. Markides, H., M. Rotherham, and A.J. El Haj, *Biocompatibility and Toxicity of Magnetic Nanoparticles in Regenerative Medicine*. Journal of Nanomaterials, 2012. **2012**: p. 11.
42. Ungaro, F., I. d'Angelo, C. Coletta, R. d'Emmanuele di Villa Bianca, R. Sorrentino, B. Perfetto, M.A. Tufano, A. Miro, M.I. La Rotonda, and F. Quaglia, *Dry powders based on PLGA nanoparticles for pulmonary delivery of antibiotics: Modulation of encapsulation efficiency, release rate and lung deposition pattern by hydrophilic polymers*. Journal of Controlled Release, 2012. **157**(1): p. 149-159.

43. Al-Qadi, S., A. Grenha, D. Carrión-Recio, B. Seijo, and C. Remuñán-López, *Microencapsulated chitosan nanoparticles for pulmonary protein delivery: In vivo evaluation of insulin-loaded formulations*. *Journal of Controlled Release*, 2012. **157**(3): p. 383-390.
44. Liu, Z., Y. Jiao, Y. Wang, C. Zhou, and Z. Zhang, *Polysaccharides-based nanoparticles as drug delivery systems*. *Advanced Drug Delivery Reviews*, 2008. **60**(15): p. 1650-1662.
45. Ma, Z., T.M. Lim, and L.-Y. Lim, *Pharmacological activity of peroral chitosan–insulin nanoparticles in diabetic rats*. *International Journal of Pharmaceutics*, 2005. **293**(1–2): p. 271-280.
46. Mendelsohn, J. and J. Baselga, *Epidermal Growth Factor Receptor Targeting in Cancer*. *Seminars in Oncology*, 2006. **33**(4): p. 369-385.
47. Selvaggi, G., S. Novello, V. Torri, E. Leonardo, P. De Giuli, P. Borasio, C. Mossetti, F. Ardisson, P. Lausi, and G.V. Scagliotti, *Epidermal growth factor receptor overexpression correlates with a poor prognosis in completely resected non-small-cell lung cancer*. *Annals of Oncology*, 2004. **15**(1): p. 28-32.
48. Howell, S.B., *Clinical applications of a novel sustained-release injectable drug delivery system: DepoFoam technology*. *Cancer journal (Sudbury, Mass.)*, 2001. **7**(3): p. 219-227.
49. Glantz, M.J., K.A. Jaeckle, M.C. Chamberlain, S. Phuphanich, L. Recht, L.J. Swinnen, B. Maria, S. LaFollette, G.B. Schumann, B.F. Cole, and S.B. Howell, *A Randomized Controlled Trial Comparing Intrathecal Sustained-release Cytarabine (DepoCyt) to Intrathecal Methotrexate in Patients with Neoplastic Meningitis from Solid Tumors*. *Clinical Cancer Research*, 1999. **5**(11): p. 3394-3402.
50. Liechty, W.B., D.R. Kryscio, B.V. Slaughter, and N.A. Peppas, *Polymers for Drug Delivery Systems*. *Annual Review of Chemical and Biomolecular Engineering*, 2010. **1**(1): p. 149-173.
51. Yoo, D., J.-H. Lee, T.-H. Shin, and J. Cheon, *Theranostic Magnetic Nanoparticles*. *Accounts of Chemical Research*, 2011. **44**(10): p. 863-874.
52. Mornet, S., S. Vasseur, F. Grasset, and E. Duguet, *Magnetic nanoparticle design for medical diagnosis and therapy*. *Journal of Materials Chemistry*, 2004. **14**(14): p. 2161-2175.
53. Choi, S.H., H.J. Byeon, J.S. Choi, L. Thao, I. Kim, E.S. Lee, B.S. Shin, K.C. Lee, and Y.S. Youn, *Inhalable self-assembled albumin nanoparticles for treating drug-resistant lung cancer*. *Journal of Controlled Release*, 2015. **197**(0): p. 199-207.

54. Long, J.T., T.Y. Cheang, S.Y. Zhuo, R.F. Zeng, Q.S. Dai, H.P. Li, and S. Fang, *Anticancer drug-loaded multifunctional nanoparticles to enhance the chemotherapeutic efficacy in lung cancer metastasis*. J Nanobiotechnology, 2014. **12**(1): p. 37.
55. Kaminskias, L.M., V.M. McLeod, G.M. Ryan, B.D. Kelly, J.M. Haynes, M. Williamson, N. Thienthong, D.J. Owen, and C.J.H. Porter, *Pulmonary administration of a doxorubicin-conjugated dendrimer enhances drug exposure to lung metastases and improves cancer therapy*. Journal of Controlled Release, 2014. **183**(0): p. 18-26.
56. Guo, X., X. Zhang, L. Ye, Y. Zhang, R. Ding, Y. Hao, Y. Zhao, and Z. Zhang, *Inhalable microspheres embedding chitosan-coated PLGA nanoparticles for 2-methoxyestradiol*. J Drug Target, 2014. **22**(5): p. 421-7.
57. Xu, H., Z. Hou, H. Zhang, H. Kong, X. Li, H. Wang, and W. Xie, *An efficient Trojan delivery of tetrandrine by poly(N-vinylpyrrolidone)-block-poly(ϵ -caprolactone) (PVP-b-PCL) nanoparticles shows enhanced apoptotic induction of lung cancer cells and inhibition of its migration and invasion*. International journal of nanomedicine, 2014. **9**: p. 231-242.
58. Sun, Q., B. Teong, I.F. Chen, S.J. Chang, J. Gao, and S.-M. Kuo, *Enhanced apoptotic effects of dihydroartemisinin-aggregated gelatin and hyaluronan nanoparticles on human lung cancer cells*. Journal of Biomedical Materials Research Part B: Applied Biomaterials, 2014. **102**(3): p. 455-462.
59. Zhao, T., H. Chen, Y. Dong, J. Zhang, H. Huang, J. Zhu, and W. Zhang, *Paclitaxel-loaded poly(glycolide-co- ϵ -caprolactone)-b-D- α -tocopheryl polyethylene glycol 2000 succinate nanoparticles for lung cancer therapy*. International journal of nanomedicine, 2013. **8**: p. 1947-1957.
60. Shen, J., G. Song, M. An, X. Li, N. Wu, K. Ruan, J. Hu, and R. Hu, *The use of hollow mesoporous silica nanospheres to encapsulate bortezomib and improve efficacy for non-small cell lung cancer therapy*. Biomaterials, 2014. **35**(1): p. 316-326.
61. Lv, S., Z. Tang, M. Li, J. Lin, W. Song, H. Liu, Y. Huang, Y. Zhang, and X. Chen, *Codelivery of doxorubicin and paclitaxel by PEG-polypeptide nanovehicle for the treatment of non-small cell lung cancer*. Biomaterials, 2014. **35**(23): p. 6118-6129.
62. Li, M., Z. Tang, J. Lin, Y. Zhang, S. Lv, W. Song, Y. Huang, and X. Chen, *Synergistic antitumor effects of Doxorubicin-loaded carboxymethyl cellulose nanoparticle in combination with endostar for effective treatment of non-small-cell lung cancer*. Adv Healthc Mater, 2014. **3**(11): p. 1877-88.

63. Maya, S., B. Sarmiento, V.-K. Lakshmanan, D. Menon, V. Seabra, and R. Jayakumar, *Chitosan cross-linked docetaxel loaded EGF receptor targeted nanoparticles for lung cancer cells*. International Journal of Biological Macromolecules, 2014. **69**(0): p. 532-541.
64. Sadhukha, T., T.S. Wiedmann, and J. Panyam, *Inhalable magnetic nanoparticles for targeted hyperthermia in lung cancer therapy*. Biomaterials, 2013. **34**(21): p. 5163-5171.
65. Nejati-Koshki, K., M. Mesgari, E. Ebrahimi, F. Abbasalizadeh, S. Fekri Aval, A.A. Khandaghi, M. Abasi, and A. Akbarzadeh, *Synthesis and in vitro study of cisplatin-loaded Fe₃O₄ nanoparticles modified with PLGA-PEG6000 copolymers in treatment of lung cancer*. J Microencapsul, 2014. **31**(8): p. 815-23.
66. Karra, N., T. Nassar, A.N. Ripin, O. Schwob, J. Borlak, and S. Benita, *Antibody conjugated PLGA nanoparticles for targeted delivery of paclitaxel palmitate: efficacy and biofate in a lung cancer mouse model*. Small, 2013. **9**(24): p. 4221-36.
67. Yordanov, G., A. Evangelatov, and R. Skrobanska, *Epirubicin loaded to pre-polymerized poly(butyl cyanoacrylate) nanoparticles: Preparation and in vitro evaluation in human lung adenocarcinoma cells*. Colloids and Surfaces B: Biointerfaces, 2013. **107**(0): p. 115-123.
68. Meenach, S.A., K.W. Anderson, J. Zach Hilt, R.C. McGarry, and H.M. Mansour, *Characterization and aerosol dispersion performance of advanced spray-dried chemotherapeutic PEGylated phospholipid particles for dry powder inhalation delivery in lung cancer*. European Journal of Pharmaceutical Sciences, 2013. **49**(4): p. 699-711.
69. McBride, A.A., D.N. Price, L.R. Lamoureux, A.A. Elmaoued, J.M. Vargas, N.L. Adolphi, and P. Muttill, *Preparation and characterization of novel magnetic nano-in-microparticles for site-specific pulmonary drug delivery*. Mol Pharm, 2013. **10**(10): p. 3574-81.
70. Patel, A.R., M.B. Chougule, T. I, R. Patlolla, G. Wang, and M. Singh, *Efficacy of aerosolized celecoxib encapsulated nanostructured lipid carrier in non-small cell lung cancer in combination with docetaxel*. Pharm Res, 2013. **30**(5): p. 1435-46.
71. Srinivasan, A.R., A. Lakshmikuttyamma, and S.A. Shoyele, *Investigation of the stability and cellular uptake of self-associated monoclonal antibody (MAb) nanoparticles by non-small lung cancer cells*. Mol Pharm, 2013. **10**(9): p. 3275-84.
72. Yin, H., H. Zhang, and B. Liu, *Superior anticancer efficacy of curcumin-loaded nanoparticles against lung cancer*. Acta Biochim Biophys Sin (Shanghai), 2013. **45**(8): p. 634-40.

73. Wang, P., L. Zhang, H. Peng, Y. Li, J. Xiong, and Z. Xu, *The formulation and delivery of curcumin with solid lipid nanoparticles for the treatment of on non-small cell lung cancer both in vitro and in vivo*. Materials Science and Engineering: C, 2013. **33**(8): p. 4802-4808.
74. Garg, N.K., P. Dwivedi, C. Campbell, and R.K. Tyagi, *Site specific/targeted delivery of gemcitabine through anisamide anchored chitosan/poly ethylene glycol nanoparticles: An improved understanding of lung cancer therapeutic intervention*. European Journal of Pharmaceutical Sciences, 2012. **47**(5): p. 1006-1014.
75. Karthikeyan, S., N. Rajendra Prasad, A. Ganamani, and E. Balamurugan, *Anticancer activity of resveratrol-loaded gelatin nanoparticles on NCI-H460 non-small cell lung cancer cells*. Biomedicine & Preventive Nutrition, 2013. **3**(1): p. 64-73.
76. Roa, W.H., S. Azarmi, M.H.D.K. Al-Hallak, W.H. Finlay, A.M. Magliocco, and R. Löbenberg, *Inhalable nanoparticles, a non-invasive approach to treat lung cancer in a mouse model*. Journal of Controlled Release, 2011. **150**(1): p. 49-55.
77. Tseng, C.-L., S.Y.-H. Wu, W.-H. Wang, C.-L. Peng, F.-H. Lin, C.-C. Lin, T.-H. Young, and M.-J. Shieh, *Targeting efficiency and biodistribution of biotinylated-EGF-conjugated gelatin nanoparticles administered via aerosol delivery in nude mice with lung cancer*. Biomaterials, 2008. **29**(20): p. 3014-3022.
78. Tigli Aydin, R.S. and M. Pulat, *5-Fluorouracil Encapsulated Chitosan Nanoparticles for pH-Stimulated Drug Delivery: Evaluation of Controlled Release Kinetics*. Journal of Nanomaterials, 2012. **2012**: p. 10.
79. Thermo Scientific (Pierce Biotechnology), *Ellman's reagent # 22582*.
80. Eggerstedt, S.N., M. Dietzel, M. Sommerfeld, R. Süverkrüp, and A. Lamprecht, *Protein spheres prepared by drop jet freeze drying*. International Journal of Pharmaceutics, 2012. **438**(1-2): p. 160-166.
81. Kokoh, K.B., F. Hahn, A. Métayer, and C. Lamy, *FTIR spectroelectrochemical investigation of the electrocatalytic oxidation of ascorbic acid at platinum electrodes in acid medium*. Electrochimica Acta, 2002. **47**(24): p. 3965-3969.
82. Yohannan Panicker, C., H. Tresa Varghese, and D. Philip, *FT-IR, FT-Raman and SERS spectra of Vitamin C*. Spectrochimica Acta Part A: Molecular and Biomolecular Spectroscopy, 2006. **65**(3): p. 802-804.
83. Li, Z., H. Chen, H. Bao, and M. Gao, *One-pot reaction to synthesize water-soluble magnetite nanocrystals*. Chemistry of materials, 2004. **16**(8): p. 1391-1393.

84. Li, Z., L. Wei, M. Gao, and H. Lei, *One-Pot Reaction to Synthesize Biocompatible Magnetite Nanoparticles*. *Advanced Materials*, 2005. **17**(8): p. 1001-1005.
85. Lu, X., M. Niu, R. Qiao, and M. Gao, *Superdispersible PVP-Coated Fe₃O₄ Nanocrystals Prepared by a "One-Pot" Reaction†*. *The Journal of Physical Chemistry B*, 2008. **112**(46): p. 14390-14394.
86. Janes, K.A., P. Calvo, and M.J. Alonso, *Polysaccharide colloidal particles as delivery systems for macromolecules*. *Advanced Drug Delivery Reviews*, 2001. **47**(1): p. 83-97.
87. Dombu, C.Y., M. Kroubi, R. Zibouche, R. Matran, and D. Betbeder, *Characterization of endocytosis and exocytosis of cationic nanoparticles in airway epithelium cells*. *Nanotechnology*, 2010. **21**(35): p. 355102.
88. Li Shang, K.N.a.G.U.N., *Engineered nanoparticles interacting with cells: size matters*. *Journal of Nanobiotechnology*, 2014. **12**(5): p. 1-11.
89. Dias, A., A. Hussain, A. Marcos, and A. Roque, *A biotechnological perspective on the application of iron oxide magnetic colloids modified with polysaccharides*. *Biotechnology advances*, 2011. **29**(1): p. 142-155.
90. Wahajuddin, S.A., *Superparamagnetic iron oxide nanoparticles: magnetic nanoplatforms as drug carriers*. *International journal of nanomedicine*, 2012. **7**: p. 3445.
91. Kolhatkar, A.G., A.C. Jamison, D. Litvinov, R.C. Willson, and T.R. Lee, *Tuning the magnetic properties of nanoparticles*. *International journal of molecular sciences*, 2013. **14**(8): p. 15977-16009.
92. Xiao, L., J. Li, D.F. Brougham, E.K. Fox, N. Feliu, A. Bushmelev, A. Schmidt, N. Mertens, F. Kiessling, M. Valldor, B. Fadeel, and S. Mathur, *Water-Soluble Superparamagnetic Magnetite Nanoparticles with Biocompatible Coating for Enhanced Magnetic Resonance Imaging*. *ACS Nano*, 2011. **5**(8): p. 6315-6324.
93. Dung, T.T., T.M. Danh, N.H. Duc, and D.M. Chien. *Preparation and characterization of magnetic nanoparticles coated with polyethylene glycol*. in *Journal of Physics: Conference Series*. 2009: IOP Publishing.
94. Hoffman-Antenbrink, M., B. Von Rechenberg, and H. Hofmann, *Superparamagnetic nanoparticles for biomedical applications*. 2009.
95. Zhou, W., R. Apkarian, Z.L. Wang, and D. Joy, *Fundamentals of Scanning Electron Microscopy (SEM)*, in *Scanning Microscopy for Nanotechnology*. 2007, Springer. p. 1-40.

96. Seraj, S., B. Mirzayi, and A. Nematollahzadeh, *Superparamagnetic maghemite/polyrhodanine core/shell nanoparticles: Synthesis and characterization*. *Advanced Powder Technology*, 2014. **25**(5): p. 1520-1526.
97. Lei, P., A.M. Boies, S. Calder, and S.L. Girshick, *Thermal plasma synthesis of superparamagnetic iron oxide nanoparticles*. *Plasma Chemistry and Plasma Processing*, 2012. **32**(3): p. 519-531.
98. Rittikulsittichai, S., B. Singhana, W.W. Bryan, S. Sarangi, A.C. Jamison, A. Brazdeikis, and T.R. Lee, *Preparation, characterization, and utilization of multi-functional magnetic-fluorescent composites for bio-imaging and magnetic hyperthermia therapy*. *RSC Advances*, 2013. **3**(21): p. 7838-7849.
99. Ko, J.A., H.J. Park, S.J. Hwang, J.B. Park, and J.S. Lee, *Preparation and characterization of chitosan microparticles intended for controlled drug delivery*. *International Journal of Pharmaceutics*, 2002. **249**(1-2): p. 165-174.
100. ChemAxon. [cited 2014 21 October]; Available from: <http://www.chemicalize.org>.
101. Wang, L., A. Roitberg, C. Meuse, and A.K. Gaigalas, *Raman and FTIR spectroscopies of fluorescein in solutions*. *Spectrochimica Acta Part A: Molecular and Biomolecular Spectroscopy*, 2001. **57**(9): p. 1781-1791.
102. Mitra, S., U. Gaur, P.C. Ghosh, and A.N. Maitra, *Tumour targeted delivery of encapsulated dextran–doxorubicin conjugate using chitosan nanoparticles as carrier*. *Journal of Controlled Release*, 2001. **74**(1-3): p. 317-323.
103. Aydın RS and Pulat M, *5-Fluorouracil Encapsulated Chitosan Nanoparticles for pH-Stimulated Drug Delivery: Evaluation of Controlled Release Kinetics*. *Journal of Nanomaterials*, 2012. **2012**: p. 10.
104. Guan, J., P. Cheng, S.J. Huang, J.M. Wu, Z.H. Li, X.D. You, L.M. Hao, Y. Guo, R.X. Li, and H. Zhang, *Optimized Preparation of Levofloxacin-loaded Chitosan Nanoparticles by Ionotropic Gelation*. *Physics Procedia*, 2011. **22**(0): p. 163-169.
105. Angeletti RH, Bibbs L, Bonewald LF, Fields GB, McMurray JS, Moore WT, and S. JT, *Formation of a disulfide bond in an octreotide-like peptide: A multicenter study*. *TECHNIQUES IN PROTEIN CHEMISTRY VII*. Vol. 7. 1996.
106. Long, J.-T., T.-y. Cheang, S.-Y. Zhuo, R.-F. Zeng, Q.-S. Dai, H.-P. Li, and S. Fang, *Anticancer drug-loaded multifunctional nanoparticles to enhance the chemotherapeutic efficacy in lung cancer metastasis*. *Journal of Nanobiotechnology*, 2014. **12**(1): p. 37.

107. Soppimath, K.S., T.M. Aminabhavi, A.R. Kulkarni, and W.E. Rudzinski, *Biodegradable polymeric nanoparticles as drug delivery devices*. Journal of Controlled Release, 2001. **70**(1–2): p. 1-20.
108. Paulino, A.T., A.R. Fajardo, A.P. Junior, E.C. Muniz, and E.B. Tambourgi, *Two-step synthesis and properties of a magnetic-field-sensitive modified maltodextrin-based hydrogel*. Polymer International, 2011. **60**(9): p. 1324-1333.
109. Xu, F., F. Inci, O. Mullick, U.A. Gurkan, Y. Sung, D. Kavaz, B. Li, E.B. Denkbas, and U. Demirci, *Release of Magnetic Nanoparticles from Cell-Encapsulating Biodegradable Nanobiomaterials*. ACS Nano, 2012. **6**(8): p. 6640-6649.
110. Hong, F.J., F. Bai, and P. Cheng, *Numerical simulation of AC electrothermal micropump using a fully coupled model*. Microfluidics and Nanofluidics, 2012. **13**(3): p. 411-420.
111. Finotelli, P.V., D. Da Silva, M. Sola-Penna, A.M. Rossi, M. Farina, L.R. Andrade, A.Y. Takeuchi, and M.H. Rocha-Leão, *Microcapsules of alginate/chitosan containing magnetic nanoparticles for controlled release of insulin*. Colloids and Surfaces B: Biointerfaces, 2010. **81**(1): p. 206-211.
112. Hu, S.-H., C.-H. Tsai, C.-F. Liao, D.-M. Liu, and S.-Y. Chen, *Controlled rupture of magnetic polyelectrolyte microcapsules for drug delivery*. Langmuir, 2008. **24**(20): p. 11811-11818.
113. Hu, S.H., S.Y. Chen, D.M. Liu, and C.S. Hsiao, *Core/Single-Crystal-Shell Nanospheres for Controlled Drug Release via a Magnetically Triggered Rupturing Mechanism*. Advanced Materials, 2008. **20**(14): p. 2690-2695.
114. Byrne, J.D., T. Betancourt, and L. Brannon-Peppas, *Active targeting schemes for nanoparticle systems in cancer therapeutics*. Advanced Drug Delivery Reviews, 2008. **60**(15): p. 1615-1626.
115. Peng, X.-H., Y. Wang, D. Huang, Y. Wang, H.J. Shin, Z. Chen, M.B. Spewak, H. Mao, X. Wang, and Y. Wang, *Targeted delivery of cisplatin to lung cancer using ScFvEGFR-heparin-cisplatin nanoparticles*. ACS Nano, 2011. **5**(12): p. 9480-9493.
116. Castillo, L., M. Etienne-Grimaldi, J. Fischel, P. Formento, N. Magne, and G. Milano, *Pharmacological background of EGFR targeting*. Annals of oncology, 2004. **15**(7): p. 1007-1012.
117. Chung, K.H., S.H. Park, M.K. Kim, H.D. Park, and T.I. Son, *Stabilization of epidermal growth factor on thermal and proteolytic degradation by conjugating with low molecular weight chitosan*. Journal of applied polymer science, 2006. **102**(5): p. 5072-5082.

118. Lesniak, A., A. Salvati, M.J. Santos-Martinez, M.W. Radomski, K.A. Dawson, and C. Åberg, *Nanoparticle Adhesion to the Cell Membrane and Its Effect on Nanoparticle Uptake Efficiency*. Journal of the American Chemical Society, 2013. **135**(4): p. 1438-1444.
119. dos Santos, T., J. Varela, I. Lynch, A. Salvati, and K.A. Dawson, *Quantitative Assessment of the Comparative Nanoparticle-Uptake Efficiency of a Range of Cell Lines*. Small, 2011. **7**(23): p. 3341-3349.
120. Davda, J. and V. Labhasetwar, *Characterization of nanoparticle uptake by endothelial cells*. International Journal of Pharmaceutics, 2002. **233**(1–2): p. 51-59.
121. Mo, Y. and L.-Y. Lim, *Mechanistic study of the uptake of wheat germ agglutinin-conjugated PLGA nanoparticles by A549 cells*. Journal of Pharmaceutical Sciences, 2004. **93**(1): p. 20-28.
122. Huang, M., Z. Ma, E. Khor, and L.-Y. Lim, *Uptake of FITC-Chitosan Nanoparticles by A549 Cells*. Pharmaceutical Research, 2002. **19**(10): p. 1488-1494.
123. de Salamanca, A.E., Y. Diebold, M. Calonge, C. García-Vazquez, S. Callejo, A. Vila, and M.J. Alonso, *Chitosan Nanoparticles as a Potential Drug Delivery System for the Ocular Surface: Toxicity, Uptake Mechanism and In Vivo Tolerance*. Investigative Ophthalmology & Visual Science, 2006. **47**(4): p. 1416-1425.
124. Li Shang, K. Nienhaus, and G.U. Nienhaus, *Engineered nanoparticles interacting with cells: size matters*. Journal of Nanobiotechnology, 2014. **12**(5).
125. Garcion, E., A. Lamprecht, B. Heurtault, A. Paillard, A. Aubert-Pouessel, B. Denizot, P. Menei, and J.-P. Benoît, *A new generation of anticancer, drug-loaded, colloidal vectors reverses multidrug resistance in glioma and reduces tumor progression in rats*. Molecular Cancer Therapeutics, 2006. **5**(7): p. 1710-1722.
126. S. Tammam, H. M.E Azzazy, and A. Lamprecht., *A High throughput Method for Determination of Amount of Surface Bound and Internalized Chitosan Nanoparticles*. (Under publication), 2014.
127. Twentyman, P.R. and M. Luscombe, *A study of some variables in a tetrazolium dye (MTT) based assay for cell growth and chemosensitivity*. Br J Cancer, 1987. **56**(3): p. 279-85.
128. Qi, L., Z. Xu, X. Jiang, Y. Li, and M. Wang, *Cytotoxic activities of chitosan nanoparticles and copper-loaded nanoparticles*. Bioorganic & Medicinal Chemistry Letters, 2005. **15**(5): p. 1397-1399.

129. Huang, M., E. Khor, and L.-Y. Lim, *Uptake and cytotoxicity of chitosan molecules and nanoparticles: effects of molecular weight and degree of deacetylation*. *Pharmaceutical research*, 2004. **21**(2): p. 344-353.
130. Ma, Z. and L.-Y. Lim, *Uptake of chitosan and associated insulin in Caco-2 cell monolayers: a comparison between chitosan molecules and chitosan nanoparticles*. *Pharmaceutical research*, 2003. **20**(11): p. 1812-1819.
131. Han, Y., S. Li, X. Cao, L. Yuan, Y. Wang, Y. Yin, T. Qiu, H. Dai, and X. Wang, *Different Inhibitory Effect and Mechanism of Hydroxyapatite Nanoparticles on Normal Cells and Cancer Cells In Vitro and In Vivo*. *Sci. Rep.*, 2014. **4**.
132. Szczepanski, C., O. Tenstad, A. Baumann, A. Martinez, R. Myklebust, R. Bjerkvig, and L. Prestegarden, *Identification of a novel lytic peptide for the treatment of solid tumours*. *Genes & Cancer*, 2014. **5**(5-6): p. 186-200.
133. Osaka, T., T. Nakanishi, S. Shanmugam, S. Takahama, and H. Zhang, *Effect of surface charge of magnetite nanoparticles on their internalization into breast cancer and umbilical vein endothelial cells*. *Colloids and Surfaces B: Biointerfaces*, 2009. **71**(2): p. 325-330.
134. Fan, C., W. Gao, Z. Chen, H. Fan, M. Li, F. Deng, and Z. Chen, *Tumor selectivity of stealth multi-functionalized superparamagnetic iron oxide nanoparticles*. *International Journal of Pharmaceutics*, 2011. **404**(1-2): p. 180-190.
135. Ulbrich, K., T. Hekmatara, E. Herbert, and J. Kreuter, *Transferrin- and transferrin-receptor-antibody-modified nanoparticles enable drug delivery across the blood-brain barrier (BBB)*. *European Journal of Pharmaceutics and Biopharmaceutics*, 2009. **71**(2): p. 251-256.
136. Dinauer, N., S. Balthasar, C. Weber, J. Kreuter, K. Langer, and H. von Briesen, *Selective targeting of antibody-conjugated nanoparticles to leukemic cells and primary T-lymphocytes*. *Biomaterials*, 2005. **26**(29): p. 5898-5906.
137. Acharya, S., F. Dilnawaz, and S.K. Sahoo, *Targeted epidermal growth factor receptor nanoparticle bioconjugates for breast cancer therapy*. *Biomaterials*, 2009. **30**(29): p. 5737-5750.
138. Kocbek, P., N. Obermajer, M. Cegnar, J. Kos, and J. Kristl, *Targeting cancer cells using PLGA nanoparticles surface modified with monoclonal antibody*. *Journal of Controlled Release*, 2007. **120**(1-2): p. 18-26.
139. Montenegro, J.-M., V. Grazu, A. Sukhanova, S. Agarwal, J.M. de la Fuente, I. Nabiev, A. Greiner, and W.J. Parak, *Controlled antibody/(bio-) conjugation of inorganic*

- nanoparticles for targeted delivery*. *Advanced Drug Delivery Reviews*, 2013. **65**(5): p. 677-688.
140. Aktaş, Y., M. Yemisci, K. Andrieux, R.N. Gürsoy, M.J. Alonso, E. Fernandez-Megia, R. Novoa-Carballal, E. Quiñoá, R. Riguera, M.F. Sargon, H.H. Çelik, A.S. Demir, A.A. Hıncal, T. Dalkara, Y. Çapan, and P. Couvreur, *Development and Brain Delivery of Chitosan–PEG Nanoparticles Functionalized with the Monoclonal Antibody OX26*. *Bioconjugate Chemistry*, 2005. **16**(6): p. 1503-1511.
 141. Raof, M., S.J. Corr, W.D. Kaluarachchi, K.L. Massey, K. Briggs, C. Zhu, M.A. Cheney, L.J. Wilson, and S.A. Curley, *Stability of antibody-conjugated gold nanoparticles in the endolysosomal nanoenvironment: implications for noninvasive radiofrequency-based cancer therapy*. *Nanomedicine: Nanotechnology, Biology and Medicine*, 2012. **8**(7): p. 1096-1105.
 142. Master, A.M. and A. Sen Gupta, *EGF receptor-targeted nanocarriers for enhanced cancer treatment*. *Nanomedicine*, 2012. **7**(12): p. 1895-1906.
 143. Salvati, A., A.S. Pitek, M.P. Monopoli, K. Prapainop, F.B. Bombelli, D.R. Hristov, P.M. Kelly, C. Aberg, E. Mahon, and K.A. Dawson, *Transferrin-functionalized nanoparticles lose their targeting capabilities when a biomolecule corona adsorbs on the surface*. *Nat Nano*, 2013. **8**(2): p. 137-143.
 144. Mahon, E., A. Salvati, F. Baldelli Bombelli, I. Lynch, and K.A. Dawson, *Designing the nanoparticle–biomolecule interface for “targeting and therapeutic delivery”*. *Journal of Controlled Release*, 2012. **161**(2): p. 164-174.
 145. Lundqvist, M., J. Stigler, G. Elia, I. Lynch, T. Cedervall, and K.A. Dawson, *Nanoparticle size and surface properties determine the protein corona with possible implications for biological impacts*. *Proceedings of the National Academy of Sciences*, 2008. **105**(38): p. 14265-14270.
 146. Adams, G.P. and R. Schier, *Generating improved single-chain Fv molecules for tumor targeting*. *Journal of Immunological Methods*, 1999. **231**(1–2): p. 249-260.
 147. Yang, L., H. Mao, Y.A. Wang, Z. Cao, X. Peng, X. Wang, H. Duan, C. Ni, Q. Yuan, and G. Adams, *Single chain epidermal growth factor receptor antibody conjugated nanoparticles for in vivo tumor targeting and imaging*. *Small*, 2009. **5**(2): p. 235-243.
 148. Zhou, Y., D.C. Drummond, H. Zou, M.E. Hayes, G.P. Adams, D.B. Kirpotin, and J.D. Marks, *Impact of single-chain Fv antibody fragment affinity on nanoparticle targeting of epidermal growth factor receptor-expressing tumor cells*. *Journal of molecular biology*, 2007. **371**(4): p. 934-947.

149. Danhier, F., E. Ansorena, J.M. Silva, R. Coco, A. Le Breton, and V. Préat, *PLGA-based nanoparticles: an overview of biomedical applications*. *Journal of Controlled Release*, 2012. **161**(2): p. 505-522.
150. Yin Win, K. and S.-S. Feng, *Effects of particle size and surface coating on cellular uptake of polymeric nanoparticles for oral delivery of anticancer drugs*. *Biomaterials*, 2005. **26**(15): p. 2713-2722.
151. Yue, Z.-G., W. Wei, P.-P. Lv, H. Yue, L.-Y. Wang, Z.-G. Su, and G.-H. Ma, *Surface charge affects cellular uptake and intracellular trafficking of chitosan-based nanoparticles*. *Biomacromolecules*, 2011. **12**(7): p. 2440-2446.
152. Rajendran, L., H.-J. Knölker, and K. Simons, *Subcellular targeting strategies for drug design and delivery*. *Nature Reviews Drug Discovery*, 2010. **9**(1): p. 29-42.
153. Allen, A., A. Neuberger, and N. Sharon, *The purification, composition and specificity of wheat-germ agglutinin*. *Biochem. j*, 1973. **131**: p. 155-162.
154. Privat, J.-P., F. Delmotte, G. Mialonier, P. Bouchard, and M. Monsigny, *Fluorescence Studies of Saccharide Binding to Wheat-Germ Agglutinin (Lectin)*. *European Journal of Biochemistry*, 1974. **47**(1): p. 5-14.
155. Ali, M.E. and A. Lamprecht, *Spray freeze drying for dry powder inhalation of nanoparticles*. *European Journal of Pharmaceutics and Biopharmaceutics*, 2014. **87**(3): p. 510-517.
156. Nandiyanto, A.B.D. and K. Okuyama, *Progress in developing spray-drying methods for the production of controlled morphology particles: From the nanometer to submicrometer size ranges*. *Advanced Powder Technology*, 2011. **22**(1): p. 1-19.
157. D'Addio, S.M., J.G.Y. Chan, P.C.L. Kwok, R.K. Prud'homme, and H.-K. Chan, *Constant size, variable density aerosol particles by ultrasonic spray freeze drying*. *International Journal of Pharmaceutics*, 2012. **427**(2): p. 185-191.
158. S N Tammam, H. M. E. Azzazy, and A.Lamprecht, *Biodegradable particulate carrier formulation and tuning for targeted drug delivery*. *Journal of Biomedical Nanotechnology*, 2015. **11**(4).
159. *Lung cancer - non-small cell*. 3 December 2014; Available from: <http://www.nlm.nih.gov/medlineplus/ency/article/007194.htm>.